REPUBLIC OF TÜRKİYE
KIRŞEHİR AHİ EVRAN UNIVERSITY
INSTITUTE OF NATURAL AND APPLIED SCIENCES
DEPARTMENT OF ADVANCED TECHNOLOGIES

# DETECTION AND MEASUREMENT OF MULTILEVEL COVID-19 INFECTION USING GAMMA CORRECTION AND FEATURES EXTRACTED BY CNN ENHANCED WITH XGBOOST FROM CT SCAN IMAGES

**RANA SABRY ABBAS AL-BAYATI**

**MSc THESIS**

**KIRŞEHİR**
**2024**

REPUBLIC OF TÜRKİYE
KIRŞEHİR AHİ EVRAN UNIVERSITY
INSTITUTE OF NATURAL AND APPLIED SCIENCES
DEPARTMENT OF ADVANCED TECHNOLOGIES

# DETECTION AND MEASUREMENT OF MULTILEVEL COVID-19 INFECTION USING GAMMA CORRECTION AND FEATURES EXTRACTED BY CNN ENHANCED WITH XGBOOST FROM CT SCAN IMAGES

**RANA SABRY ABBAS AL-BAYATI**

**MSc THESIS**

**SUPERVISOR**
**ASSIST. PROF. DR. MUSTAFA AKSU**

**KIRŞEHİR**
**2024**

**KIRŞEHİR AHİ EVRAN UNIVERSITY**

**INSTITUTE OF NATURAL AND APPLIED SCIENCES**

**MSc THESIS**

**ETHICS DECLARATION**

In this thesis study, which I have read and understood the Kırşehir Ahi Evran University Scientific Research and Publication Ethics Directive and which I have prepared in accordance with the Kırşehir Ahi Evran University, Institute of Natural and Applied Sciences Department of Advanced Technologies Thesis Writing Rules;

- I have obtained the data, information and documents I have presented in the thesis within the framework of academic and ethical rules,
- I present all information, documents, evaluations and results in accordance with scientific ethical rules,
- I have cited all the works I have benefited from in the thesis by making appropriate references,
- I have not made any changes in the data used and the results,
- This study, which I have presented as a thesis, is original,

Otherwise, I declare that I accept all legal actions to be taken against me in this regard and all loss of rights that may arise against me. 29/03/202024

RANA SABRY ABBAS AL-BAYATI

**LIST OF CONTENTS**

**Page No**

**ACKNOWLEDGEMENTS**

For their continual encouragement and counsel during my master programme Assist. Prof. Dr. Mustafa AKSU, my supervisor, have my sincere gratitude. Their knowledge and tolerance have been a great help to me and were essential to the achievement of this thesis.

I want to convey my most profound appreciation to the Engineering and Architecture Faculty at Kırşehir Ahi Evran University for giving me the chance to pursue my master's degree. Their support and assistance throughout this research journey have been invaluable.

I appreciate my friends and family's affection and assistance throughout this journey. I would not have finished my adventure if it were not for their support and inspiration.

Last, I thank everyone who participated in my study and was willing to share their knowledge. With their help, this work was completed.

March, 2024 RANA SABRY ABBAS AL-BAYATI

**GENİŞLETİLMİŞ ÖZET**

**YÜKSEK LİSANS TEZİ**

# BT TARAMA GÖRÜNTÜLERİNDEN GAMA DÜZELTME VE XGBOOST İLE GELİŞTİRİLMİŞ CNN KULLANILARAK ÇOK DÜZEYLİ COVID-19 ENFEKSİYONUNUN ÖLÇÜMÜ VE TESPİTİ

**RANA SABRY ABBAS AL-BAYATI**

**KIRŞEHİR AHİ EVRAN ÜNİVERSİTESİ**
**FEN BİLİMLERİ ENSTİTÜSÜ**
**İLERİ TEKNOLOJİLER ANABİLİM DALI**

**Danışman:** **Dr. Öğr. Üyesi Mustafa AKSU**
**Yıl: 2024 / Sayfa: 99**
**Jüri:** **Dr. Öğr. Üyesi Mustafa AKSU**
**Doç. Dr. Mustafa YAĞCI**
**Doç. Dr. Murat CANAYAZ**

Radyasyon teşhisi alanı, yapay zekâ (AI), bilgisayarlı görüş ve gelişmiş tıbbi görüntüleme teknikleri gibi yenilikçi teknolojilerin desteklediği hızlı ilerlemelerden geçmektedir. Bu dinamik ortamda bilgisayarlı tomografi (BT) görüntüleme, özellikle hem COVID-19 hem de akciğer tümörleriyle ilişkili klinik değişikliklerin tanımlanmasında öne çıkan bir yöntem olarak ortaya çıkmıştır. Göğüs röntgeni, çeşitli tıbbi görüntüleme teknikleri ve BT taramalarının kullanımı, COVID-19'un hızlı ve doğru tanısı için pratik ve etkili bir araç olarak önerilmiştir. Özellikle BT taramaları, aşırı koşullar altında yanlış negatif sonuçların ortaya çıkabileceği durumlarda bile, COVID-19'un varlığını tespit etmede yüksek hassasiyet göstermiştir. Ancak COVİD-19 pozitifliğini belirlemek için röntgen ve BT görüntülerinin uzmanlar tarafından analiz edilmesi zaman alıcı ve zorlu bir süreçtir. Bu çalışma, zorlukların üstesinden gelmek ve teşhis sürecini iyileştirmek için evrişimli sinir ağlarının (CNN'ler) uygulanmasını ele alıyor. Bu CNN'ler, transfer öğrenimi yoluyla elde edilen bir başarı olan ilgisiz öğeleri filtrelerken görüntüleri doğru bir şekilde kategorize etmede çok önemli bir rol oynuyor. Transfer öğreniminde önceden var olan yöntemler, ImageNet gibi kapsamlı veri kümelerinden temel özellikleri toplayarak bunları yeni görevlere etkili bir şekilde uygular. Makine öğrenimi tekniklerindeki ilerlemelere rağmen, CNN'lerin etkinliği hala CT görüntülerinden ilgili niteliklerin çıkarılmasına bağlıdır.

Bu nedenle çalışma, göğüs BT taramaları ve X-ışını görüntülerinin kullanımının, COVID-19'u tespit etmek için önemli bir potansiyele sahip olduğunu ve bu potansiyelin, DenseNet, ResNet ve VGG-16 gibi önceden eğitilmiş CNN'ler kullanılarak daha da artırılabileceğini öne sürüyor.

İki farklı veri kümesinden (Covid Veri 1 ve Covid Veri 2) elde edilen sonuçlar ile CNN net ve XGBoost sınıflandırıcısını içeren çeşitli modellerin sonuçları karşılaştırıldı ve analiz edildi. Her iki veri kümesinde de XGBoost, görüntü boyutu ve eğitim ayarlarından bağımsız olarak doğruluk açısından sürekli olarak CNN ağını geride bırakıyor. Covid Veri 1, test edilen tüm modellerde ve ayarlarda genellikle Covid Veri 2'ye kıyasla daha yüksek doğruluk sergiliyor. Özellikle XGBoost, GC ($\Upsilon$=1.5) ile eğitildiğinde ve 128x128 ve 256x256 piksel görüntü boyutlarını kullandığında, Covid Veri 1 için %97.94'e ve Covid Veri 2 için %97.76'ya ulaşarak en yüksek doğruluğu elde ediyor. Öte yandan CNN ağı hem GC'siz hem

de 256x256 piksel görüntü boyutlarını kullanarak, en yüksek oranlar Covid Veri 1 için %79.54 ve Covid Veri 2 için %79.74 olmak üzere daha düşük doğruluk oranları elde ediyor. Bu nedenle, sağlanan sonuçlara göre XGBoost sınıflandırıcı, sınıflandırma görevleri için üstün bir seçim gibi görünüyor; modeller ve ayarlar genelinde tutarlı olarak daha yüksek doğruluk oranı nedeniyle tercih edilen veri seti ise Covid Veri 1'dir.

Çalışma, bu modelin tanı amaçlı terapötik uygulamasına yönelik önemli ilerlemeler kaydederken, potansiyelini tam olarak gerçekleştirmek için daha fazla araştırmaya ihtiyaç duyulduğunu da kabul ediyor. Gelecekteki araştırmaların gama düzeltme ve ön işleme araçlarını kullanan ek tasarımları keşfetmesi bekleniyor. Daha karmaşık platformları eğitmek için daha büyük bir GPU bellek sınırına izin veren model eğitim seçeneklerine ilişkin hususlar önerilmektedir. Bu, gelişmiş yetenekler için başlangıç modüllerinin ve birden fazla yoğun katmanın dahil edilmesini içerebilir.

Çalışmada özetlenen bir sonraki araştırma alanı, belirli mimari tarzların belirli rahatsızlıkların tedavisinde daha etkili olup olmadığını belirlemeyi amaçlayan çeşitli rahatsızlıkların sınıflandırılmasına odaklanmaktadır. Farklı hastalıklarla ilgili performans farklılıklarını araştırmak, altta yatan nedenlere dair içgörü sağlayabilir. Ek olarak, analiz sürecini geliştirmek ve model performansının daha kapsamlı ve sağlam bir şekilde değerlendirilmesini sağlamak için k-fold veri bölme gibi alternatif veri bölme yöntemleri önerilmektedir.

**Anahtar Kelimeler**: Yapay zekâ, COVID-19, Akciğer hastalığı, BT (Bilgisayarlı Tomografi), Derin öğrenme, Görüntü işleme.

**ABSTRACT**

**MASTER'S THESIS**

**DETECTION AND MEASUREMENT OF MULTILEVEL COVID-19 INFECTION USING GAMMA CORRECTION AND FEATURES EXTRACTED BY CNN ENHANCED WITH XGBOOST FROM CT SCAN IMAGES**

**RANA SABRY ABBAS AL-BAYATI**

**KIRŞEHİR AHİ EVRAN UNIVERSITY**
**INSTITUTE OF NATURAL AND APPLIED SCIENCES**
**DEPARTMENT OF ADVANCED TECHNOLOGIES**

| | |
|---|---|
| **Supervisor:** | **Assist. Prof. Dr. Mustafa AKSU** |
| | **Year: 2024 / Page: 99** |
| **Jury:** | **Assist. Prof. Dr. Mustafa AKSU** |
| | **Assoc. Prof. Dr. Mustafa YAĞCI** |
| | **Assoc. Prof. Dr. Murat CANAYAZ** |

The field of radiation diagnosis is undergoing rapid advancements, propelled by innovative technologies such as artificial intelligence (AI), computer vision, and sophisticated medical imaging techniques. In this dynamic landscape, computed tomography (CT) imaging has emerged as a prominent method, especially in the identification of clinical changes associated with both COVID-19 and lung tumors. The utilization of chest X-rays, various medical imaging techniques, and CT scans has been proposed as a practical and efficient means for the rapid and accurate diagnosis of COVID-19. Notably, CT scans have demonstrated high sensitivity in detecting the presence of COVID-19, even in cases where false negatives may occur under extreme circumstances. However, the analysis of X-rays and CT images by specialists to determine COVID-19 positivity is a time-consuming and challenging process. To address these challenges and improve the diagnostic process, the study addresses the application of convolutional neural networks (CNNs). These CNNs play a crucial role in accurately categorizing images while filtering out irrelevant elements, a feat achieved through transfer learning. In transfer learning, pre-existing methods gather essential characteristics from extensive datasets like ImageNet, effectively applying them to new tasks. Despite the advancements in machine learning techniques, the efficacy of CNNs still hinges on the extraction of relevant attributes from CT images.

Therefore, the study suggests that the use of chest CT scans and X-ray images holds significant potential for detecting COVID-19, and this potential can be further enhanced by employing pre-trained CNNs such as DenseNet, ResNet, and VGG-16.

The results from two distinct datasets, namely Covid Data 1 and Covid Data 2, along with various models including CNN net and XGBoost classifier, have been compared and analyzed. Across both datasets, XGBoost consistently outperforms the CNN net in terms of accuracy, regardless of the image size and training settings. Covid Data 1 generally exhibits higher accuracies compared to Covid Data 2 across all models and settings tested. Specifically, XGBoost achieves the highest accuracy, reaching up to 97.94% for Covid Data 1 and 97.76% for Covid Data 2, when trained with GC ($\Upsilon$=1.5) and using image sizes of 128x128 and 256x256 pixels. On the other hand, the CNN net achieves lower accuracies, with

the highest being 79.54% for Covid Data 1 and 79.74% for Covid Data 2, both without GC and using image sizes of 256x256 pixels. Therefore, based on the provided results, the XGBoost classifier appears to be the superior choice for classification tasks, with Covid Data 1 being the preferred dataset due to its consistently higher accuracies across models and settings.

While the study makes significant strides toward the therapeutic application of this model for diagnostic purposes, it acknowledges the need for further research to fully realize its potential. Future investigations are expected to explore additional designs utilizing gamma correction and pre-processing tools. To train more complex platforms, considerations for model training options that allow for a larger GPU memory limit are suggested. This could involve incorporating inception modules and multiple dense layers for enhanced capabilities.

The next area of research outlined in the study focuses on the classification of various ailments, aiming to determine whether specific architectural styles are more effective in treating certain conditions. Exploring performance differences related to different illnesses could provide insights into the underlying causes. Additionally, alternative data splitting methods, such as k-fold data splitting, are suggested to enhance the analysis process, providing a more comprehensive and robust evaluation of the model's performance.

**Keywords:** Artificial intelligence, COVID 19, Lung disease, CT, deep learning, image processing.

**LIST OF TABLES**

**Page No**

**LIST OF FIGURES**

**Page No**

## LIST OF ICONS AND ABBREVIATIONS

| **Icons** | | **Described** |
|---|---|---|
| % | : | Percentage |
| **Abbreviations** | | **Described** |
| **ACC** | : | Accuracy |
| **AUC** | : | Area under the Curve |
| **BNN** | : | Backpropagation Neural Network |
| **CAP** | : | Community-acquired pneumonia |
| **CI** | : | Confidence interval |
| **CNN** | : | Convolutional neural networks |
| **COPD** | : | Chronic obstructive pulmonary disease |
| **COVID** | : | Corona virus |
| **CRD** | : | Chronic respiratory diseases |
| **CT** | : | Computed tomography |
| **CXR** | : | Chest x-rays |
| **DCNN** | : | Densely connected CNN |
| **DL** | : | Deep learning |
| **DNN** | : | Deep Neural Network |
| **EMR** | : | Electronic medical record |
| **GAN** | : | Generative Adversarial Network |
| **GWAS** | : | Genome-wide association studies |
| **HDLA** | : | Hybrid Deep Learning Algorithm |
| **ILD** | : | Interstitial lung disease |
| **IPF** | : | Idiopathic pulmonary fibrosis |
| **ML** | : | Machine learning |
| **PROM** | : | Protracted rupture of the membranes |
| **ResNet** | : | Residual network |
| **RF** | : | Random Forest |
| **RT-PCR** | : | Reverse transcription polymerase chain reaction |
| **SEN** | : | Sensitivity |
| **SPE** | : | Specificity |
| **SVM** | : | Support Vector Machine |
| **TB** | : | Tuberculosis |
| **VGG** | : | Visual Geometry Group |
| **XGBoost** | : | eXtreme Gradient Boosting |

## 1. INTRODUCTION

Many techniques have been developed in computer science. Image processing and machine learning have been involved in solving many aspects of life's problems. Apps using modern technologies have become commonplace recently to help people make decisions and speed up work completion. Most fields today cannot survive without the presence of computer science on the way to get things done. The field of medicine is one of the fields that use computer vision and artificial intelligence techniques in diagnosis, examination, and decision-making (Ahuja, 2019).

Smart medical applications that rely on data analysis and processing, like other smart applications, depend primarily on the data used to create them. The selection of key algorithms and tools and the design and creation of the application are done in the early stages, and then the system needs to be trained to reach the decision-making stage. Data collected in the medical field can be relied upon to build, train, and test the system. Once the accuracy of the system has been measured, it can be recommended to be used in real-time to assist the clinician in diagnosis and decision-making (Canayaz et al., 2019).

Radiation diagnosis is a rapidly developing field of medicine that actively incorporates concepts such as artificial intelligence, computer vision, and new medical imaging modalities. Recently, CT imaging techniques of the lung have become the more popular pathogenic method to detect clinical changes related to COVID-19 and lung tumors. The research aims to use the algorithmic help generated in conjunction with geometric analysis to highlight the many markers that characterize the clinical status of the item of interest (COVID-19, tumors, and nodules) (Canayaz, 2021).

The key to building any intelligent system or application was, and still is, reducing performance time and increasing efficiency and productivity. As for the medical aspect, accuracy and speed in decision-making are essential. Computer-aided techniques play a vital role in medical image analysis. In the old days, there was more time to analyze and identify diseases in all areas of medical diagnosis (Halalli & Makandar, 2018).

It often leads to failure in the accurate and timely diagnosis of the patient. In this case, especially lung cancer, it needs more support from computer-assisted techniques. Early detection of lung cancer increases human life expectancy. Advances in medicine offer many techniques for observing patient conditions, such as chest x-rays (CXR). It is

essential to understand the existing techniques in the literature to develop an intelligent system through images, CT images, and magnetic resonance. Chest CT and X-ray samples are presented in Figure 1.1 (Bharati et al., 2021).

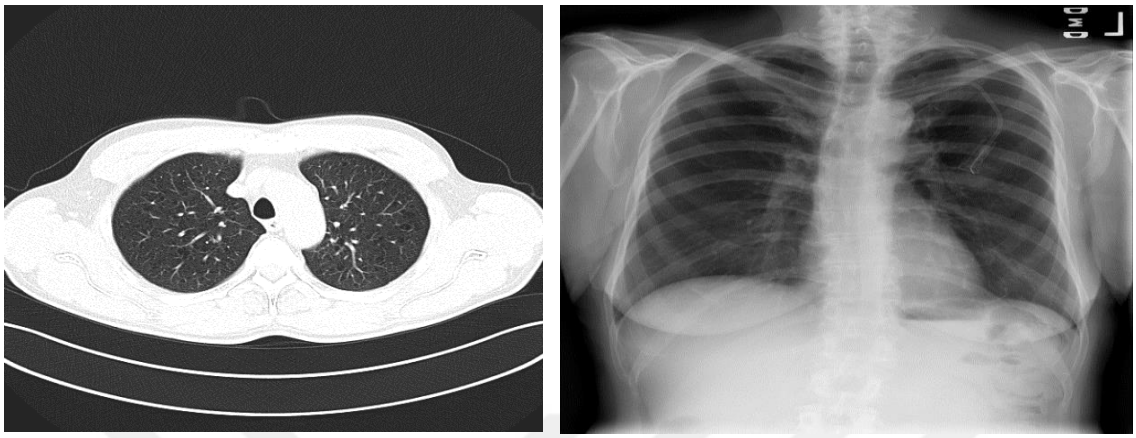

**Figure 1.1.** Chest CT and X-ray images

Healthcare facilities can share data to treat COVID-19 patients properly. It is a challenging task to securely share data and train a worldwide algorithm to identify impacted patients. The collection of data from many sources is a major issue and a roadblock to the creation of intelligent methods. Organizations may disseminate their data among universities and store it discreetly by using block chain-based federated learning. A block chain-based electronic medical record (EMR) offers a lot of potential to offer secure, trustworthy, and resilient EMR storage. Additionally, it will improve access to research data so that academics, medical professionals, and government organizations may examine it and use it to inform better decisions. The decentralized mechanism used by many facilities to share information does so safely and without jeopardizing the institutions' privacy. In order to enhance the global deep learning (DL) model for identifying contaminated patients, this dispersed information may be evaluated. For storing and maintaining any patient data, the key issues are privacy, confidentiality, and data consistency (Chan et al., 2020).

The main benefit of DL is its ability to learn from unlabeled data, often known as "unsupervised learning." Deep learning is commonly employed in a variety of sectors, including self-driving cars, face recognition, identifying objects, and image classification, due to features such as unlabeled data application, operating without feature engineering, forecast with high accuracy and precision, and image classification. Convolutional neural networks are deep learning techniques that have been widely employed to handle issues including document analysis, picture categorization, posture

recognition, and action detection. Convolutional neural networks (CNNs) have proved successful at detecting a number of ailments, including coronary artery disease, malaria, Alzheimer's disease, several dental disorders, and Parkinson's disease. One area where CNN has shown promising results is in medical imaging. Additionally, CNN has a good chance of distinguishing COVID-19 infections from non-COVID-19 infections using medical pictures such chest X-rays and CT scans that are available in public databases (Subramanian et al., 2022).

### 1.1. Research Importance

For more than a decade, lung cancer has been causing serious losses in human survival. It requires early and timely detection of the disease, and it's a step-by-step process for several radiologists to accurately detect lung cancer. Computer-assisted techniques and computer-aided diagnosis are the computer age that reduces complications in medical image diagnosis. Confidence in information technology and medical technological devices has played an important role in bringing about a fundamental change in the quality of healthcare services and raising the level of operation.

Related literature has investigated a lot of various machine learning tools, like supervised, unsupervised, and deep learning approaches. In this research, we will investigate the performance of CNN in detecting lung cancer after implementing Fourier transform and gamma correction on images as pre-processing and removing some brightness in CT segments, and compare the performance of implementing CNN without the pre-processing stage.

### 1.2. Research Problem

The use of deep learning (DL) in the detection of lung diseases is a topic that is expanding and becoming a cutting-edge technology for automated picture identification and computer vision. It routinely produces extremely effective detection, segmentation, or identification tasks, demonstrating considerable strength in the field of medical imaging computers. Despite the effectiveness reported in the research, there are still a number of fundamental obstacles that must be overcome before a true transfer to clinical practice can be achieved.

In this study, we focus on the textural qualities of medical pictures that can cause COVID patients to be misclassified using CT imaging.

### 1.3. Research Objectives

This research will integrate image processing and deep learning to identify lung CT images as healthy or COVID. First, a pre-processing step with a gamma correction on CT images is implemented before the CNN model. Then, using CNN to extract deep features and another gamma correction on the latter to enhance its resolution, Finally, compare recognition effectiveness with and without gamma correction. This study is anticipated to provide a tool for physicians to correctly interpret CT image findings, increasing the odds of a cure for lung disease patients.

### 1.4. Research Methodology

The main proposed methodology in this research includes the following: (1) preparing the COVID-19 CT dataset for analysis; (2) implementing gamma correction on medical images; (3) implementing a CNN model for deep feature extraction; and (4) discussing the difference in detection performance between the presence and absence of gamma correction. In this research, all computation and programming are carried out using the Colab website and Python deep learning and image processing packages.

## 2. LITERATURE REVIEW

### 2.1. Introduction

The utilization of chest X-rays, medical imaging, or CT scans has been proposed as a practical means of rapidly and accurately diagnosing COVID-19. The CT scan has demonstrated a high sensitivity in initially detecting the presence of COVID-19 in patients and can even correct false negatives under extreme circumstances. However, the analysis of X-rays and CT imaging by a specialist to determine COVID-19 positivity is a time-consuming and challenging process. The initial diagnostic method for detecting COVID-19 is through a chest X-ray. Convolutional neural networks (CNNs) are capable of accurately categorizing images while excluding irrelevant elements. Transfer learning is employed in this feature extraction, where pre-trained methods gather the main characteristics from large datasets like ImageNet and apply them effectively. Despite the advancements in machine learning techniques, the efficacy of CNNs still relies on extracting relevant attributes from CT images. Thus, the use of chest CT scans and X-ray images for COVID-19 detection shows promise and could benefit from the utilization of pre-trained CNNs like DenseNet, ResNet, and VGG-16. Transferring learned information from a pre-trained CNN that has already performed a specific function to a new one is a systematic approach to training CNN architecture. This method is faster and more efficient, as it does not require extensive annotation training datasets, making it a preferred choice for many academics, especially in the medical field.

### 2.2. Related Work

Ucar et al. (2020) have created an AI-powered framework specifically designed for COVID-19 patient screening that surpasses existing research in terms of effectiveness. The framework enhances the diagnostic capabilities through Bayesian optimization additives and optimizes SqueezeNet's lightweight network architecture (depicted in Figure 2.1). By fine-tuning hyperparameters and augmenting the dataset, the proposed network outperforms current designs, achieving a higher level of accuracy in COVID-19 diagnostics. The suggested model demonstrates accuracy rates of 100% for pneumonia cases, 98.04% for healthy cases, and 96.73% for COVID-19 cases.

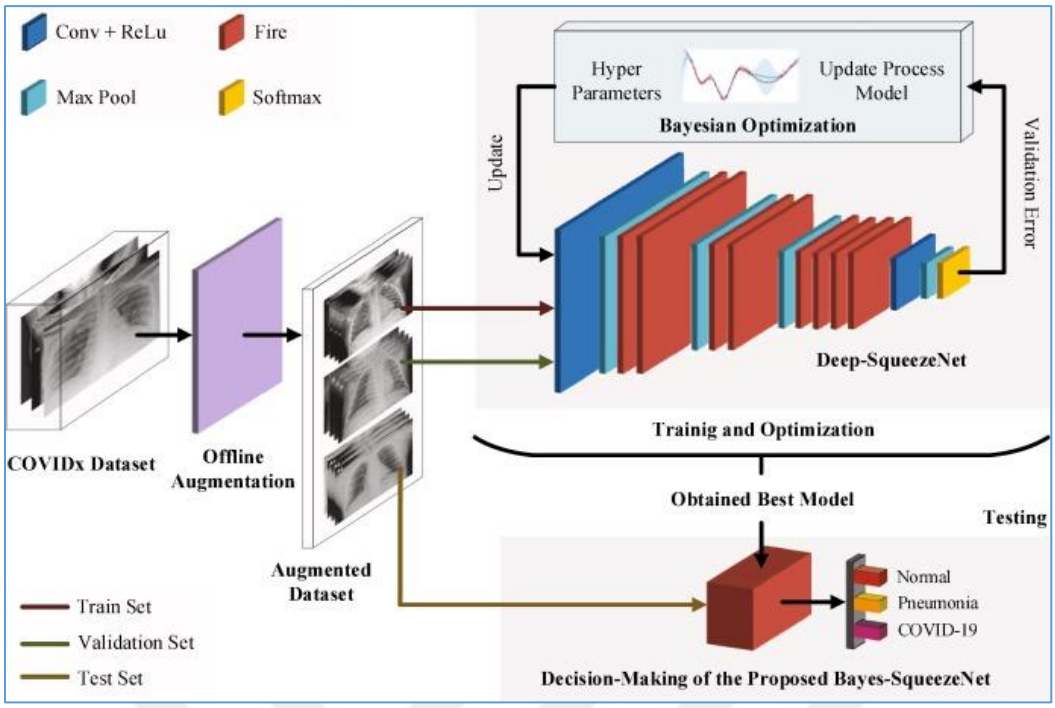


**Figure 2.1.** Proposed CNN model to classify CXR images (Ucar & Korkmaz, 2020).

Hammoudi et al. (2021) created a deep transfer learning-based model for the screening and diagnosis of COVID-19 patients based on InceptionResNetV2. Using chest X-ray pictures, their DenseNet169 model had an average accuracy of 96% for diagnosing pneumonia cases. The accuracy is 92.8%, while the sensitivity is 99.3%. There are 5,863 CXR samples of children in the group.

Rajaraman et al. (2020) introduced a specialized CNN in their study, aiming to classify chest X-ray (CXR) images into three categories: normal, bacterial pneumonia, or COVID-19-related abnormalities. To train the model, they utilized CXR images and incorporated ImageNet techniques to acquire modality-specific feature representations on a patient level. Their methodology involved transferring and fine-tuning learned knowledge to enhance performance and generalization. In order to reduce complexity and improve memory efficiency, the researchers applied iterative pruning. This technique resulted in the removal of redundant or less significant network parameters. Furthermore, they implemented ensemble techniques to aggregate predictions from the top-performing pruned models, effectively boosting the classification accuracy. The empirical evaluations of the proposed approach demonstrated remarkable outcomes.

By utilizing the weighted average of the pruned models, the researchers achieved an impressive accuracy of 99.01% in the detection of COVID-19 findings on CXRs. Additionally, the area under the curve (AUC) for their classification model

reached a high value of 0.9972. In summary, Rajaraman et al.'s research showcases the successful utilization of a customized CNN, combined with CXR images and ImageNet approaches, to accurately classify CXRs and detect COVID-19-related abnormalities.

Hall et al. (2020) developed a pre-trained ResNet50 with 10-fold cross-validation for identifying COVID and pneumonia patients. The AUC of the finding was 95%, and the total accuracy was 89.2%. Their study focuses on CXRs, which are less costly and simpler to get than CT scans, although they are less helpful. To assess individuals with COVID-19, Rahimzadeh and colleagues (Mohammad & Abolfazl, 2020) developed two models, namely Xception and ResNet50V2. These models were utilized to perform multiclass categorization, distinguishing between healthy individuals, patients with pneumonia, and those affected by COVID-19. The proposed methodology included the extraction of deep features from the data using the Xception and ResNet50V2 models, followed by the application of a softmax classifier for multiclass classification. The dataset employed in this study consisted of various types of CXR images, including COVID-19, pneumonia, and regular cases. Remarkably, the accuracy of this approach reached an impressive 99.56%. As further research progresses, it is recommended to explore the effectiveness of this method on larger datasets to potentially enhance its accuracy.

In a comparative study for the identification of COVID-19, Hemdan et al. (2020) used the VGG19, Inception-ResNet-V2, and MobileNetV2 DL models. In their research investigation, the VGG19 and dense nets performed well when compared to other CNN models. The VGG and dense CNN models had F1 scores of 89% and 91%, respectively. 25 normal subjects' CXR pictures and 25 images of COVID-19-positive cases make up the dataset. The proposed method's updated version can be utilized in the healthcare industry together with mobile devices to categorize cases of positive COVID-19.

Wang et al. (2014) developed a three-stage deep learning (DL) technique aimed at enhancing the analysis of COVID-19 in chest CT images. The technique involved three key steps: automated lung separation, reduction of non-lung areas, and diagnostic and predictive analysis for COVID-19.

To accomplish this, the researchers utilized two DL networks within their system. Firstly, they proposed a novel network known as COVID-19Net, specifically designed for the diagnostic and predictive analysis of COVID-19. Additionally, they employed the DenseNet121-FPN network for effectively separating the lungs in chest CT images. Similar to the DenseNet structure, each of the four dense units in this

COVID-19Net model includes several stacks of convolution and ReLU activation layers. The accuracy was 85%, the sensitivity was 79.35%, the AUC was 86%, and the specificity was 71.43%. A large dataset is made up of CT scan pictures from 5372 people. To improve performance, generative adversarial networks may one day be utilized to transform CT pictures with various slice thicknesses into CT images with a single slice thickness.

In order to identify COVID-19, Zheng et al. (2020) created a software system based on poorly supervised deep learning. To forecast the likelihood of COVID-19 infection, their method divided the lung area into segments using a pre-trained UNet, which were then input into a 3D deep neural network (Figure 2.3).

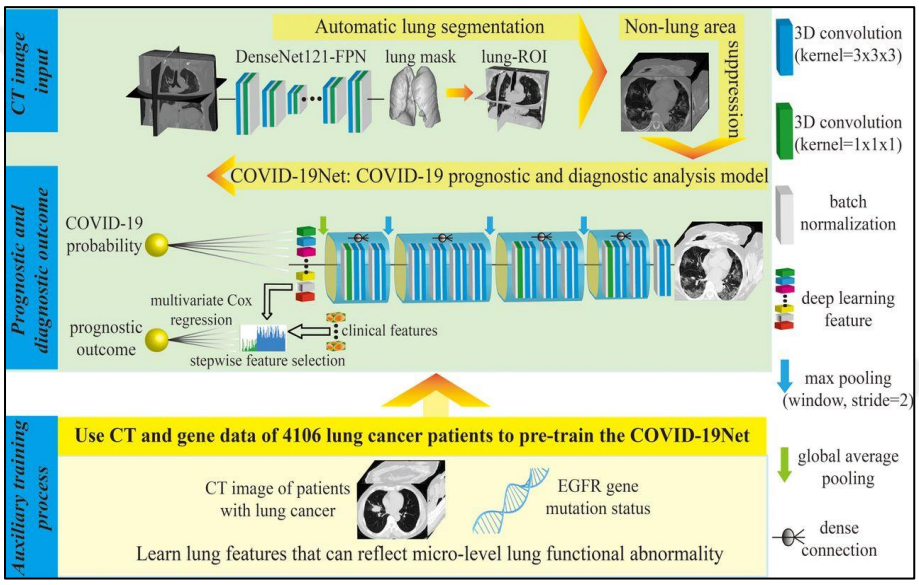


**Figure 2.2.** Proposed CNN model to classify lung CT images (Wang et al., 2020).

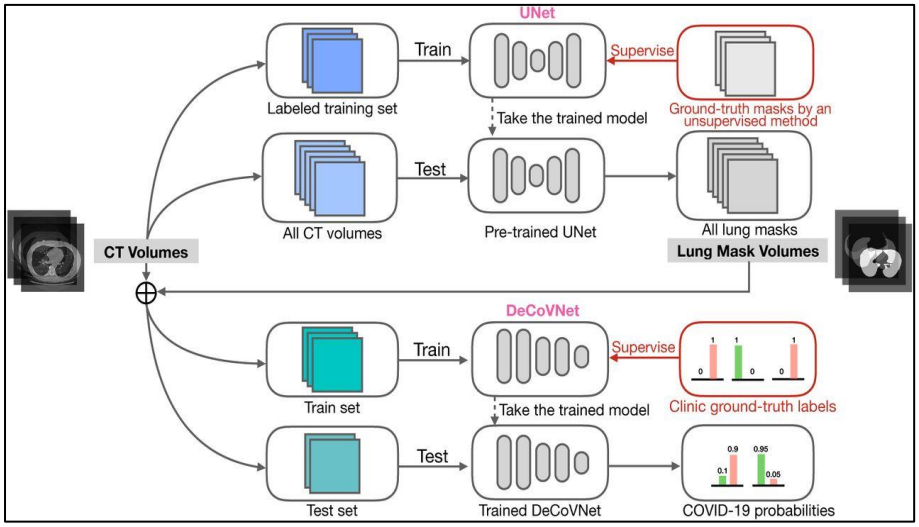


**Figure 2.3.** Proposed DL model to classify lung CT images (Zheng et al., 2020).

In the given study, the accuracy rate achieved was 90.1%, demonstrating the effectiveness of the method used. Additionally, the sensitivity rate was 90.7%, indicating the ability of the model to accurately detect infected areas. Moreover, the specificity rate reached 91.7%, highlighting the model's capability to correctly identify non-infected regions. Lastly, the AUC (area under the curve) value was measured to be 97.6%, further confirming the model's robustness in effectively distinguishing between infected and non-infected lung areas.

Using the ResNet50 architecture, Fu et al. (2020) presented a deep learning-based diagnostic tool that employs multi-class categorization to classify CT scan images into seven different categories. These categories include COVID-19, pneumonia, bacterial pneumonia, and normal lung conditions. The objective of this tool is to accurately identify and differentiate between these various lung conditions. The performance of the tool was evaluated, resulting in an impressive accuracy rate of 98.8%, a sensitivity rate of 98.2%, and a specificity rate of 98.9%. To train the model and validate its performance, a dataset of 60,427 CT scan images was collected from the Wuhan Jin Yin-Tan Hospital.

Ardakani et al. (2020) conducted a comparative analysis using various deep learning models, namely ResNet-101, VGG-19, SqueezeNet, ResNet-18, and Xception, to differentiate between COVID-19 and non-COVID-19 cases. It was found that the ResNet-101 models yielded the most favorable results. The researchers also compared the real-time performance of radiologists with the diagnostic outcomes obtained from these ten deep learning models for the identification of COVID-19. The results showed an accuracy rate of 99.51%, 100% sensitivity, an AUC of 99.4%, and a specificity of 99. The dataset consists of CT scan pictures from 108 COVID-19 patients and 86 patients with viral pneumonia who had conditions that were not COVID-19. The performance of the diagnostic system based on the DL models will be compared in the future with that of clinicians in real-time.

A self-powered technique for the diagnosis of COVID-19 patients was suggested by Rehman et al. (2022). Their approach frequently distinguishes between COVID-19 patients and viral and normal cases using multiclass categorization. Their study examined the seven CNN DL pre-trained designs, which were as follows: (1) AlexNet has three fully connected layers and five convolutional layers. (2) The VGG consists of 3 fully linked layers and 16 convolutional layers. (3) SqueezeNet features a five-module expanded layer. (4) The GoogleNet network, which comprises one fully connected

layer, one linear layer, two convolutional layers, four max-pooling layers, and nine inception models. (5) Three distinct applications of ResNet were made. Five convolutional blocks with two residual blocks each make up ResNet 18. There are two convolution layers in a residual block. Each of the five residual blocks in ResNet50 has an identity and a convolution block. Three convolution layers are used in the convolution and identity blocks. ResNet101 has an identity block, three convolutional blocks, and three residual blocks. (6) DenseNet has max-pooling layers and 1x1 convolutional filters.

Khalifa et al. (2022) created a method for identifying COVID-19 cases based on GAN (Generative Adversarial Network) using tailored DL models. AlexNet, GoogleNet, and RestNet18, which had 8, 18, and 22 layers, respectively, were three of the four DL models they employed. These models were selected because they utilize less memory, have fewer layers, and are faster to process.

For the purpose of diagnosing COVID-19 sickness, Loey et al. (2020) developed an approach using a generative adversarial network. These models included AlexNet, GoogleNet, and RestNet 18. In their model, GoogleNet attained 99.9% validation accuracy and 100% testing accuracy.

Then, using data from chest CT scans, Shan et al. (2020) suggested a precise DL-based algorithm for automatically segmenting and quantifying infection zones of COVID-19. The infectious region was properly segmented and quantified using VB-Net segmentation in the suggested model. The accuracy of the suggested model is 91.6%.

Using data from multiple centers and scanners, Hu et al. (2020) presented a deep learning framework that utilizes chest CT scans to automatically detect areas affected by COVID-19. This not only facilitates the diagnosis of COVID-19 patients based on the detected areas but also explores the ability of the model to distinguish between COVID-19 patients with community-acquired pneumonia (CAP) and those without pneumonia (NP), leveraging CT radiological features through their deep neural networks. The study findings suggest that the binary classification tasks, such as NP/COVID-19 and NP/CAP, outperform the three-way classification tasks. This can be attributed to the fact that binary classification is relatively simpler and less unpredictable compared to three-way classification. The proposed model demonstrates promising results, achieving a mean accuracy (ACC) of 96.2%, precision (PRC) of 97.3%, sensitivity (SEN) of 94.5%, specificity (SPE) of 95.3%, and area under the curve (AUC) of 0.970. These metrics indicate the model's proficiency in distinguishing

COVID-19 cases from non-pneumonia instances. The high performance can be attributed to the model's ability to accurately identify the specific patterns and features associated with COVID-19 in the CT scans. In summary, the study highlights the efficacy of the weakly supervised deep learning architecture in automatically detecting COVID-19-contaminated areas on chest CT scans. Furthermore, it demonstrates the model's capability to differentiate between COVID-19 patients and those with community-acquired pneumonia based on CT radiological features. The binary classification tasks exhibit superior performance compared to three-way classification, providing a more straightforward and reliable approach to distinguishing between different conditions.

Research conducted by Wang et al. (2020) introduced a system that uses CXR images for the detection of COVID-19. The study utilized a collaborative approach between humans and machines to develop COVID-Net, a network architecture specifically designed for identifying instances of COVID-19 from CXR images. The design process involved a combination of human-guided network design prototyping and machine-driven design exploration. Additionally, a benchmark dataset called COVIDx was created to facilitate the training and testing of COVID-Net. This paraphrased text provides a detailed explanation of the creation of the COVIDx dataset, the implementation and architectural design of COVID-Net, the effectiveness of the network architecture, and the use of explainability in auditing COVID-Net. The accuracy of the VGG-19 and COVID-Net deep learning technologies used was 83.0% and 93.3%, respectively.

Li et al. (2020) introduced a neural network called COVNet for the detection of COVID-19 by analyzing volumetric chest CT images and extracting visual characteristics specific to COVID-19 identification. To assess the model's robustness, the researchers also included cases of community-acquired pneumonia (CAP) and other anomalies in the CT scans. The study collected data from a span of four and a half years, from August 2016 to February 2020, encompassing 4352 chest CT images from 3322 patients across six hospitals. In terms of gender distribution, the male population slightly outnumbered females, with 1838 males and 1484 females (P =.29). The average age of the patients was reported as 49 years and 15 days, although the standard deviation was not specified. In order to evaluate the diagnostic performance of COVNet, various metrics were used, including the area under the receiver operating characteristic curve (AUC), sensitivity, and specificity. Remarkably, COVNet achieved

an impressive AUC of 0.96 (P <.001) for COVID-19 detection in the independent test set. The per-scan sensitivity was reported as 90% (95% confidence interval [CI]: 83%, 94%), with a total of 114 out of 127 scans correctly identified as COVID-19 cases. Additionally, the specificity was measured at 96% for COVID-19 detection. Regarding the identification of community-acquired pneumonia (CAP) in the same test set, COVNet demonstrated a per-scan sensitivity of 87% (152 out of 175 scans correctly identified) and a specificity of 92% (239 out of 259 scans correctly identified).

The AUC for CAP detection was reported as 0.95. These findings highlight the promising performance of COVNet in accurately detecting both COVID-19 and CAP cases in chest CT scans. The study outcomes provide valuable insights into the potential application of AI-based algorithms in the field of medical imaging for efficient and reliable disease identification.

The researchers, Minaee et al. (2020), have developed a method to identify COVID-19 in chest X-ray (CXR) images. In their study, they compiled a dataset consisting of 5000 CXR images sourced from publicly available databases. To ensure accurate identification of COVID-19, they sought the expertise of a board-certified radiologist, who reviewed the images and identified those displaying symptoms of the virus. For training their models, the researchers employed four widely recognized convolutional neural networks: ResNet18, SqueezeNet, and DenseNet-121. Through transfer learning, they fine-tuned these models using a subset of 2000 radiograms. Notably, SqueezeNet outperformed the other models, exhibiting a sensitivity of 98% and a specificity of 92.9% in detecting COVID-19 in the examined CXR images. In a separate study by Basu et al. (2020), a model for diagnosing COVID-19 was established using a gradient class activation map and domain extension transfer learning. In their investigation, the researchers employed pre-trained deep learning (DL) models such as AlexNet and ResNet. These models achieved accuracy rates of 82.98% and 85.78%, respectively, demonstrating their effectiveness in diagnosing COVID-19. The suggested model introduced by Basu et al. is capable of carrying out various types of classification, including distinguishing COVID-19 cases from normal, pneumonia, and other disease cases. This comprehensive approach aids in accurately identifying and categorizing a range of conditions based on CXR images.

In their study on COVID-19 detection, Khalifa et al. (2021) presented a new approach that explores the influence of neutrosophic sets on deep transfer learning models. The main objective of this research was to assess the effectiveness of

Restnet18, Googlenet, and Alexnet models, which have simpler structures, in the neutrosophic domain. Using different training and testing procedures with dataset splits of (90-10%, 80-20%, and 70-30%), a total of 36 experiments were conducted to evaluate the conversion to the neutrosophic domain.

The experiments encompassed testing the original domain as well as the true (T), indeterminacy (I), and false (F) domains. The performance of the deep transfer models was assessed across these domains using various training and testing methodologies. The results of the experiments revealed that the indeterminacy (I) neutrosophic domain achieved the highest testing accuracy of 87.1% and demonstrated good performance in terms of precision, recall, and F1 score. The findings of this study suggest that the use of neutrosophic sets in deep learning models holds promise for improving testing accuracy, especially when working with limited COVID-19 datasets.

Deep feature concatenation (DFC) has been employed in two different ways by Saad et al. (2022) to connect the deep characteristics of X-ray and CT images. The first method involves combining one-way DFC with a CNN. This approach aims to establish a link between the deep features extracted from X-ray and CT scans. In the second method, two pre-trained CNN models, namely ResNet and GoogleNet, are utilized to aggregate the retrieved attributes from X-ray or CT scans. To address the issue of significant time consumption, the researchers propose a three-tiered approach. With their initial strategy, they achieved an impressive accuracy of 96.13%, precision of 94.37%, recall of 97.04%, and an f_score of 95.69%. When applying their second approach with CT images, they achieved a correct classification rate of 98.9%, along with an accuracy of 93.6%, a recall of 98.5%, and an f_score of 98.29%. However, when utilizing X-ray images, their second approach yielded an accuracy of 99.3%, precision of 99.79%, and an f_score of 99.3%.

In their study, Serte et al. (2021) introduced a novel artificial intelligence (AI) technique aimed at classifying COVID-19 and standard CT volumes. This innovative approach utilizes the ResNet-50 deep learning model to predict the presence of COVID-19 in each CT image within a 3D CT scan. What sets this method apart is its integration of image-level predictions to specifically diagnose COVID-19 within the entire 3D CT volume. The results of their research demonstrate the impressive performance of the deep learning model, achieving an AUC value of 96% for the detection of COVID-19 on CT images. This highlights the model's ability to accurately identify cases of COVID-19 through the analysis of CT scans.

Another notable contribution in the field of COVID-19 diagnosis comes from Singh et al. (2021), who developed a deep transfer learning ensemble approach. Specifically, they employed the ResNet152V2 and densely connected CNNs (DCCNs) to create a powerful ensemble deep learning model for classifying COVID-19 in chest CT scan images. The suggested ensemble model incorporated not only the DCCNs and ResNet152V2 models but also the well-known VGG16 model. By combining the strengths of these three popular models, the ensemble approach successfully addresses the sensitivity problem associated with RT-PCR. To validate their ensemble model, Singh et al. utilized a large chest CT dataset and compared its performance against fifteen rival models. Based on their experimental findings, the suggested ensemble model outperforms the existing models in terms of accuracy, f-score, sensitivity, and specificity, with improvements of 1.2738%, 1.3274%, 1.283%, and 1.8382%, respectively. These advancements in AI and deep learning techniques for COVID-19 diagnosis offer a clearer understanding of the disease's presence through CT imaging. The integration of image-level predictions and the employment of an ensemble approach contribute to more accurate and reliable analysis, paving the way for improved diagnostic capabilities in the fight against COVID-19.

The researchers, Kedia et al. (2021), have developed a model called CovNet-19, which is an ensemble deep convolution neural network model. The purpose of this model is to aid radiologists and medical professionals in identifying individuals infected with COVID-19 by analyzing chest X-ray images.

The experimental results of this study clearly demonstrate the effectiveness of the suggested technique, achieving an impressive overall classification accuracy of 98.28% for the three-class classification (COVID-19, pneumonia, and normal). The average precision and recall for this classification were found to be 98.33% each. Furthermore, when it comes to the binary classification of non-COVID and COVID chest X-ray pictures, the model achieved an impressive total accuracy of 99.71%. In another study conducted by Ieracitano et al. (2022), a diagnostic method for accurately differentiating between COVID-19 pneumonia cases and non-COVID-19 interstitial pneumonia cases in portable CT scans was suggested.

This method utilizes a fuzzy augmented deep learning-based architecture called CovNNet, which is employed in a CAD (computer-aided diagnosis) system. The CAD system generates images by combining portable CXR (chest X-ray) and fuzzy images, allowing CovNNet to extract crucial and in-depth information from these images.

Overall, this CAD system achieved an encouraging accuracy rate of over 80% when tested on a local dataset. In summary, these studies showcase the effectiveness of CovNet-19 and CovNNet models in detecting and differentiating COVID-19 cases in chest X-ray images and portable CT scans, respectively. The high accuracy rates achieved by these models provide valuable insights for medical professionals in the fight against the COVID-19 pandemic.

### 2.3. Lung Diseases and COVID 19 Infection

#### 2.3.1. Obstructive lung disease

Lung diseases, which are also known as respiratory disorders, are medical conditions that impact the organs and tissues involved in breathing, leading to a disruption in the exchange of gases. These encompass a wide range of respiratory illnesses, ranging from minor and temporary ailments like the common cold, flu, and throat infection to severe and life-threatening diseases such as bacterial pneumonia, pulmonary embolism, tuberculosis, acute lung cancer, asthma, and severe respiratory disorders such as COVID-19. The classification of respiratory infections can be determined by various factors, including the symptoms' type and progression, the specific organ or tissue affected, or even the underlying cause of the disease (Patel et al., 2022). The aim of this information is to educate readers about lung diseases, also known as respiratory disorders. These conditions impact the organs and tissues involved in breathing, thereby disrupting the exchange of gases. They span a wide spectrum, ranging from common ailments like the cold, flu, and throat infections to more severe, life-threatening diseases such as bacterial pneumonia, pulmonary embolism, tuberculosis, acute lung cancer, asthma, and serious respiratory disorders like COVID-19. Respiratory infections can be classified based on factors like symptom type and progression, affected organs or tissues, and underlying causes (Patel et al., 2022).

Pulmonology, a specialized field of medicine, focuses on the study and treatment of respiratory diseases. Professionals in this field, like pulmonologists, chest medicine specialists, respirologists, or thoracic medicine specialists, specialize in diagnosing and managing respiratory ailments. Conditions such as asthma, chronic bronchitis, bronchiectasis, and chronic obstructive pulmonary disease (COPD) are classified as obstructive lung diseases, which can result in airway obstruction. Inflammation within the bronchial tree narrows the air passages, limiting the intake of air into the tiny air sacs called alveoli. To detect signs of obstructive lung diseases, medical practitioners

frequently rely on spirometry, a widely used pulmonary function test that assesses lung capacity and airflow. This test enables them to evaluate respiratory function and identify potential indications of obstructed airways.

To prevent various obstructive lung diseases, such as dust mite allergies and smoking-related conditions, managing symptoms with bronchodilators and, in severe cases, reducing inflammation with corticosteroids prove to be effective treatment options. Factors such as severe infections and cystic fibrosis commonly contribute to bronchiectasis, whereas smoking plays a significant role in COPD, comprising emphysema and chronic bronchitis. The exact cause of asthma remains uncertain.

### 2.3.2. Restrictive lung diseases

In infants experiencing respiratory distress syndrome, the expansion of the lungs is inadequate, and there is an increase in lung stiffness, which results in a loss of lung compliance. These conditions are referred to as restrictive lung disorders. Restrictive lung disorders can be categorized into two types: those caused by internal factors and those caused by external factors. Internal factors may lead to tissue loss due to chemical exposure or inflammation, resulting in restrictive lung diseases. On the other hand, external factors such as neuromuscular dysfunction and abnormal chest wall movements can contribute to restrictive lung diseases that originate outside of the lungs (Martinez-Pitre et al., 2020).

### 2.3.3. Chronic respiratory disease

Long-term lung structures, including the airways, are impacted by chronic respiratory diseases (CRCs). They can be identified by either a damaging infection cycle or a significant recruitment of inflammatory cells (neutrophils).

Acute breathing difficulties, asthma, and persistent obstructive pulmonary disease are among the most frequent. Despite the fact that there is no cure for CRDs, there are a number of therapies that can help expand the major airways and lessen shortness of breath, which can help manage symptoms and enhance quality of life. The most recent research indicates that initial pulmonary rehabilitation and maintenance therapy for persons with chronic respiratory diseases provided via telerehabilitation achieve outcomes comparable to center-based rehabilitation. Despite the fact that no safety concerns have been found, the conclusions are supported only by a small amount of research (Shukla et al., 2020).

### 2.3.4. Respiratory tract infections

The respiratory system is susceptible to infections, which can affect different components. These infections can be classified into two categories: upper respiratory tract infections and lower respiratory tract infections. The upper airway, which connects the glottis to the mouth and nose, encompasses these structures. The common cold is the most common upper respiratory tract illness, while other conditions such as sinusitis, tonsillitis, otitis media, pharyngitis, and laryngitis can also impact specific organs within the upper respiratory system (File, 2000).

With a fatality rate of 7% in adults and 1% in children, epiglottitis is characterized by a bacterial infection of the larynx leading to dangerous swelling of the epiglottis. Despite vaccinations, Haemophilus influenzae remains the primary agent responsible for this condition, although Streptococcus pyogenes can also provoke it. Clinical manifestations of epiglottitis include drooling, stridor, dysphagia, respiratory distress, and a husky voice.

Croup, a viral infection impacting the vocal cords, typically lasts for approximately five to six days. Key symptoms comprise a cough resembling a barking sound and a low-grade fever. Physicians often identify croup by observing the "steeple sign" on an X-ray, denoting tracheal narrowing. This condition predominantly affects children between 3 months and 5 years of age and is more prevalent in the winter months. Conversely, bacterial tracheitis is a serious bacterial-induced ailment.

Tonsillitis is an infectious disease, whether bacterial or viral in nature, that leads to the swelling of the tonsils. This inflammation can potentially cause blockage in the airway. Predominantly affecting the young population, peritonsillar abscess is the most common upper airway infection that can develop from tonsillitis. The enlargement of one of the tonsils may cause the uvula to be displaced towards the unaffected side. Typically, the diagnosis involves a thorough examination and symptom presentation. Common signs of tonsillitis include fever, sore throat, difficulty in swallowing, and a muffled voice known as a "hot potato" sound (Zoorob et al., 2012).

Pneumonia, a prevalent respiratory ailment impacting the lungs, is frequently instigated by bacterial agents, notably Streptococcus pneumoniae in Western nations. It stands as the most prevailing type of infection affecting the lower respiratory tract. Globally, tuberculosis (TB) serves as a significant etiology of pneumonia. Various pathogens, such as viruses and fungi, have the potential to induce pneumonia, which encompasses pneumocystis pneumonia, COVID-19, and severe acute respiratory

syndrome. Complications of pneumonia can include infection-triggered lung cavities, lung abscesses, or pneumonia extension into the pleural cavity.

The transmission of bacteria from periodontal disease to the respiratory system can lead to a lower respiratory tract infection; hence, inadequate oral hygiene may act as a predisposing element. Primary ciliary dyskinesia, an inherited disorder, disrupts the coordinated movement of cilia. This condition can result in chronic respiratory infections, persistent coughing, and nasal congestion, potentially leading to the development of bronchiectasis and subsequent life-threatening respiratory issues.

### 2.3.5. Pleural cavity diseases

Pleural effusion refers to a buildup of fluid in the pleural cavity. This could be the result of illnesses like congestive heart failure and cirrhosis, which cause fluid to move from the circulation into the pleural cavity. Additionally, it might be brought on by pleural inflammation, which can happen as a result of infections, pulmonary emboli, TB, mesothelioma, and other disorders (Kim et al., 2020).

A pneumothorax is a hole that develops in the pleura, the membrane that covers the lung, enabling lung air to leak into the pleural cavity. When the air in the pleural cavity cannot escape, the pneumothorax becomes larger and larger until it crushes the heart and blood vessels, creating a potentially fatal scenario. This condition is known as a tension pneumothorax.

### 2.3.6. Pulmonary vascular disease

The pulmonary circulation is impacted by pulmonary vascular disorders. Examples include (Brittain et al., 2022):

A condition known as a pulmonary embolism, which involves the development of a blood clot in a vein that then travels through the heart and lodges in the lungs, can have fatal consequences. In addition to blood clots, substances such as fat (often resulting from bone injuries), amniotic fluid (in cases of labor and delivery complications), and air (due to invasive medical procedures) can also travel through the bloodstream and reach the lungs, although these occurrences are less frequent.

• Pulmonary arterial hypertension, or high pulmonary artery pressure. Although COPD, in particular, can have an impact, it is most frequently idiopathic. Cor pulmonale, a disorder that puts strain on the right side of the heart, might result from this.

• Pulmonary edema is a medical condition characterized by the leakage of fluid from tiny blood vessels called capillaries in the lungs into the air sacs known as alveoli.

• Blood can enter the air sacs (alveoli) of the lungs due to conditions such as pulmonary hemorrhage, inflammation, and injury to the lung capillaries. Consequently, coughing up blood may occur. Examples of autoimmune disorders that can lead to pulmonary bleeding include granulomatosis with polyangiitis and Goodpasture's disease.

### 2.3.7. Neonatal diseases

About 1% of all newborns in the United States develop infant respiratory distress syndrome within the first six hours of life. Prematurity is the greatest risk factor, and in newborns weighing less than 750g, the probability of it happening increases to 71%. Other risk factors include fetal hypoxia, protracted rupture of the membranes (PROM), genetics, the infant of a diabetic mother (IDM), manner of delivery, maternal toxemia, chorioamnionitis, and male sex. Respiratory distress syndrome is believed to be a result of immature lung and vascular development, inadequate surfactant production, and other factors. The absence of surfactant causes the lungs to become atelectatic, which results in a mismatch between ventilation and perfusion, decreased compliance, and increased air resistance.

Hypoxia and respiratory acidosis are brought on by this, and they might result in pulmonary hypertension. On an x-ray, it seems to be ground glass. Tachypnea, nasal flare-up, paradoxical chest movement, grunting, and subcostal retractions are a few symptoms that might occur (Camacho-Gonzalez et al., 2013). After birth, bronchopulmonary dysplasia is a disorder that typically results from using oxygen and mechanical assistance. It is characterized by pulmonary vascular injury and inflammation, in addition to occurring virtually exclusively in premature newborns. A patient with BPD may continue to experience complications as an adult. They could grow up with hearing issues, pulmonary hypertension, and learning impairments. Asthma and exercise intolerance are more likely to develop in adults.

Infants who aspirate meconium at full term or after the term have meconium aspiration syndrome. Fetal hypoxia, premature birth, a diabetic mother, and high blood pressure in the mother are risk factors. Meconium stains in the amniotic fluid during delivery and stains on the skin, nails, and umbilical cord are used to make the diagnosis.

Aspiration can result in pneumonia, pulmonary edema, air embolism, and inactivated surfactant.

On an x-ray, it appears as patchy atelectasis and hyperinflation, with the possibility of a pneumothorax or pneumomediastinum. A disorderly transition to life outside the womb can result in the illness known as persistent pulmonary hypertension in newborns (PPHN). A right-to-left shunt of the blood through the foramen ovale or ductus arteriosus is caused by high pulmonary vascular resistance and vasoconstriction. PPHN has three basic causes: parenchymal illnesses, including diaphragmatic hernia and meconium aspiration syndrome; idiopathic; and hypoplastic vasculature. Most infants will ultimately recover from it. The FDA has only authorized inhaled nitric oxide for this condition (Gallacher et al., 2016).

The temporary tachypnea experienced by newborns is caused by the buildup of fluid in their lungs. This condition mainly occurs in infants delivered through a caesarean section before the onset of labor, as the absorption of amniotic fluid in the lungs has not yet begun. Other factors that increase the risk include being male, having a larger than average birth weight, multiple pregnancies, and having maternal asthma.

Usually, tachypnea and harder breathing are the first symptoms. Diffuse infiltrates, interlobar fissures, and occasionally pleural effusions can all be visible on an x-ray. Due to its resemblance to other conditions, it is a diagnosis of exclusion, and CPAP is commonly used to assist in pushing lung fluid into the pulmonary capillaries.

Air escaping from overextended alveoli and entering the lung interstitium causes pulmonary interstitial emphysema. Although it can manifest in adulthood, it is an uncommon condition that mostly affects preterm newborns. It frequently manifests as a gradual decline requiring more ventilatory assistance. The gold standard for diagnosis when it manifests as cystic or linear translucencies spreading to the margins of the lungs is a chest x-ray.

The swelling and mucus accumulation in the bronchioles are known as bronchiolitis. RSV, which spreads when a newborn comes in contact with an infected person's nasal or throat secretions, is typically to blame. After infecting the cells, the virus results in ciliary malfunction and death. The symptoms ultimately develop as a result of the debris, edema, and inflammation. It is the most typical justification for a child under a year old being admitted. From a little respiratory infection to respiratory failure, it can appear in many different ways. The only way to manage the condition is supportively, with fluids and oxygen, as there is no medicine to treat it.

### 2.3.8. Interstitial lung disease

A diverse set of approximately 200 illnesses with varying clinical presentations and prognoses is referred to as interstitial lung disease (ILD). In spite of the ongoing COVID-19 pandemic and its associated difficulties, significant progress has been made in this field over the past ten years. In 2021, research on ILD made significant strides in pathogenic mechanisms of disorder, new efficient therapeutic targets, and the discovery of notable biomarkers (Smith et al., 2023).

#### 2.3.8.1. Genesis of ILD

Idiopathic pulmonary fibrosis (IPF), a progressive lung disease characterized by the formation of scar tissue, currently has no cure. The survival rate for individuals with IPF is typically between three and five years. Among the various types of fibrotic interstitial lung diseases, IPF is the most commonly encountered.

To gain a better understanding of the condition, recent genome-wide association studies (GWAS) have consistently highlighted a particular genetic variation present in the MUC5B promoter region. This genetic variation leads to an augmented function, thus representing the primary genetic risk factor associated with IPF development. Through these studies, scientists have been able to shed light on the underlying mechanisms and contributing factors of this debilitating disease. Excessive levels of MUC5B protein have been observed in animal models of bleomycin-induced fibrosis and can also be detected in areas of pulmonary fibrosis in patients with idiopathic pulmonary fibrosis (IPF). The reason why MUC5B mutations are relatively common in the general population but IPF cases are rare remains unknown. In a study by Dobrinskikh et al., different strains of rats treated with bleomycin were observed, revealing a diverse range of phenotypes. These included strains with extensive fibrosis and high expression of Muc5b, strains with localized fibrosis and low expression, and variants where there was no association between Muc5b and fibrosis. Cluster analysis further suggested that factors, either independently or in combination with Muc5b, are likely to contribute to the development of fibrosis (Cottin et al., 2018).

After examining the genetic makeup of 99 young individuals and identifying 20 people with TRG gene variants, researchers conducted a comprehensive analysis of each participant's family. This investigation unveiled five family members who exhibited fibrosis, even though they did not possess the TRG mutation. Additionally, the researchers discovered that individuals carrying non-TRG genetic variations

exhibited shortened telomere lengths in their blood or lungs. This shortening was likely inherited from an ancestor who possessed the TRG mutation. Consequently, this suggests that although the TRG mutation may not be directly passed on, the associated risks can still be present. In order to enhance our understanding of the intricate molecular environment of IPF, Konigsberg et al. conducted a comprehensive study using a systems biology approach. They compared the lungs of individuals with IPF to those of healthy controls and analyzed various types of data, including DNA methylation patterns, coding and non-coding gene expression, and protein profiles. This analysis corroborated previously reported pathways that are known to be irregular in IPF while also identifying additional molecular characteristics. Our multiomic method revealed that 10 long non-coding RNAs and 18 regions of variable methylation are important for the function of matrix metalloproteinase 7 (MMP7) control, potentially opening up novel therapy options for this system (Constantino et al., 2023).

McErlean et al. also investigated epigenetic changes in IPF patients' alveolar macrophages. They observed a unique DNA methylation structure in alveolar macrophages, as opposed to circulating monocytes. They also observed differences in methylation between IPF and controls (n = 11) and areas (n = 49). The severity of the IPF illness was connected to the differentially methylated areas, which included genes that regulate lipid and glucose metabolism. It is also noteworthy that epigenetic diversity is not related to accelerated aging. According to Cui et al. (2021), increased lactate from myofibroblast sources in the fibrotic rat lungs was taken up by macrophages and induced histone lactylation, which in turn produced profibrotic gene up-regulation. This study also demonstrated how lactate is responsible for inducing epigenetic changes in macrophage activity.

#### 2.3.8.2. Fibroblast and epithelial cell structure

Certain microbial antigens have previously been shown to activate B cells, prompting them to release profibrotic metalloproteases and chemokines. Ali et al. discovered that profibrotic and inflammatory proteins are released by B cells in reaction to CpG or glucan, two microbial antigens, in a study of B cells from IPF patients. Microbial antigens increased the production of IL6, IL8, and MMP7 in B cells; as a consequence, fibroblasts were triggered with antigen-exposed B cell supernatant. They discovered that, as compared to controls, being exposed to activated B cells significantly increased fibroblast motility and activation. Moreover, they showed that

both nintedanib and pirfenidone affected the secretory behavior of B cells. Additionally, nintedanib exhibited the ability to decrease fibroblast migration and stimulation induced by A-cells, while pirfenidone did not, indicating distinct modes of action and divergent results (Berger et al., 2023). The differentiation of fibroblasts into myofibroblasts and their activation play a crucial role in the development of fibrosis. Research conducted by Vera et al. focused on the involvement of the Notch pathway in myofibroblast differentiation by studying the impact of Notch3 ablation on lung collagen-expressing cells in animal models. The mice with a knockout of Notch3 demonstrated a significant decrease in the number of myofibroblasts expressing smooth muscle actin (SMA) and a lower activation of profibrotic genes after bleomycin injury compared to the control group. fibroblast viability and differentiation.

These findings suggest that the Notch pathway plays a role in lung fibrogenesis and could be a promising target for future therapies. Investigating fibroblast deactivation further could lead to the discovery of new therapeutic approaches, considering that fibroblast activation is persistent in fibrotic diseases but temporary in other conditions like wound healing and the resolution of fibrosis in bleomycin-induced injury. Tan et al. conducted a study comparing the gene signature of fibroblasts from healthy mice with those collected at day 14 and day 30 after bleomycin treatment, which corresponds to the peak of extracellular matrix (ECM) deposition and early stages of fibrosis clearance.

Freshly isolated fibroblasts were subjected to RNA sequencing, revealing the identification of new potential genes and mechanisms that could serve as antifibrotic agents. Among these genes, Aldh2 and Nr3c1 experienced a decline on day 14, followed by a subsequent recovery on day 30. Subsequent experiments involving the upregulation of these genes in cultured fibroblasts demonstrated a reduction in profibrotic gene expression, decreased fibronectin deposition, and lessened collagen gel compaction, indicating their significant contributions to fibroblast deactivation.

#### 2.3.8.3. Therapeutic methods

Researchers have recently discovered a new pathway in fibrosis involving the interaction between fibrocytes and fibroblasts. This pathway is responsible for the increased production of pro-fibrotic miR-21-5p and collagen type 1 in fibrotic lung tissue. Additionally, the transcriptome characteristics of cellular senescence in alveolar type 2 cells, rather than cell loss, have been identified as key drivers of fibrosis in a p53-

dependent manner. Understanding these senescence-related processes could potentially lead to therapeutic interventions for early fibrosis treatment (Constantino et al., 2023).

### 2.3.9. COVID-19 in lungs

#### 2.3.9.1. Overview

The advent of COVID-19 in December 2019 triggered a significant global impact stemming from the SARS-CoV-2 virus, causing various clinical symptoms, including fever, respiratory issues, pneumonia, and the potential onset of acute respiratory distress syndrome (ARDS). The gravity of this illness necessitated a pandemic declaration.

Treating COVID-19 patients effectively required a substantial portion, approximately 31.7%, to receive intensive care unit (ICU) services. Within this cohort, 29% experienced ARDS, and 5% required extracorporeal membrane oxygenation for respiratory support. Sadly, the reported fatality rate stood at 15%. Notably, as of February 29, 2020, Wuhan, identified as the infection's epicenter, exhibited a comparatively lower fatality rate of less than 1.4% (Singhal et al., 2020).

Johns Hopkins University estimates the median fatality rate among COVID-19 patients in various countries to fall within the range of 1.5% to 2%. In the United States, COVID-19 has emerged as the foremost cause of death, particularly affecting the elderly population. The SARS-CoV-2 virus impacts the nasal passages and lungs, resulting in a spectrum of symptoms of differing intensities. While some individuals may remain asymptomatic, others may exhibit signs such as upper respiratory tract infections, loss of taste and smell, pneumonia, and, in severe cases, acute respiratory distress syndrome (ARDS).

Coronaviruses, utilizing angiotensin-converting enzyme 2 (ACE) receptors, infect the airways, particularly targeting type 2 alveolar and goblet cell types. COVID-19 patients often face decreased oxygen levels, especially if they have pre-existing lung conditions that exacerbate their comorbidities. Moreover, the inflammatory response triggered by the SARS-CoV-2 infection can induce lung impairment, leading to conditions like ARDS and pulmonary fibrosis. The virus may also possess mechanisms to evade the body's natural immune response. In addition to compromising the immune system and exacerbating pre-existing lung ailments such as cancer and chronic obstructive pulmonary disease (COPD), COVID-19 is linked to heightened mortality rates. Furthermore, COVID-19 can interfere with the identification and management of

lung disorders, which typically require invasive procedures and imaging methods, as well as chemotherapy or immunotherapy. Regrettably, comprehensive information on the risks and advantages of clinical diagnostic procedures and treatment options remains limited (Panahi et al., 2020).

#### 2.3.9.2. Pathophysiology of the Coronavirus

In the first phases of SARS-CoV-2 infection, the spike protein of the virus attaches itself to the ACE2 receptor found in a variety of lung cells, including epithelial, alveolar, and vascular cells. The S glycoprotein, a member of the TMPRSS2 family of membrane serine proteases, facilitates this interaction. Once within the host cells, the virus enters the cytoplasm and uses the machinery to replicate its RNA, which starts the replication process and spreads to other host cells. The immune system's antigen-presenting cells recognize the viral antigens, which triggers the production of cells that draw CD8+ cytotoxic T cells and natural killer (NK) cells. Both the innate and adaptive immune systems produce pro-inflammatory cytokines and chemokines in response to the infection (Hu et al., 2021).

Throughout history, the immune system has depended on key elements like monocytes, macrophages, and neutrophils to naturally combat viral infections. These immune cells are equipped with specialized receptors referred to as pattern recognition receptors (PRRs). PRRs play a pivotal role in identifying and detecting molecular patterns associated with pathogens, known as pathogen-associated molecular patterns (PAMPs). For viral infections, specific endosomal PRRs such as TLR3, TLR7, and TLR8 are responsible for recognizing extracellular PAMPs like viral RNA. Additionally, cytoplasmic RNA sensors known as RIG-I and MDA5 serve as additional PRRs. Certain transcription factors, including nuclear factor-kappa B (NF-B), RIG-1/MDA5, and interferon response factor 3 (IRF3), are stimulated by the activation of these PRRs. These transcription factors, which are also known as activation protein 1, are vital for producing pro-inflammatory cytokines and other critical elements of the immune response. Notably, type I interferon (T1IFN), a powerful antiviral cytokine, is produced in greater quantities when IRF3 is activated. On the other hand, innate pro-inflammatory cytokines like interleukin-1 (IL-1), interleukin-6 (IL-6), and tumor necrosis factor-alpha (TNF-) are produced in greater amounts when the NF-B pathway is activated. It is noteworthy that some viral infections, such as the Middle East Respiratory Syndrome coronavirus (MERS-CoV), the severe acute respiratory

syndrome coronavirus (SARS-CoV), and maybe the SARS-CoV, show importance in this regard. In addition to controlling blood pressure and fluid balance, the renin-angiotensin-aldosterone system (RAAS) has the ability to activate nuclear factor kappa B (NF-B).

An essential enzyme that transforms angiotensin II (Ang II) into angiotensin is called angiotensin-converting enzyme 2 (ACE2), which is inhibited by the SARS-CoV-2 virus in the early stages of infection (1–7). As a result, Ang II builds up and attaches to the surface of immune cells' angiotensin type 1 receptor (AT1R). The NF-B pathway is first activated by this binding. When Ang II and AT1R interact, the NF-B pathway is activated, which sets off a chain of events that include the manufacturing of several cytokines such as interleukin-6 (IL-6), tumor necrosis factor-alpha (TNF-), interleukin-1 (IL-1), and interleukin-18 (IL-18). Certain sensors, such as proteins known as NLRs (nucleotide-binding domain leucine-rich repeat family), are able to identify intracellular danger-associated molecular patterns (DAMPs) inside the cytosol. The ability of these NLR proteins to identify DAMPs inside cells is essential. NLR proteins are recognized and cause the molecular complexes known as inflammasomes to form, which are essential for immunological responses. Moreover, pro-caspase-1, an inactive precursor enzyme, is activated by inflammasomes to become active caspase-1, an essential element for immunological activation.

Among the many tasks performed by caspase-1 is the transformation of pro-IL-1, a precursor molecule, into IL-1, the active form. This body's immune response cascade is aided by activated IL-1. Adaptive immune cells identify and eliminate invaders by producing cytokines from CD4+ T lymphocytes, B cell antibodies, and CD8+ T lymphocytes that cause cytotoxicity when innate immunity is activated. It's possible that SARS-CoV-2 will strengthen CD4+ T cells and help them develop into Th1 cells. IL-6 and granulocyte macrophage colony-stimulating factor (GM-CSF) are then released by these Th1 cells. Then, CD14+ and CD16+ monocytes are carried by blood into the lungs, where they may differentiate into alveolar macrophages. Perforin is implicated in the cytolytic release of granulysin by CD8+ T cells as part of adaptive immunity. As a result, antigen-presenting cells and cytotoxic T cells go through apoptosis, which stops the over-activation of antigenic activity (Abebe et al., 2020). Bioactive lipid mediators called eicosanoids, which include prostaglandins and leukotrienes, are recognized for inducing inflammation. Eicosanoid storms and inflammasome activation may be caused by the SARS-CoV-2 virus. Levels of some

pro-resolving mediators (SPMs) drop during an eicosanoid storm. By preventing the synthesis of pro-inflammatory cytokines and encouraging the clearance of debris by macrophages, SPMs are essential in the reduction of inflammation.

Additionally, they lessen the inflammatory response to influenza. In a similar vein, arachidonic acid is the source of epoxyeicosatrienoic acids (EETs), which have anti-inflammatory qualities. EETs may increase the synthesis of mediators that function in pathways that reduce inflammation. Boosting macrophage phagocytosis, lowering pro-inflammatory cytokine levels, minimizing excessive white blood cell buildup, and reducing the presence of inflammatory cells in organs are all potential benefits of SPM or EET treatment. The generation of antibodies against SARS-CoV-2 and adaptive immune responses may be aided by these anti-inflammatory actions. Notably, EETs are metabolites produced by soluble epoxide hydrolase (sEH). Research has shown that eicosanoid storms may be suppressed by SPMs and sEH inhibitors via the inhibition of NF-B transcriptional regulator expression.

Individuals who were found to be positive for COVID-19 and have been diagnosed have higher quantities of macrophages and monocytes in their system. Additionally, cytokines produced from endothelial, macrophage, and epithelial cells are released from the lungs of infected patients. A variety of cytokines, such as interferon-gamma-inducible protein 10 (IFN-), granulocyte colony-stimulating factor (GCSF), monocyte chemoattractant protein 1, and macrophage inflammatory protein 1-alpha, are also elevated in these infected people. When COVID-19 pneumonia patients have significant lung damage, these cytokines are intimately linked to that condition. For example, elevated IL-6 is associated with a poor outcome in COVID-19 patients, but the anti-inflammatory cytokine IL-10 helps to lower neutrophil and monocyte activity. Nonetheless, even in the presence of IL-10, monocytes' persistent suppression of the human leukocyte antigen-DR isotype (HLA-DR) may be a factor in increased death rates. A cytokine storm—a prodigious influx of various immune cells, including neutrophils, T cells, and macrophages—from the circulation into the lungs causes severe lung damage. As a result, endothelial cells, vascular barriers, capillaries, and alveoli are harmed by these immune cells. Additionally, severe COVID-19 instances cause T lymphocytes to produce more naïve helper T cells while producing fewer memory helper T cells (Wiersinga et al., 2020). In severe COVID-19 instances, the numbers of NK cells and CD4+ and CD8+ T lymphocyte subtypes drop, leading to lymphocytopenia. Patients have large amounts of HLA-DR and CD38 expression on

their lymphocytes, even with decreased lymphocyte counts and severe COVID-19 lymphocytopenia.

#### 2.3.9.3. COVID-19 with different cases

COVID-19 in smokers: Considering the clinical features of individuals diagnosed with COVID-19 pneumonia, comorbidities such as COPD are recognized as significant risk factors. A preliminary meta-analysis conducted by Lippi et al. in 2020 suggested that the link between smoking and severe COVID-19 is not conclusively established. However, this study was limited to five research populations. Conversely, Alqahtani et al. explored both COPD and smoking habits as variables related to the risk of COVID-19. Another study conducted by Leung and colleagues investigated ACE2 expression levels across various participant groups, including Cornell (n = 211) and the British Columbia Cancer Agency (n = 238) (Leung et al., 2020). The findings indicated that current smokers exhibit significantly higher ACE2 expression compared to control subjects. Similarly, a group of researchers at Ghent University Hospital in Belgium noted that mRNA expression of ACE2 is higher in current tobacco users, based on studies involving lung tissue biobanks. However, further analysis showed that increased ACE2 mRNA expression is not associated with COPD or smoking status when considering other variables. This observation remained consistent when assessing type II alveolar cells and alveolar material using immunohistochemical staining for ACE2 and measuring protein concentrations.

A plausible theory posits that the impact of nicotine on the renin-angiotensin system might result in modifications to the ACE2 receptor expression profile or an upregulation of ACE2 receptor expression as a consequence of nicotine exposure. It is important to remember that people with asthma have lower levels of ACE2 expression than those with chronic obstructive pulmonary disease (COPD), which has important ramifications for COVID-19. It's also interesting to note that SARS-CoV-2 is more severe in transgenic mouse models that overexpress human ACE2, but animals missing ACE2 cannot get the virus. This discrepancy may be related to the interaction function of the spike protein (S protein). SARS-CoV-2 has a greater hydrogen bond occupancy (>90%) in the receptor-binding region of the S protein at the ACE2 interface, in contrast to SARS-CoV, despite their structural similarities. This suggests that, in comparison to SARS-CoV, SARS-CoV-2 has a higher propensity for binding to ACE2.

The SARS-CoV-2 virus suppresses the expression of ACE2. ACE2 inhibits the expression of Ang II by functioning as a negative regulator of the renin-angiotensin system. Since ACE2 is essential for vasodilation, low ACE2 levels are linked to pneumonia and acute respiratory distress syndrome (ARDS).

COVID-19 with lung cancer: Cancer comorbidity is associated with a worse outcome and is considered a risk factor for COVID-19, especially in China. A registry study conducted by the Thoracic Cancers International COVID-19 Collaboration found a correlation between high death rates and low ICU admission rates in cases of lung cancer. Significant death rates have been seen in COVID-19-positive lung cancer patients, as well as an increase in ARDS and hospitalizations. Smoking and COPD history are risk factors for lung cancer patients because they are associated with more severe instances of COVID-19 (Abebe et al., 2020).

Immunotherapy-induced alterations in the immune system have the potential to worsen coronavirus infection. On the other hand, COVID-19 pneumonia could resemble the pulmonary adverse effects of anti-cancer medication. Immunotherapy such as nivolumab may exacerbate systemic inflammation mediated by T cells and elicit an unanticipated immune response against the influenza virus. Additionally, people with lung cancer may become more vulnerable to COVID-19 as a result of anti-cancer therapy. A possible side effect of bevacizumab is an increased risk of thrombosis. Gemcitabine, cisplatin, and taxanes may increase the risk of immunosuppression and myelosuppression. Gemcitabine, anti-PD-1 drugs, and treatments aimed at the epidermal growth factor receptor increase the risk of interstitial pneumonitis. Radiation treatment also has the potential to worsen lung interstitial fibrosis. Patients with MET exon 14 skipping mutation-diagnosed non-small-cell lung cancer are usually administered the c-Met kinase inhibitor crizotinib. SARS-CoV-2 infection and crizotinib-induced interstitial lung disease (ILD) might, however, co-occur. Ground-glass opacity and consolidation are seen in imaging comparable to COVID-19 PCR ILD and lung cancer instances in real-world circumstances.

Furthermore, antineoplastic therapies may make lung cancer patients more susceptible to COVID-19. For instance, bevacizumab may make thrombosis more likely. Gemcitabine, cisplatin, and taxanes may increase the risk of immunosuppression and myelosuppression.

Gemcitabine, anti-PD-1 medicines, and treatments that target the epidermal growth factor receptor increase the risk of interstitial pneumonitis. Radiation treatment

makes interstitial fibrosis in the lungs worse. In patients with non-small-cell lung cancer who have the MET exon 14 skipping mutation, crizotinib, a c-Met kinase inhibitor, may cause interstitial lung disease (ILD) as well as SARS-CoV-2 infection.

Because lung adenocarcinoma, drug-induced ILD, and COVID-19 have many symptoms, including consolidation and ground-glass opacity, it may be difficult to distinguish between them in real-world situations. During the COVID-19 epidemic, the European Society for Medical Oncology (ESMO) has created recommendations for the care and management of patients with lung cancer. Lung cancer patients are categorized into three priority categories by ESMO in partnership with Cancer Care Ontario, Huntsman Cancer Institute, and the Magnitude of Clinical Benefit Scale: high, medium, and low. Patients in serious conditions or in need of urgent care are given high priority. Patients with stable conditions are considered medium-priority if postponing therapy for more than 6 to 8 weeks might have a detrimental effect on the overall result. The possible benefit to the patient determines the intermediate priority. Low priority enables services to be delayed in the event of the COVID-19 pandemic or in cases where there are no appreciable benefits from the intervention. In order to reduce any possible negative consequences of care during the COVID-19 pandemic, lung cancer identification, staging, and treatment should be prioritized. It is advised that people who have lung cancer in addition to the COVID-19 infection stop their treatment. Furthermore, COVID-19-related fatalities are more likely to occur in lung cancer patients who have poor lung function and cardiopulmonary comorbidities (Wiersinga et al., 2020). For patients with lung cancer who are also afflicted by the coronavirus, chemotherapy-immunotherapy is a frequently used treatment. A mix of medications, including carboplatin, pemetrexed, and pembrolizumab, is used in this therapy. This strategy also makes use of tocilizumab, a humanized recombinant monoclonal antibody that targets the IL-6 receptor.

In one particular case report, a 65-year-old man who had previously smoked and was diagnosed with stage IV lung adenocarcinoma with bilateral lung metastases was highlighted by Bonomi et al. in 2020. At ASST Cremona in the Lombardia area of Italy, the patient got two doses of tocilizumab, an anti-IL-6 receptor treatment.

It is encouraging to note that the patient's need for oxygen assistance significantly decreased after tocilizumab delivery. His condition then became better, and he had no trouble continuing his chemotherapy therapy after that. This course of treatment is in line with the European Society for Medical Oncology's (ESMO)

guidance, which states that after COVID-19 has stabilized, chemotherapy should resume. According to the guidelines, individuals with lung cancer who are receiving chemotherapy should not be treated for COVID-19, nor should they get tocilizumab and chemotherapy at the same time. Therefore, it is imperative that patients with lung cancer who get a COVID-19 diagnosis during this pandemic have their treatment plans closely monitored.

Lung cancer diagnosis delays brought on by the COVID-19 pandemic provide another difficulty. According to research from the UK Lung Cancer Coalition, there may be a correlation between the rising demand for respiratory healthcare services and the possible overlap of COVID-19 symptoms in the number of people receiving a late-stage lung cancer diagnosis.

COVID-19 and lung transplantations: Patients who have received lung transplants and are using immunosuppressive medications might display either asymptomatic or moderate symptoms upon infection with SARS-CoV-2. However, COVID-19 pneumonia can lead to varying clinical outcomes in lung transplant recipients, highlighting the necessity for further research. The treatment for lung transplant patients with COVID-19 might involve a combination of immunosuppressive and antiviral medications.

Lung transplant patients who contracted COVID-19 have been prescribed lopinavir or ritonavir after the transplant procedure. This medication is often used alongside tacrolimus, a drug that impedes T cell proliferation. A study conducted by Saez-Gimenez et al. in 2020 discovered a significant interaction between tacrolimus and lopinavir/ritonavir. The study revealed that lopinavir and ritonavir slowed down the metabolism of tacrolimus, intensifying its effects. Regrettably, 39% of the total patients did not survive, while 84% required either oxygen treatment or ventilator assistance (Hu et al. 2021).

Moreover, investigations of lung tissue from lung transplant patients and post-mortem results from individuals who succumbed to COVID-19 revealed severe end-stage pulmonary fibrosis. It was noted that for a patient experiencing COVID-19-induced end-stage pulmonary fibrosis, lung transplantation was essential for survival. Cypel et al. (2020) outlined ten factors to consider before lung transplantation for COVID-19-associated acute respiratory distress syndrome (ARDS) (Cypel, 2020).

COVID-19 and medical imaging: When probable pneumonia is suspected, chest X-rays are useful and time-saving, especially in portable radiography. However, there

are worries about possible contamination. Comparing chest radiographs to CT and ultrasound imaging, however, revealed a limited association between the radiographic findings and the clinical condition of COVID-19. Considering that COVID-19 pneumonia is characterized by peripheral lung involvement, lung ultrasonography is used to assess the severity of both ARDS and pneumonia. Initially, COVID-19 in the lungs was evaluated using lung ultrasonography by Vetrugno et al. (2020), who assigned a severity score ranging from 0 to 36. The need for CT and chest radiography may be minimized since different kinds of lines in the ultrasound pictures showed different degrees of pneumonia severity (moderate, severe, and critical).

In around 10% of pneumonia patients, CT imaging revealed bilateral patchy buildup or ground-glass opacities, which may resemble a crazy-paving pattern. Rapid identification of COVID-19 pneumonia is facilitated by the absence of pleural effusion and the possibility of consolidation in conjunction with an air-bronchogram. Ground-glass opacities, a growing crazy-paving pattern, consolidation, and resolution without the crazy-paving pattern were the separate phases of the illness's development shown on CT scans. Typically, the peak of lung involvement was seen ten days after the beginning of symptoms. Each chest CT scan is given a score by the COVID-19 Reporting and Data System, which helps in the diagnosis of COVID-19 pneumonia. Still, CT's specificity is not high enough to differentiate COVID-19 in lung cancer patients.

COVID pathology: Pathological reports, often constructed based on autopsy findings or radiological presentations, reveal various changes within the lung tissue due to SARS-CoV-2 infection. Examination of the lung parenchyma during autopsies revealed reduced alveolar flexibility along with patchy peripheral hemorrhage. Fibrous cords containing exudate were observed in the bronchus, trachea, and pulmonary alveoli. The lung tissue exhibited signs of diffuse alveolar injury characterized by interstitial and alveolar inflammation. Hematoxylin-eosin staining and immunohistochemistry confirmed findings of acute respiratory distress syndrome (ARDS) showing edematous alveolar septa, congested blood vessels, and the presence of immune cells like macrophages, lymphocytes, and monocytes. Additionally, there were indications of hyperplasia of type II alveolar epithelial cells and their shedding in specific regions, along with evidence of focal bleeding, fluid accumulation in alveolar cavities, and loose fibrosis in the pulmonary interstitium. The presence of organizing

pneumonia was identified by the observation of organized fibrin and loose fibrous plugs within the alveoli. 2

Using electron microscopy, coronavirus particles were identified in type II alveolar epithelia and bronchial mucosal epithelia. Immunohistochemical staining for SARS-CoV-2 antigen was positive in desquamated cells, macrophages, and alveolar epithelial cells. Real-time PCR results for SARS-CoV-2 were also potentially positive.

SARS-CoV-2 infection through the ACE2 receptor might affect endothelial cells, leading to a tendency for thrombosis. Elevated inflammatory mediators and immunoglobulins may contribute to increased blood viscosity, while the detection of anti-cardiolipin antibodies suggests an immune complex-mediated vasculitis. These changes could result in localized bleeding, thickened blood vessel walls, and the accumulation of monocytes and lymphocytes in and around blood vessels, potentially increasing the risk of deep vein thrombosis and pulmonary thromboembolism in COVID-19 patients.

### 2.4. Deep Learning in Lung COVID Diagnosis

Lung diseases have an impact on the respiratory system, including the airways and other structures related to the lungs. They are also known as respiratory disorders. According to the statistics provided by the International Respiratory Society Forum, approximately 334 million individuals worldwide suffer from asthma. Additionally, TB claims the lives of 1.4 million people annually, while 1.6 million individuals succumb to lung cancer. Moreover, pneumonia causes the loss of millions more lives. The numbers clearly indicate that lung diseases are a leading global cause of both mortality and disability. Early detection is vital, as it improves long-term survival rates and increases the chances of achieving a cure.

Clinical examinations, biological testing (skin, sputum, blood, or pathology), respiratory function tests, chest x-ray examinations, and computed tomography (CT) have historically been used to investigate respiratory illness (Huffman et al., 2022). The recent emergence of new technical advancements in artificial intelligence (AI) has demonstrated great promise when applied to medical images, including lung diseases, particularly in terms of its ability to synthesize multiple pertinent pieces of information. clinical or paraclinical examinations for the purpose of detection, quantification, classification, and long-term survival prediction.

Despite its fast development, artificial intelligence is still a relatively new topic. The technique has not been thoroughly evaluated in many prospective clinical studies. Software validation for medical devices often falls under the responsibility of commercial companies due to the complex administrative procedures required to obtain regulatory approval. However, these companies typically prioritize products with clear commercial potential. Consequently, researchers who focus on technical innovation without an immediate clinical application may not be as inclined to engage in software validation. This aspect may be of lesser importance to researchers in the field of basic sciences (Hohr et al., 2020). Physiological and pathophysiological information serve as the cornerstone of algorithms used to manage patients' health issues because it is the essence of medicine. In this scenario, stronger cooperation between academia and business, as well as between technology researchers and physicians, may be required.

Medically speaking, the applications of AI, which are predicted to take off in the next few years, should be guided by a fundamental understanding of physiology and prioritize the needs of the patient over the deployment of any software or algorithms. For these reasons, we decided to base our physiological argument, prior to using AI in scientific research, on the morphological and functional alterations seen in respiratory disorders.

Generally, deep learning (DL) and convolutional neural networks (CNN), specifically, have been popular techniques for identifying and categorizing COVID-19. In general, CNN is quite good at classifying people who are at risk of contracting illnesses. From binary classification to multiclass classification, CNN systems are employed in a variety of classification applications. With multilayer capabilities and high-dimensional datasets, CNN has already produced amazing findings for locating complex structures. CNN employs 2D convolutional layers for 2D image processing. An input layer, an output layer, and hidden layers make up a CNN (Figure 2.4). Convolution, pooling, fully linked, and regression layers are some of the hidden layers (Shazia et al. (2021).

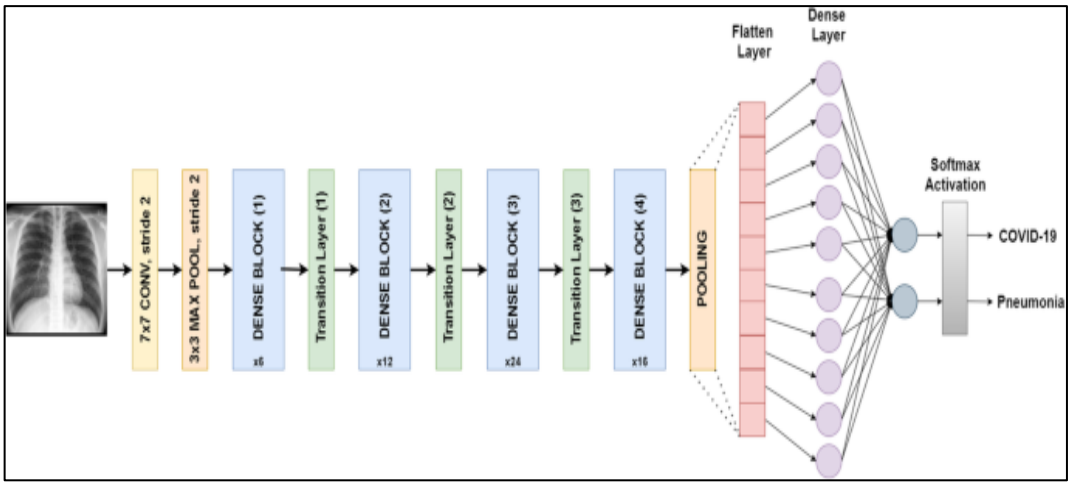


**Figure 2.4.** CNN model for x-rays lung images classification (Shazia et al., 2021).

In this thesis, we examine Alexnet, a deep learning model that is useful for picture categorization. The described model has a number of defined layers, and each layer obtains the data it requires from all preceding layers. Our model is assessed using data from the COVID-19 radiography dataset. Our carefully thought-out methodology divides the dataset into three categories and yields reliable findings.

### 2.4.1. Lung disease pathology and phenotype

CT has great power thanks to the rapid advancement of medical imaging technologies in both hardware and software. Computed tomography has been used over the past 20 years to characterize the anatomy of the lungs in great detail and to describe respiratory disorders.

Volumetric collection has made it possible to do more complex analyses of CT data using computer methods, such as quantitative computer tomography (or QCT) (Newell et al., 2013). As a result, the visuals basically transformed into digital data, which is particularly well suited for examination using computers. Computers would be able to notice details that the human eye cannot, and they would be able to ignore minute differences in the photos they analyzed, helping with diagnosis, spotting early indications of sickness, and even forecasting its path. Numerous QCT parameters have been created and evaluated against clinical, functional, and prognostic biomarkers after the analysis of hundreds of thousands of CT images.

Chest X-rays employ a minimal amount of ionizing radiation to capture internal chest images. These images are utilized to evaluate the condition of the heart, lungs, and chest wall, aiding in the identification of injuries, fever, chest discomfort, shortness of breath, and chronic coughing. Additionally, chest X-rays can play a crucial role in the

diagnosis and treatment of various lung disorders, such as pneumonia, COVID-19, emphysema, and cancer. Due to their efficiency and simplicity, chest X-rays are highly valuable when it comes to emergency diagnosis and treatment (Guarnera et al., 2022). An autosomal recessive condition called primary ciliary dyskinesia (PCD) causes problems with ciliary structure and function, impairing mucociliary clearance and leading to chronic otosinopulmonary illness. Since the symptoms are ambiguous, late diagnosis is frequent, and therapy is typically started at an advanced stage of the disease, its frequency in the Caucasian population is about 1/15,000. The prognosis is mostly connected to respiratory failure brought on by secretions obstructing the airways and subsequent infections that progressively bring on bronchiectasis. As of now, patients should have their respiratory and otolaryngology (ENT) systems checked every six to twelve months. Despite the fact that there has been a lot of study on PCD, the published imaging series are frequently tiny, and current care is mostly based on professional consensus inferred from CF data.

Despite the similarities between these two conditions, current research has shown that PCD and cystic fibrosis differ significantly in terms of pathogenesis, clinical characteristics, pulmonary function results, and imaging, particularly CT imaging. In contrast to cystic fibrosis, which mostly affects the upper lobes, PCD lung abnormalities are primarily found in the middle and lower lobes (Damseh et al., 2017).

Since determining functional and structural alterations is crucial for managing PCD, several researchers have looked into the relationship between the two using a variety of approaches, such as case-control studies or long-term follow-up, with mixed findings. These examinations have in common that the evaluation of CT severity is still mostly descriptive or semi-quantitative. The Brody computed tomography score, which was initially created to evaluate airway involvement in cystic fibrosis, is the most widely used semi-quantitative method. This score has various restrictions that make it difficult to utilize. First, it necessitates intensive training, costs money, and, most importantly, depends on a subjective evaluation of scanner irregularities. Recent research on chest computed tomography in primary ciliary dyskinesia evaluated the ratios between neighboring artery size and airway diameter. Their findings, which indicated that children with PCD had more dilated airways than controls and did not exhibit bronchial wall thickening, were unexpected. However, according to preliminary CT results of PCD disease, the main abnormalities include atelectasis, bronchiectasis, thickening of the bronchial walls, the presence of mucoid impactions, consolidation of

the lungs, and bronchiectasis. These abnormalities are all likely to change the image density parameters by altering the density of the lung tissue. using studies on larger populations and quantitative research techniques, investigated.

It has been suggested to use the Glanville-originalized term Chronic Lung Allograft Dysfunction (CLAD) to characterize the clinical signs and symptoms of a variety of disease processes in the airways. as well as lung allograft parenchymal compartments that develop more than 3 months after the transplant procedure, which cause a severe and long-lasting decline in lung function. Due to chronic rejection, CPGD is the most common long-term complication among lung transplant patients (LTx), who have a 60% death rate after 5 years. Physiological and imaging studies that can identify early airway damage are required since subclinical alloreactivity can substantially impair allograft integrity (Verleden et al., 2014).

The authors' recommended opacities are likely to result in limiting physiology and are parenchymal opacities and/or pleural thickening consistent with a diagnosis of pulmonary and/or pleural fibrosis. Air entrapment may be distinguished from other types of mosaic attenuation, such as vascular occlusive and infiltrative lung illnesses, using exhalatory computed tomography. Large airway abnormalities, such as moderate columnar bronchiectasis and thickening of the bronchial wall, are frequently seen. Along with a budding tree, other signs of bronchiolar impaction and/or thickening of the bronchial wall include small centrilobular nodules. Depending on the disease's stage when it is identified, RAS has different imaging characteristics. Opacification and ground-glass consolidation are frequently observed in the early stages of acute exacerbations. Once these lesions have healed, fibrosis typically follows, leading to traction and reticulation bronchiectasis. In later stages, individuals have confluent peripheral consolidation zones that are advancing and signify pleuro-parenchymal fibrosis. It is common to see a distinct separation between normal and pathological lung parenchyma. Loss of volume causing hilar retraction, traction bronchiectasis, and bronchiolectasis are examples of secondary characteristics (Chua et al., 2019).

Pneumonia is a condition when the lungs' air sacs fill with fluid, causing inflammation in the lungs as a result. This leads to additional problems, including chills, weariness, and fever, as well as breathing difficulties, coughing, and chest discomfort. Other symptoms that some people may have include appetite loss and nausea, which is followed by vomiting. Typically, physicians will recommend painkillers as well as cough and fever medications. Only in dire circumstances could the patients need to go

to the hospital and be placed on a ventilator. COVID-19 and the flu and pneumonia seasons are converging. All three are risky respiratory conditions, particularly for vulnerable groups, including those with asthma and chronic obstructive pulmonary disease (COPD) (Galani et al., 2021). In cases of chest discomfort or difficulty breathing, seek emergency assistance right away. Otherwise, you should schedule a visit with your primary care physician if you think you may have pneumonia or COVID-19, depending on the severity of your symptoms. They can assess your risk and recommend a course of therapy to hasten your recovery with the least chance of life-threatening consequences.

The coronavirus disease, also known as COVID-19, is an infectious illness caused by the recently identified SARS-CoV-2 virus. It primarily affects the respiratory system, leading to a range of symptoms that can vary in severity. Certain populations, particularly older adults and those with underlying medical conditions like cancer, diabetes, heart disease, and respiratory issues, are at a higher risk of experiencing severe complications or even death as a result of contracting the virus.

### 2.4.2. AI and DL in medicine

Recent advances in perception (the interpretation of sensory information) made possible by artificial intelligence enhance medical diagnosis systems to more accurately represent and comprehend complicated facts. This has resulted in significant advancements in applications like image processing, disease detection and diagnosis, prediction, and treatment—tasks that, up until a few years ago, could only be completed by humans. The neural network topology used in deep learning, a subclass of machine learning, is roughly modeled on that of the human brain. Because they learn discriminative properties from input, such frameworks are capable of modeling exceedingly intricate nonlinear interactions. In task-specific applications, recent DL algorithms can match or even surpass humans, in contrast to most initial AI techniques, which created applications with human-like performance (Sunarti et al., 2021).

This is due to recent developments in AI research, the vast quantities of digital data that are now accessible to train algorithms, and the most up-to-date, most potent computer gear. Researchers anticipate that, in the decades to come, AI will automate a variety of jobs, including translating languages, creating best-selling novels, and conducting surgery, continuing the trend towards human-level general AI (Figure 2.5).

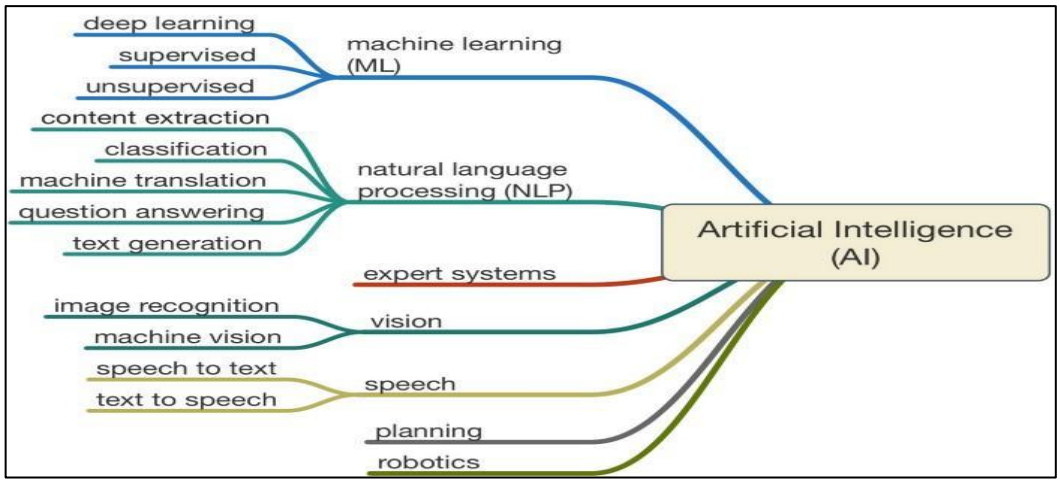


**Figure 2.5.** Artificial intelligence branches (Yeasmin et al., 2019).

Artificial intelligence is becoming more and more significant in a variety of healthcare applications, including risk management, wearable technologies, virtual assistants, medication creation, remote patient monitoring, medical imaging, and diagnostics. It is anticipated that the use of AI would also help industries dealing with massive data processing, such as RNA and DNA sequencing. Because they work with a lot of imaging data, medical fields including radiology, pathology, dermatology, and ophthalmology have already started to benefit from using AI approaches. In radiography, skilled medical practitioners visually assess radiographic pictures to identify, characterize, and monitor diseases. This evaluation has historically been based on their expertise and experience, which may sometimes be interpreted differently. In contrast to qualitative thinking, artificial intelligence (AI) provides a more quantitative approach.

Artificial intelligence (AI) is very adept at automatically generating quantitative evaluations and identifying complex patterns in imaging data. Through the incorporation of AI into the clinical workflow, healthcare personnel may use it as a helpful tool to perform radiological examinations that are more accurate and consistent. Due to the fact that imaging data is gathered during routine clinical procedures, it is essential for large datasets to be easily accessible to enable extensive academic and medical research. Radiographic images and patient outcome data have played a pivotal role in the emergence and rapid growth of radiomics as a medical field.

Initially, radiomics research concentrated on extracting various pre-designed characteristics that define the shape, intensity, and texture of radiographic images. DL techniques have recently been employed in radiomics research to automatically create depictions of features from sample images, offering insight into the clinical significance

of numerous of these radiological traits. In principle, it is convenient to access extensive amounts of information, as imaging data is routinely collected during clinical practice. This vast dataset serves as a valuable resource for both academic and medical research. Radiological images and medical outcomes have played a significant role in the development and rapid growth of radiomics as a research field. Initially, radiomics research primarily involved examining images to identify various pre-defined features that describe the shape, intensity, and texture of the radiographic data. DL techniques have recently been employed in radiomics research to automatically create representations of features from sample images, revealing the clinical significance of several of these radiographic traits. The primary driver behind the advancement of AI in medical imaging is the pursuit of improved effectiveness and efficiency in clinical treatment. As the volume of radiological imaging data surpasses the availability of skilled professionals, healthcare providers are facing the challenge of increasing productivity to compensate for diminishing imaging reimbursements. The demands on radiologists have significantly risen due to these factors. Research indicates that in order to meet these demands, an average radiologist may have to analyze an image every 3–4 seconds over the course of an 8-hour workday. In the field of radiology, errors are inevitable as they involve both visual perception and making uncertain decisions, particularly in such constrained situations.

By incorporating an AI component into the imaging workflow, qualified radiologists can benefit from pre-screened images and recognized characteristics. This integration not only enhances productivity but also reduces errors and meets targets with minimal manual intervention. Consequently, substantial efforts and regulations are being implemented to drive advancements in AI technology, specifically in the field of medical imaging. The analysis and assessment of radiographic properties play a crucial role in various image-based radiology tasks, such as disease identification, categorization, and monitoring. The concept of utilizing logic and statistical pattern recognition to address medical issues has been in existence since the early 1960s.

As the use of computers increased in the 1980s, radiography changed from being a perceptually subjective art to a quantitatively calculable area thanks to the AI-powered automation of numerous clinical activities. Similar to other application fields, radiology is undergoing an AI revolution at a rate that is proportionate to the exponential development of data and computing capacity.

There are two categories of AI techniques that are now popular. The first makes use of hand-engineered qualities that may be quantified using computer programs because they are expressed in terms of mathematical equations (for example, tumor texture). Modern machine learning models that are taught to categorize patients in ways that might aid clinical decision-making employ these variables as inputs. Even though these characteristics are thought to be discriminative, their expert definition means that they may not always reflect the best feature quantification strategy for the given discriminating problem. Additionally, due to the differences in imaging modalities, including CT, positron emission tomography (PET), and magnetic resonance imaging (MRI), as well as their corresponding signal-to-noise characteristics, preset features are sometimes unable to adjust. Deep learning, the second technique, has drawn a lot of interest recently. Without the help of human specialists, deep learning computers can autonomously learn feature representations from data. This data-driven method is more informative and generalizable since it allows for more abstract feature descriptions. Thus, deep learning can automatically measure the phenotypic traits of human tissues, promising significant advancements in clinical diagnosis and treatment.

Deep learning also eliminates the requirement for human preprocessing processes. For instance, precise segmentation of sick tissues by experts is frequently required in order to retrieve predetermined characteristics. Deep learning is data-driven; thus, when given enough example data, it may autonomously detect sick tissues without the help of a specialist. Deep learning, which can learn complicated data representations, is frequently resilient against undesirable variance, such as inter-reader variability, and may thus be used to model a wide range of clinical characteristics and situations. In many respects, deep learning can be comparable to what skilled radiologists do, which is to discover picture characteristics and then assess their significance in light of other aspects to make a clinical conclusion. Numerous studies have contrasted deep learning techniques with their preset feature-based equivalents in light of the expanding number of applications of deep learning in medical imaging and have found significant performance advantages with deep learning. Deep learning methods have also been demonstrated in studies to perform as well as radiologists in detection and segmentation tasks in ultrasonography and MRI, respectively. Deep learning outperformed radiologists in terms of sensitivities but lagged behind them in terms of specificities for the categorization of lymph node metastases in PET-CT. A greater understanding of the trade-off between sensitivity and specificity is anticipated

when these technologies are continually improved and tuned for particular applications. Deep learning may also speed up development times because it doesn't require domain knowledge because it just uses curated data and the information that goes with it. On the other hand, conventional preset feature systems have recently displayed performance plateauing and, as a result, seldom satisfy the strict criteria for clinical usefulness. Only a handful have been translated into the clinic as a result. It is anticipated that in the near future, high-performance deep learning techniques will transcend the bar for clinical value and may quickly be applied in clinical settings. In the field of radiology, skilled professionals rely on their perceptual abilities to spot potential anomalies during the manual detection process. They then use their cognitive skills to confirm or reject the findings.

To thoroughly examine stacks of images, radiologists frequently adjust viewing angles, window widths, and level settings. By drawing on their training, experience, and knowledge of normal radiographic patterns, radiologists are trained to identify abnormalities through changes in imaging intensities or unexpected patterns. These assessments, along with others, form a subjective evaluation framework that aids in detecting various issues, from identifying breast tumors to detecting colon polyps and lung nodules. Computer-aided detection techniques, which involve automated recognition and processing of predetermined characteristics, have been proposed for quite a while but have not been widely utilized in clinical settings despite our growing reliance on computers. Using computer vision algorithms, these techniques emphasize conspicuous elements in radiographic images based on criteria defined by radiologists in a pattern-recognition challenge.

These algorithms do not, however, generalize across illnesses and imaging modalities and are frequently task-specific. With continued attempts to decrease false positives, the accuracy of conventional preset feature-based CAD systems nonetheless remains debatable. It is sometimes necessary for radiologists to evaluate results before deciding if a particular automated annotation needs additional examination, which adds to the workload.

Fully convolutional networks, or networks made entirely of convolutional layers, are recently suggested deep learning architectures for segmentation that provide segmentation probability maps for the complete picture. Other architectural designs, like the U-net, were created especially for medical pictures. A single advanced AI model has demonstrated its ability to perform various segmentation tasks in different

types of medical imaging, including brain MRI, breast MRI, and cardiac CT angiography (CTA). Remarkably, this model can accomplish these tasks without requiring specific training for each individual task. Others propose deep learning techniques for segmenting brain MRI data that totally do away with the necessity for image registration, an atlas-based technique's prerequisite preprocessing step.

Additionally, several radiographic parameters are used in the ensuing tasks of diagnosis. These are essential for determining, for example, if a lung nodule is solid or if it comprises ground-glass opacity (GGO) nodules, which are nodules that are not solid. Due to the lack of concomitant radiographic markers of malignancy or invasiveness, GGO nodules are frequently difficult to identify and necessitate particular therapeutic strategies. The size, maximal diameter, sphericity, internal texture, and margin definition of a tumor can all be determined by its radiographic properties. These frequently arbitrary qualities serve as the foundation for diagnosis and allow items to be categorized into classifications denoting benign or malignant conditions. Computer-aided diagnosis (CADx) systems relate to several techniques for automating diagnostics. They frequently use predetermined, designed discriminative characteristics, just like CADe. As with screening mammography, several technologies are already in clinical use. Their apparent effectiveness has prompted the creation of comparable systems for other imaging modalities, including ultrasonography and MRI, and they often serve as a second opinion to supplement a radiologist's judgment.

Traditional CADx systems, for instance, have been proven to enhance the performance of relatively novice radiologists and decrease variability among them when used with ultrasound pictures to identify cervical cancer in lymph nodes. Other application areas include prostate cancer in multiparametric MRI, where automated segmentation for candidate detection is performed after a malignancy probability map is first created for the whole prostate. Traditional preset feature-based CADx systems' accuracy depends on a number of variables, including how well prior object segmentations performed. Errors frequently get worse as they spread through the several image-based jobs in the clinical oncology process. We also discover that several conventional CADx techniques do not generalize to other objects. For instance, despite the fact that tracking growth rates over time is thought to be an important aspect of determining risk, pulmonary nodule CADx systems built around this criterion frequently fail to correctly identify rare nodules like cavity and GGO nodules. Additional descriptors, which are not discriminative when applied to the more typical

solid nodules, are needed for the proper identification and diagnosis of such nodules. This ultimately results in a variety of solutions with limited generalizability that are designed for particular situations.

Deep learning-based CADx is able to automatically learn from patient populations and create a basic grasp of variances in anatomy without the need for explicit predefinition of these discriminative traits. This enables it to capture a representation of both frequent and exceptional situations.

### 2.4.3. Deep learning in lung disease

A novel Hybrid Deep Learning Algorithm (HDLA) architecture was introduced by Farhan and Yang (2023) for automated lung disease classification from chest X-ray images. The method involves pre-processing chest X-ray images in addition to automated feature extraction and identification. To improve the quality of raw chest X-ray images, a combination of efficient filtering and no-data-loss pre-processing is intended. The pre-trained model is recommended to be used with the robust CNN for autonomous lung feature extraction. They used the 2D CNN model to extract the greatest characteristics in the shortest amount of time and space.

The proposed 2D CNN model uses a very efficient 1D feature estimate from the pre-processed input image to provide dependable feature learning. They had high scale variability, so they used min-max scaling to enhance the recovered 1D characteristics. They classified the CNN properties using a number of machine learning classifiers, such as AdaBoost, Support Vector Machine (SVM), Random Forest (RF), Backpropagation Neural Network (BNN), and Deep Neural Network (DNN). The experimental results show that the proposed model reduces computational complexity by 16.91% and beats state-of-the-art methods in terms of overall accuracy by 3.1%.

Li et al. (2020) divided the data into three categories using DL models such as CheXNet, InceptionV3, and squeezeNet. A 97.94% accuracy rate was achieved by a model constructed using 423 COVID-19 images, 1,485 viral pneumonia photos, and 1,575 normal shots. Li et al. (2020b) suggested CovXNet as a network architecture for the detection of bacterial pneumonia and COVID-19. There are 1,583 photographs of healthy people in the collection, 1,493 images of viral pneumonia, 2980 samples of pneumonia, and 305 images of COVID-19 scans from a variety of patients. 89.1% of their predictions came true.

COVID-Net was created by Gunraj et al. to help physicians differentiate between pneumonia associated with COVID-19 and pneumonia unrelated to COVID-19. Researchers showed a fresh set of 13,975 CXR scans from 13,870 subjects and found that their approach was 93.3 percent accurate. On the other hand, the validity of the 3-class categorization was simply examined in relation to the article. A deep 3D multiple-case learning technique based on attention was used by Han et al. (2020) to distinguish COVID-19 from other cases. In the examination of 230 CT scans, data from 79 individuals, 100 pneumonia cases, and 130 healthy individuals were included. They found that the overall accuracy of their approach was 97.9%. An incrementally trimmed DL ensemble was used by Rajaraman et al. (2020) to identify COVID-19 in chest X-ray pictures. In doing so, they used two models.

Using the transfer learning approach, the first model was trained to discriminate between normal and abnormal chest X-rays, and the second model was taught to use the learning weights from the first model to distinguish between COVID-19 and pneumonia cases. They were able to increase the model's overall prediction performance by using an ensemble technique, and they were able to achieve an accuracy of 99.01%. Customized models were developed by Hammoudi et al. (2021) to detect COVID-19 aspiratory side effects at every stage of the medication's production. They used conventional chest X-ray images, viruses, bacteria, and data from two types of pneumonia to train the models. The main track COVID-19 classification network, or FCONet, is a 2D DL architecture that was created by Ko et al. (2020) to assess a chest CT scan for COVID-19 pneumonia. The transfer mechanism for learning in the FCONet model is based on state-of-the-art deep learning models. With values of 99.8%, 100%, and 99.87%, respectively, the ResNet50 FCONet model demonstrated the best results for accuracy, true positive rate, and true negative rate on the validation dataset. An approach for COVID-19 pneumonia identification using CXR images was described in a paper (Dorr et al., 2020). A model for forecasting COVID-19 anomalies was shown in Dorr et al. (2020) using deep learning and laboratory data. Six hundred patients' worth of laboratory findings were made available for the model's testing.

An optimization technique was applied to diagnose COVID-19 using a hybrid CNN (Ezzat et al., 2021). Using the Xception architecture, researchers developed CorNet, a photo-based DCNN, to detect COVID-19 infections (Khan et al., 2020). Deep learning was utilized in this method to diagnose COVID-19 (Nayak et al., 2021). There were many CNN models applied. Deep learning was used to identify COVID-19 on

CXR (Oluwasanmi et al., 2021). There were three stages. Prior to a diagnosis being established, the condition was originally determined to be pneumonia, then COVID-19 and pneumonia. They achieved a 97 percent accuracy rate using 6523 CXR images. By using a patch-based CNN, the authors (Oh et al., 2020) demonstrated that they could correctly detect COVID-19 in CXR pictures. The authors of Panwar et al. (2020) presented a method that makes use of CNNs, feed-forward neural networks, and COVID-19 CXR image descriptors to diagnose diseases from COVID-19 images. CXR and CT imaging were used in this study to identify illnesses linked to COVID-19 (Alshayeji et al., 2022).

### 2.4.4. DL models

#### 2.4.4.1. Asight on DL networks

A research trend in the development of artificial intelligence and machine learning is deep learning. It simulates the learning process of the human brain using deep neural networks and employs unsupervised feature extraction to handle massive amounts of data (music, text, photos, etc.).

In the realm of neuroscience, the human brain consists of a vast network of interconnected neurons, each serving as a mini-information processor. These neurons form a complete deep neural network, with their connections dictating the flow of information. This intricate network structure has paved the way for the development of end-to-end image processing techniques. Deep learning, a phenomenon characterized by the multiplication of hidden layers within a network, has become the focal point of research and innovation. Layer-by-layer initialization and batching techniques are crucial in overcoming the formidable task of training deep networks.

The main applications of DL in computer vision are pattern recognition, handwritten number identification, data dimensionality reduction, and handwritten number reduction. Image recognition, image restoration, picture segmentation, object tracking, and scene analysis are some examples of methods with extraordinarily high efficacy.

#### 2.4.4.2. Convolutional neural networks

The convolutional neural network, which combines deep learning with image processing, is a widely recognized model in the field of deep learning technology. It has made significant strides in image analysis and processing, establishing itself as one of

the most prominent neural networks. Numerous achievements have been accomplished using convolutional neural networks on ImageNet, a standard image annotation dataset commonly employed in academic research. These accomplishments include tasks such as image feature extraction, classification, pattern recognition, and more. By utilizing spatial relative connections and weight sharing between different regions of the previous layer network, the convolutional neural network employs supervised learning to improve training performance while reducing the number of parameters required. From the time the convolutional neural network was first proposed until its widespread use now, it has basically gone through the stages of theoretical development, experimental growth, widespread application, and in-depth study. An important notion in the early stages of theory is the idea that human visual information is processed by receptive fields and neurocognitive machinery. Hubel et al. demonstrated in 1962, using biological studies, that multilayer receptive field excitation is the mechanism by which visual information from the retina is transmitted to the brain (Figure 2.6).

The idea of a receptive field was initially put forth in this manner. Fukushima suggested a neurocognitive device based on the idea of receptive fields in 1980. It is recognized as the first convolutional neural network implementation network. LeNet5 started the experimental development stage in 1998, when Lécun et al. presented it utilizing a gradient-based backpropagation technique for supervised network training. Convolutional neural networks first came to the attention of academics when the LeNet5 network was proposed and successfully used for handwriting recognition.

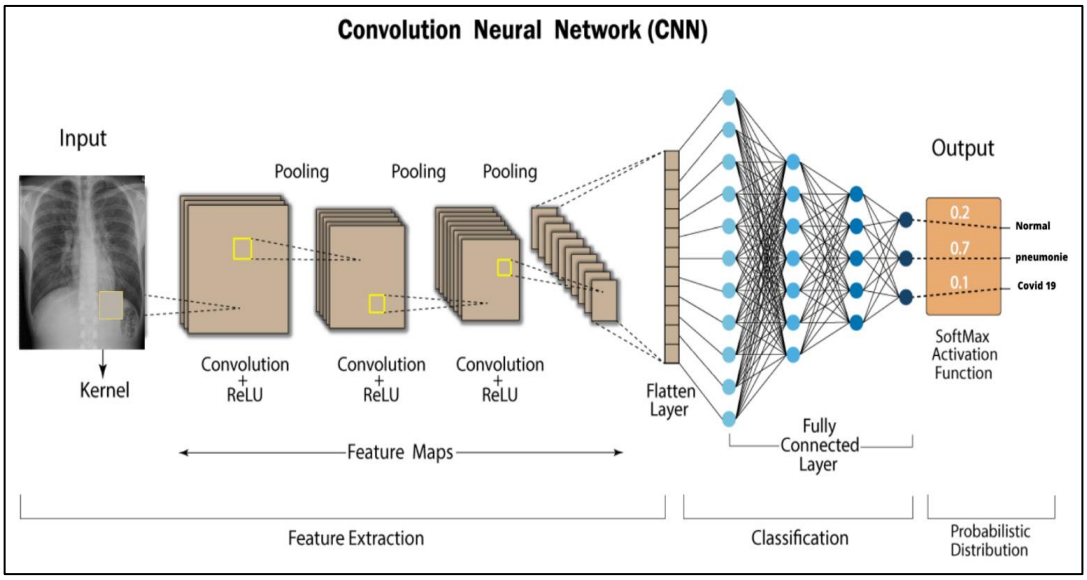


**Figure 2.6.** Convolutional neural network in image classification (Rguibi et al., 2022).

After the LeNet5 network, the convolutional neural network has been in the development stage. Convolutional neural networks did not have a specific role in deep learning applications until the 2012 introduction of the AlexNet network. Convolutional neural networks have emerged as the primary study topic in computer vision, and this research is still ongoing. Krizhevsky et al.'s AlexNet was the most effective in classifying images from the ImageNet training set.

In a 2D-CNN model, an input layer, an output layer, and a number of hidden layers make up CNN. Convolution, pooling, and activation are only a few of the various operations carried out by each layer in the hidden layer. The number of neurons in the input layer, which is coupled to the input image, equals one pixel of the input picture. The middle convolutional layer uses a convolution operation to extract features from the input data and create a feature map. The convolution operation's outcome is determined by how the parameters of the convolution kernel are specified. The feature maps are filtered and chosen by the pooling layer, which is located after the convolutional layer. This reduces the computational cost of the overall network. All of the neurons in the layer above are linked completely through this layer. The classifier receives the output value and returns a classification result. The 2D CNN is a general-purpose convolutional neural network.

ResNet, VGG (Visual Geometry Group), and other 2D convolution kernels are examples of the convolution kernel. A 2D image serves as the input image. Assume the input image is H x W in size and contains three RGB channels. The convolution kernel of size (c, h, w), where c, h, and w stand for the convolution kernel's channel count, height, and width, respectively, slides on the input image's spatial dimension. The image value and the value of (h, w) are entered on each channel with the intention of executing a convolution operation and getting a value.

#### 2.4.4.3. 3D-CNN

The majority of medical imaging, including CT and MRI, is often 3D. Despite being a 2D picture, the CT image we often view is only a portion of the whole. Therefore, a 3D convolution kernel must be used if you wish to segment any sick tissues. The 3D U-Net segmentation network is an example of a network that utilizes a 3D convolution kernel. It transforms the 2D convolution kernel of the U-Net network into a 3D convolution kernel, specifically designed for 3D medical image segmentation. By employing a 3D CNN, it enables the extraction of a more powerful volume

representation along the X, Y, and Z axes. Incorporating three-dimensional information in segmentation fully utilizes the advantages of spatial information. The 3D convolution kernel has one additional 2D slice compared to the 2D convolution kernel in medical images. To represent a 3D image, the convolution kernel uses the dimensions C, N, H, and W, where C represents the channels, N represents the slice layers, H represents the height, and W represents the width. Similar to the 2D convolution process, a value is obtained by sliding the window over the height, width, and layer dimensions for each channel (see Figure 2.7).

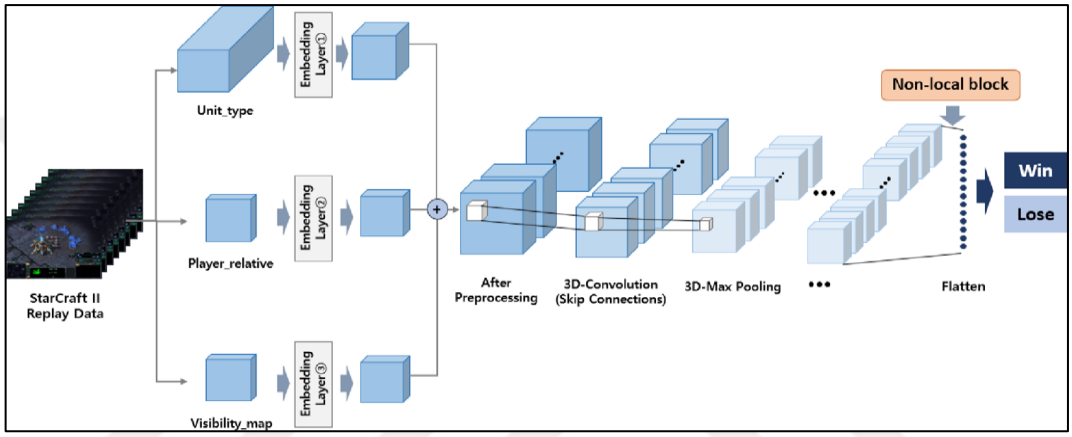


**Figure 2.7.** 3D CNN in image classification (Baek et al., 2022).

### 2.4.5. Segmentation using DL models

In conventional CNN construction, the segmentation network is also modified. The final two fully connected layers of the classification network were converted to convolutional layers for the first segmentation network. The encoder-decoder structure and deep structures like VGG and ResNet form the backbone of the network used to segment medical images. Early models of networks include LeNet and AlexNet. The two network architectures are associated with shallow networks and are comparably comparable. Compared to the LeNet network, AlexNet has a lot more parameters. Its suggestion to follow the convolutional layer with a pooling layer is still widely used today. Deepening the number of network layers is one way that VGG outperforms AlexNet. It replaced the bigger convolution kernel in AlexNet with a series of three convolution kernels. The depth of the network and the impact of feature extraction are advanced under the constraint of maintaining the same receptive field.

VGG has a clean, straightforward structure. The maximum pooling size and convolution kernel size are the same across the board, demonstrating that performance

may be enhanced by progressively deepening the network structure. By adding more network layers, all of the networks previously discussed improve the results of training.

However, issues like overfitting and disappearing gradients may result from this. In order to address these issues, GoogleNet enhanced it from a different angle by segmenting the evacuation network structure into modules. The inception structure is suggested to boost the network's depth and width while decreasing the network's parameters. Convolution kernels of various sizes are used in Inception, along with pooling. The convolution and pooling results are then combined into a series. The overall depth of the network is composed of 22 levels. It starts with AlexNet's seven layers, followed by VGG's 19 layers, and finally extends to GoogleNet's 22 layers. As the depth increases beyond a certain threshold, the addition of more layers does not enhance the classification performance; instead, it hinders the network's convergence. He et al. introduced a pioneering network structure called ResNet, consisting of 152 layers, to effectively train deeper networks. ResNet tackles this issue by utilizing shortcuts, which are composed of residual blocks. Each module includes a shortcut and multiple subsequent layers.

The shortcut connects the module's input and output before applying the ReLU activation function. By combining the outputs with ReLU activation, this block's output is generated. Squeeze-and-excitation blocks, along with other structural elements, enhance the network model's expressive design capabilities from the perspective of the new network model, focusing on channel connections. The encoder-decoder architecture is a combination of a CNN-based encoder and a decoder, which forms the basis for semantic segmentation networks. It shares similarities with the encoder used in segmentation tasks, where CNNs are commonly employed for classification purposes. The encoder extracts picture features from the input image, creating a low-resolution feature map through encoding. The decoder then takes the encoder's low-resolution discriminative feature map and transfers it to the high-resolution pixel space to achieve category labeling for each pixel. An example of an encoder-decoder structure is SegNet, which has both the encoder and the decoder having the same channel count and spatial dimension and corresponding to each other one-to-one. The constant development of the encoder and decoder structure and the enhancement of its effectiveness are primarily responsible for the creation of the semantic segmentation network. For the complete segmentation network's output, the decoder's impact and complexity are very significant.

Recent advancements in the field of deep learning have opened up new possibilities for identifying COVID-19 in a cost-effective and efficient manner, without the need for direct contact with medical professionals. These methods utilize chest X-ray, CT, and ultrasound images to automatically detect the presence of the virus. However, further research is needed to address certain challenges and limitations. Specifically, there is a requirement for extensive training and evaluation of deep learning models on large datasets of CXR and CT images, with input from radiologists, in order to achieve more accurate results. Additionally, there should be efforts made to develop a real-time program that can effectively identify COVID-19 using various imaging techniques. To improve the performance of deep learning algorithms, it is important to extract clinical information from images that show different signs of illness rather than relying solely on the posterior-anterior (PA) view of X-rays. Furthermore, future research should focus on differentiating COVID-19 cases from other viral diseases like SARS and MERS, as well as different forms of pneumonia.

## 3. MATERIAL AND METHOD

### 3.1. Material

#### 3.1.1. Introduction

The section outlines the proposed methodology for categorizing COVID and healthy CT images of lungs through the utilization of gamma correction, the CNN network, and the XGBoost classifier. The suggested approach encompasses the following steps (Refer to Figure 3.1):

(1) Importing the images into the dataset-defined category (labels: COVID, normal).

(2) Segmenting samples into 80% for training and validation purposes, and 20% for testing.

(3) Processing and classifying CT lung images involves the subsequent actions:

a) Loading CT images

b) Implementing gamma correction (GC) on images

c) Constructing and training CNN Net

d) Deriving new features via CNN

e) Categorizing new deep features using XGBoost

(4) Assessing the classification efficacy by utilizing testing samples and examining the distinction between classifying images employing CNN as a classifier versus a feature extraction tool.

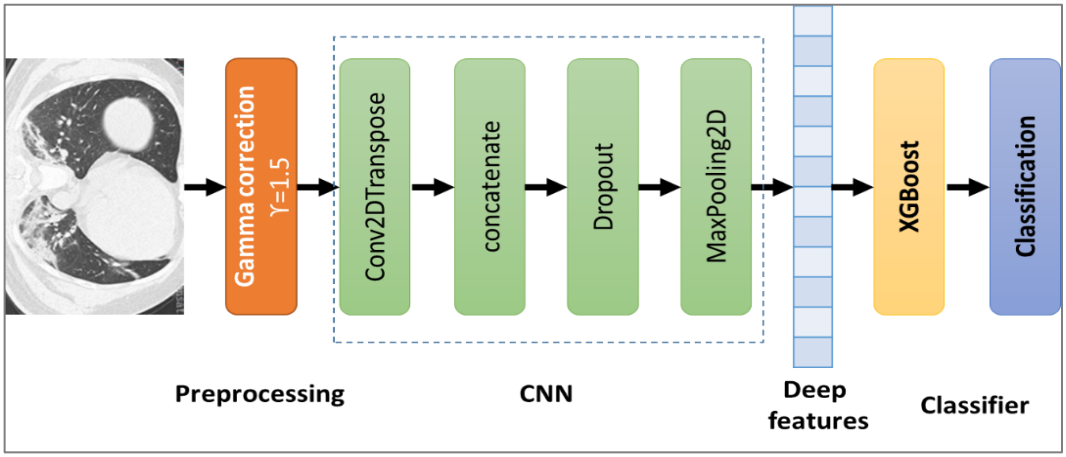


**Figure 3.1.** The proposed and implemented methodology for classifying COVID CT images.

```
# Step 1: Loading the images dataset based on category
        images_dataset = load_dataset("path/to/dataset")
# Step 2: Splitting samples into training, validation, and testing sets
        training_validation_split_ratio = [0.8, 0.2], [0.7, 0.3], [0.6, 0.4]
        for split_ratio in training_validation_split_ratio:
        training_set, validation_set = split_dataset(images_dataset, split_ratio[0])
        testing_set = get_testing_set(images_dataset, validation_set)
# Step 3: Processing and classifying CT lung images
        ct_images = preprocess_images(training_set)
    # Step 3.1: Applying gamma correction (GC) on images
        ct_images_gc = apply_gamma_correction(ct_images)
    # Step 3.2: Building and training CNN net
        cnn_model = build_cnn_model()
        trained_cnn_model = train_cnn_model(cnn_model, ct_images_gc, labels)
    # Step 3.3: Extracting new features using CNN
        extracted_features = extract_features(trained_cnn_model, ct_images)
    # Step 3.4: Classifying new deep features using XGBoost
        xgboost_model = train_xgboost_model(extracted_features, labels)
# Step 4: Evaluation
        testing_images = preprocess_images(testing_set)
        testing_images_gc = apply_gamma_correction(testing_images)
        cnn_predictions = cnn_model.predict(testing_images_gc)
        xgboost_predictions = xgboost_model.predict(extracted_features)
    # Step 4.1: Evaluate CNN classification performance
        cnn_accuracy = calculate_accuracy(cnn_predictions, testing_set.labels)
    # Step 4.2: Evaluate XGBoost classification performance
        xgboost_accuracy = calculate_accuracy(xgboost_predictions, testing_set.labels)
        print(f"Performance comparison for {split_ratio[0]*100}% training, {split_ratio[1]*100}% testing:")
        print(f"CNN Accuracy: {cnn_accuracy}")
        print(f"XGBoost Accuracy: {xgboost_accuracy}")
```

**Figure 3.2.** Pseudocode of methodology

### 3.1.2. Datasets

**Dataset #1:** The COVID-19 CT dataset employed in this study is a valuable resource, providing a comprehensive collection of medical imaging data for the investigation of the respiratory effects of the virus. The dataset, meticulously curated by Yang et al. in 2020 and accessible through the link (https://doi.org/10.48550/arXiv.2003.13865), comprises a total of 349 CT scans. These scans offer a detailed portrayal of the clinical findings associated with COVID-19, specifically highlighting ground-glass-patterned regions indicative of the infection. Remarkably, these scans originate from 216 individuals, contributing to the diversity and depth of the dataset. In addition to the COVID-19 positive instances, the dataset encompasses 397 CT images representing COVID-19 negative cases. This inclusion of negative instances is vital for establishing a comprehensive and well-balanced dataset that facilitates the robust training and evaluation of machine learning models. By incorporating both positive and negative instances, the dataset provides a holistic view of the variations in imaging patterns associated with COVID-19, enabling the

development of more accurate and reliable diagnostic models. To offer a visual insight into the dataset, Figure 3.2 has been included in the study. This figure serves as a representative display, showcasing select COVID-19 positive and negative CT images. The visual representation not only enhances the comprehensibility of the dataset but also aids in conveying the distinct features and characteristics associated with COVID-19, such as the ground glass-patterned regions. In summary, the COVID-19 CT dataset utilized in this study is a robust compilation of medical images that captures the nuances of the virus's impact on respiratory health. With a focus on ground glass-patterned regions, the dataset encompasses a diverse range of CT scans from both positive and negative instances, fostering a thorough understanding of the imaging patterns associated with COVID-19. Figure 3.2 serves as a visual aid, providing a glimpse into the rich and informative content of the dataset, which is instrumental in advancing research and diagnostics in the context of the ongoing global health crisis.

**Dataset #2**: For comparison, we used datasets that studies by Amin et al. (2021) (https://www.kaggle.com/datasets/paultimothymooney/chest-xray-pneumonia, https://github.com/ieee8023/covid-chestxray-dataset ), Panwar et al. (2020) (https://arxiv.org/abs/2003.11597), Demir et al. (2021) (https://www.kaggle.com/bachrr/covid-chest-xray), and Sheykhivand et al. (2021) (https://www.kaggle.com/paultimothymooney/chest-xray-pneumonia, https://www.kaggle.com/andrewmvd/convid19-x-rays, https://www.pyimagesearch.com/2020/03/16/detecting-covid-19-in-x-ray-images-with-keras-tensorflow-and-deep-learning), particularly focusing on pneumonia, normal, and COVID-19 cases. Amin et al. used a dataset consisting of 194 images from the original pneumonia dataset and 163 images from the COVID-19 dataset. Their DL model achieved a remarkable 98% accuracy, with precision, recall, and F1 scores all equaling 0.97. Panwar et al. utilized the VGG model for feature extraction on a dataset comprising 142 COVID-19 images and 5863 Kaggle CXR healthy images, resulting in an accuracy of up to 99%. Demir et al. implemented a DL model with 20 convolutional layers on a dataset of 1061 chest X-ray (CX) images, achieving 100% accuracy in 80% of tests. Lastly, Sheykhivand et al. achieved a 92.43% accuracy on a diverse dataset containing healthy, COVID-19, bacterial, and viral images, demonstrating a high accuracy of 90% for all scenarios except one. These studies collectively showcase the effectiveness of DL models in accurately classifying COVID-19 and related conditions, with varying dataset sizes, compositions, and class distributions. The reported high

accuracy rates highlight the potential of DL models in contributing significantly to medical image analysis and diagnosis across different datasets and scenarios.

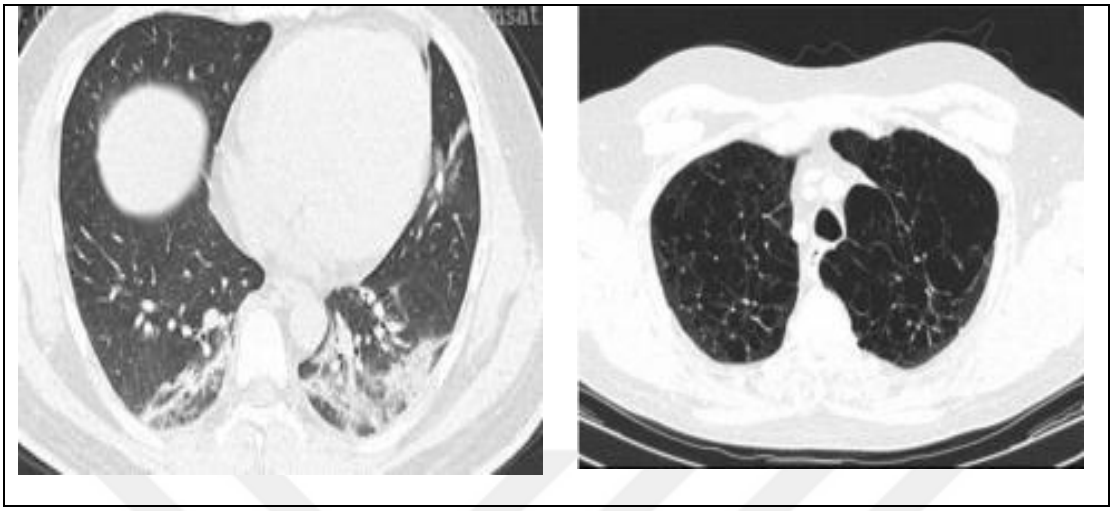

**Figure 3.3.** Positive (left) and negative COVID CT images from the proposed dataset.

**Table 3.1.** Training and testing samples based on labels.

| Dataset/classes | Normal | COVID-19 |
|---|---|---|
| Training and validating set (# images) (80%) | 317 | 279 |
| Test set (# images) (20%) | 80 | 70 |
| Total | 397 | 349 |

### 3.2. Method

#### 3.2.1. Gamma Corrections

Gamma correction is a pivotal process in image processing, aiming to adjust the brightness of an image to ensure accurate color representation on-screen. Despite the seemingly uniform brightness of an image, the intensity of light emitted from each pixel on the screen can vary, mimicking the natural variations in light. The essence of gamma correction lies in harmonizing the visual output on the screen with the actual colors captured by the camera, thereby enhancing the fidelity of the displayed image.

In the realm of medical imaging, such as CT scans, where precision is paramount, gamma correction plays a crucial role. CT scans, when displayed, might exhibit discrepancies in color intensity or brightness, particularly in regions of interest as illustrated in Figure 3.3. Gamma correction intervenes in such instances, rectifying these discrepancies to ensure that the colors are accurately represented. The mechanism of gamma correction involves raising the input value to the power of the inverse of gamma. This mathematical operation recalibrates the color intensities, aligning them with the intended representation. The formula for gamma correction is a fundamental

aspect of this process, acting as a mathematical guideline to achieve the desired adjustment. In essence, gamma correction is a vital tool in image processing, ensuring that the visual representation of an image on the screen faithfully mirrors the original colors captured by the camera. Its application is particularly significant in medical imaging, where precise interpretation of visual data, as exemplified in CT scans, holds paramount importance. The formulaic approach to gamma correction underscores its systematic nature, providing a standardized method to enhance the accuracy and reliability of displayed images in various imaging contexts.

$$I' = 255 \times \left(\frac{I}{255}\right)^{1/\gamma} \qquad (3.1)$$

In this study, (ϒ=0.5, ϒ=1 and ϒ=1.5) is used in implementing gamma correction.

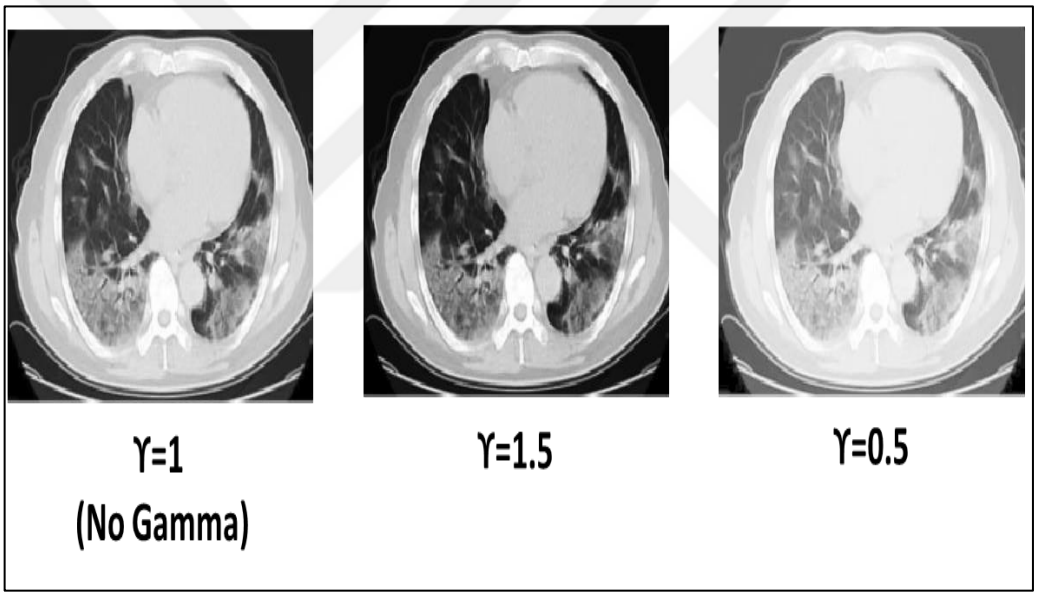


**Figure 3.4.** COVID CT images with different values of gamma correction.

### 3.2.2. Convolutional Neural Network

The model (network) in this study is built with Keras (and Tensorflow in the background). In this study, the CNN was implemented using Python as follows:

First, call the required libraries.

Second: load the training set and divide it into two training and test sets. And then convert the shape of the matrices to what is suitable for the input layer (number of examples, number of channels, width, length) in order.

Third: Normalization. To achieve this, the color values of the images must be converted to within the range (0–1), and since the images in the training set are within grayscale (color values within the range 0-255), we divide the values by the maximum value (255).

Fourth: the output encoding. Our question is one of multiple classifications. We have 2 categories (0–1). We will convert the integer values of the categories into a binary array using the to_categorical method.

Fifth: network construction. The initial hidden layer in this model is a convolution layer called Convolution2D. It consists of 16 attribute maps, each with a size of 3*3. The activation function used is rectifier, or relu. Following this, there is a pooling layer with a window size of 2*2. Then comes the dropout layer, where the goal is to randomly eliminate 20% of the neurons in order to prevent overfitting. After that, there is a flattening layer that converts the 2D data matrix into a single vector in order to process it further with the fully connected network. The subsequent layer is a fully connected layer that contains three neurons and uses the relu activation function. Lastly, there is an output layer with 10 neurons representing the two classes. The softmax activation function is applied to produce the probability of each class. The error function used is categorical cross-entropy loss, and the training algorithm employed is Adam.

Sixth: training and evaluation. The task of the network is generalization, and we reach it through training using appropriate algorithms. Above all, the training is to find the optimal set of weights to achieve the correct prediction. Our network training method is supervised by a batch-training learner. That is, the weights are modified after entering all the examples, unlike the corresponding type (online training), in which the weights are modified after entering each example.

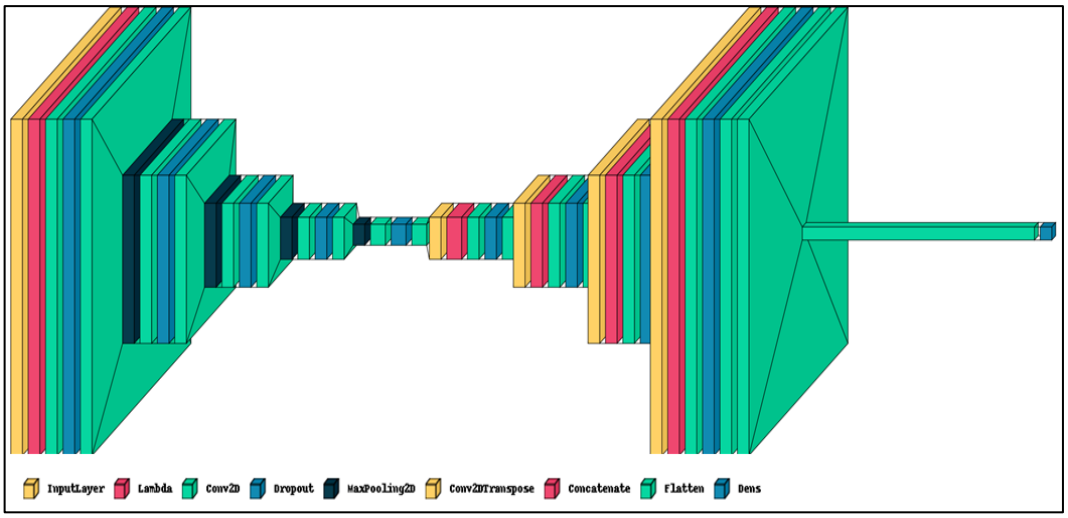


**Figure 3.5.** The main architecture of implemented CNN.

The training algorithm utilized is known as the Adam optimization algorithm. While multiple algorithms can be utilized for training purposes, the efficiency and effectiveness of the Adam algorithm have been demonstrated across various neural network structures. Additionally, it is highly recommended as a valuable tool for random optimization due to its ability to minimize the need for extensive storage capacity, relying instead on first-order regression.

It is a combination of two algorithms: (Gradient Descent with Momentum: GDM) and (Root Mean Square Prop: RMSprop). The number of training epochs is 100,, and the batch size of data in each epoch is 200.

#### 3.2.2.1. Using CNN as feature extraction tool

This method aims to extract learned image features from a trained CNN network and use those features to train the XGBoost classifier. The proposed method (Figure 1) consists of (1) implementing and training CNN using the dataset; (2) selecting the fully connected layer 'Conv2D_7'; (3) getting feature representations (layer output contains extracted features); (4) building an XGBoost classifier model based on the training dataset; and (5) evaluating the performance of CNN and XGBoost using extracted features from the testing set.

### 3.2.3. XGBoost Classifier

One of the most widely utilized algorithms in existence today is extremely popular due to its exceptional potency. It bears semblance to the gradient batch algorithm, yet boasts additional attributes that significantly enhance its capabilities. Notably, it offers a more direct path to the lower bounds rather than a gradual descent,

resulting in significantly accelerated performance. Furthermore, this algorithm effectively diminishes correlation among trees, ultimately bolstering the overall strength of the group.

XGBoost operates by utilizing Newton's method within the function space. Unlike gradient boosting, which functions as gradient descent within the function space, XGBoost employs a quadratic Taylor approximation in the loss function to establish a link with the Newton-Raphson method.

Algorithm parameters:

***eta [default = 0.3]****:* The shrink parameter is employed to adjust the weight of leaf nodes, ensuring that it does not exceed a certain threshold by multiplying it with a modulus value. This helps prevent the step size from becoming excessively large. Increasing the value of this parameter increases the likelihood of convergence. It is advisable to lower the learning rate to a smaller value. A reduced learning rate facilitates more cautious learning in later stages.

***min_child_weight [default = 1]:*** By default, this parameter is set to 1, representing the minimum sum required in each sheet. In cases of unbalanced positive and negative samples for 0-1 classification, considering a value of approximately 0.01 for h, a min_child_weight of 1 implies that a leaf node should include a minimum of 100 samples. This parameter has a significant impact on the outcome as it governs the minimum threshold for the sum of second derivatives within the leaf nodes. Remarkably, the smaller the value of this parameter, the more effortless it becomes to fill in the gaps.

***max_depth [default = 6]:*** The greater the height of a tree, the more effortless it becomes to occupy, indicating that the maximum depth of each tree plays a significant role.

***max_leaf_nodes:*** The role of max_depth coincides with the maximum number of leaf nodes.

***gamma [default = 0]:*** *The* parameter is utilized for regulating whether or not to truncate text after removing unnecessary elements.

***max_delta_step [default = 0]:*** The role of this parameter becomes significant during the update process. When set to 0, it signifies the absence of any constraints. However, if a positive value is selected, it results in a more cautious approach to the update step. This cautiousness prevents numerous update steps, thereby promoting a more gradual update process.

***Subsample [default = 1]:*** When the algorithm is randomly sampled, a smaller value leads to a more cautious approach, avoiding overfitting. However, it is important to note that if the value is too small, it can result in inappropriate fitting.

***colsample_bytree [default = 1]:*** Typically, in the process of generating each tree, column sampling, specifically the sampling of features, is often set within the range of 0.5 to 1. This technique allows for a more comprehensive representation of the data.

***lambda [default = 1]:*** The L2 tuning term parameter determines the weight assigned to the model complexity. A higher value leads to decreased chances of the model becoming overly complex.

***alpha [default = 0]:*** The weight value's L1 normal term parameter is responsible for controlling the model's complexity. Increasing the parameter value reduces the likelihood of the model surpassing its performance.

***scale_pos_weight [default = 1]:*** If the value exceeds zero, it can aid in achieving rapid convergence, particularly when dealing with imbalanced class samples.

### 3.2.4. Performance Measures

The performance is measured using formula of accuracy (Eq. 3.2), sensitivity (Eq. 3.3) and F1-score (Eq. 3.4):

$$Accuracy = \frac{TP + TN}{TP + TN + FP + FN} \quad (3.2)$$

$$Sensitivity = \frac{TP}{TP + FN} \quad (3.3)$$

$$F1 - score = \frac{2 \cdot \Pr ecision \cdot \mathrm{Re}\, call}{\Pr ecision + \mathrm{Re}\, call} \quad (3.4)$$

Where:

$$\Pr ecision = \frac{TP}{TP + FP} \quad (3.5)$$

$$\mathrm{Re}\, call = \frac{TP}{TP + FN} \quad (3.6)$$

- True Positive (TP): The number of correctly classified data indicating the correct case.
- False Positive (FP): The number of incorrectly categorized data that is not indicative of the correct case.

True Negative (TN): The number of data classified as not the correct case and not indicative of the case. False Negative (FN): The number of data classified as not the correct case and indicative of the case

# 4. RESULT AND DISCUSSIONS

## 4.1. The results of the 1st (Covid Data 1) Dataset

### 4.1.1 Results of splitting Covid Data-1 into 80% training and 20% testing

The training procedure for the CNN involves the meticulous process of fine-tuning the last seven layers of the network. This targeted fine-tuning allows for the optimization of specific parameters, enhancing the network's ability to extract and learn intricate features from the input data.

Table 4.1 illustrates the performance metrics of a CNN employed as a classifier to discern between COVID-19 and normal cases. The evaluation is conducted under two distinct training conditions: one without the application of gamma correction (GC) and the other incorporating gamma correction. The essential metrics considered include accuracy, sensitivity, and F1-score, each providing valuable insights into the classifier's capabilities.

In the absence of gamma correction during training, the CNN achieves an accuracy of 79.03%. Sensitivity values, representing the ability to correctly identify positive instances, are 78.12% for COVID-19 and 76.54% for normal cases. Additionally, the F1-scores for COVID-19 and normal cases stand at 76.32% and 74.74%, respectively. Conversely, when gamma correction is applied during training, the classifier demonstrates substantial improvement across all metrics. The accuracy significantly increases to 92.19%, indicating a more precise overall classification performance. Sensitivities for both COVID-19 and normal cases show remarkable enhancements, reaching 94.12% and 92.02%, respectively. The F1-scores experience notable improvements as well, reaching 92.23% for COVID-19 and 91.01% for normal cases.

These results collectively suggest that the integration of gamma correction during the training process positively influences the CNN classifier's ability to distinguish between COVID-19 and normal cases (Figure 4.1). The higher accuracy underscores the efficacy of gamma correction in refining the learning process, while the increased sensitivities and F1-scores affirm its impact on correctly identifying instances of both classes. The findings advocate for the beneficial role of gamma correction as an image enhancement technique, contributing to the improved performance of the CNN in the classification of medical images.

**Table 4.1**. Covid-19 data-1 (80% training and 20% testing) the performance of training and testing the CNN net as a classifier.

| | **Image size 128x128** | | | | | |
|---|---|---|---|---|---|---|
| | **Training without GC (ϒ=1)** | | **Training with GC (ϒ=1.5)** | | **Training with GC (ϒ=0.5)** | |
| | Covid-19 | Normal | Covid-19 | Normal | Covid-19 | Normal |
| Accuracy (%) | 79.03 | | 92.19 | | 78.52 | |
| Sensitivity (%) | 78.12 | 76.54 | 94.12 | 92.02 | 79.12 | 75.54 |
| F1-score (%) | 76.32 | 74.74 | 92.23 | 91.01 | 77.32 | 75.74 |
| | **Image size 256x256** | | | | | |
| | **Training without GC (ϒ=1)** | | **Training with GC (ϒ=1.5)** | | **Training with GC (ϒ=0.5)** | |
| | Covid-19 | Normal | Covid-19 | Normal | Covid-19 | Normal |
| Accuracy (%) | 79.54 | | 92.62 | | 78.23 | |
| Sensitivity (%) | 78.23 | 76.54 | 94.32 | 92.54 | 79.54 | 75.52 |
| F1-score (%) | 76.56 | 74.76 | 92.65 | 91.01 | 77.20 | 75.74 |

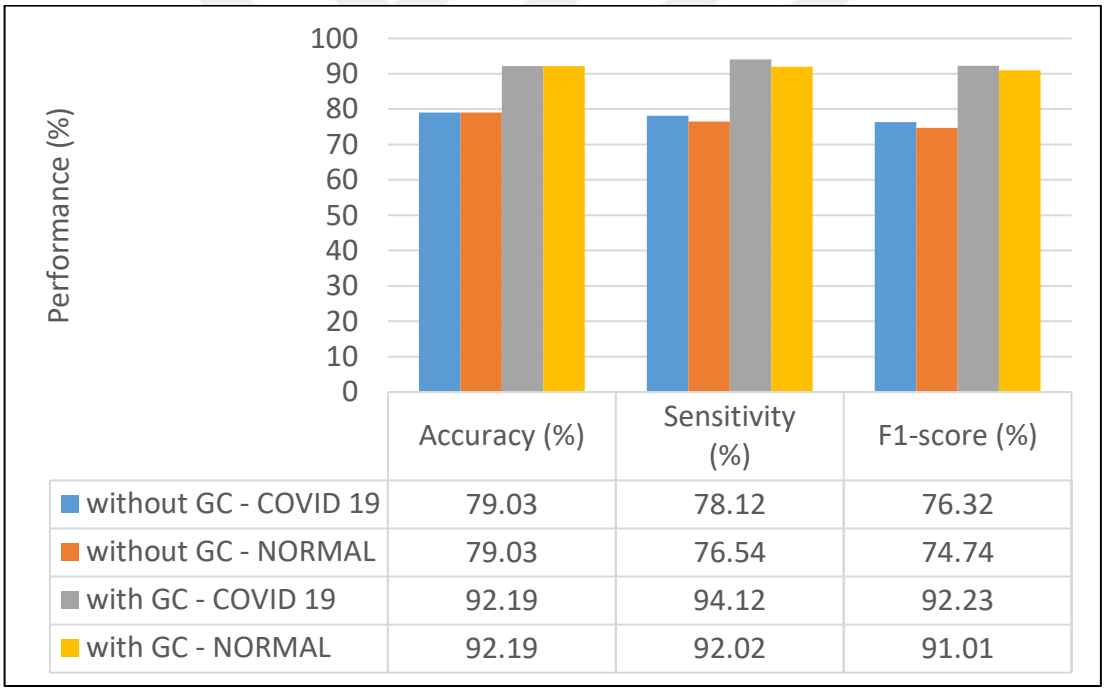


**Figure 4.1.** Covid-19 data-1 (80% training and 20% testing) the performance of training and testing the CNN net as a classifier.

This section addresses the classification performance of the XGBoost model, leveraging a multi-step approach that involves utilizing extracted features from images through a CNN and subsequently implementing Gradient Correction (GC) on the deep features. Table 4.2 outlines the performance metrics of an XGBoost classifier utilized for the classification of COVID-19 and normal cases, under two distinct training

conditions: without and with GC. The primary evaluation metrics considered are accuracy, sensitivity, and F1-score, providing a comprehensive view of the classifier's performance.

**Table 4.2.** Covid-19 data-1 (80% training and 20% testing) the performance of training and testing XGBoost classifier.

| **Image size 128x128** | | | | | | |
|---|---|---|---|---|---|---|
| | **Training without GC (ϒ=1)** | | **Training with GC (ϒ=1.5)** | | **Training with GC (ϒ=0.5)** | |
| | Covid-19 | Normal | Covid-19 | Normal | Covid-19 | Normal |
| Accuracy (%) | 95.02 | | 97.94 | | 89.42 | |
| Sensitivity (%) | 94.22 | 89.02 | 98.32 | 90.21 | 86.22 | 88.02 |
| F1-score (%) | 96.45 | 92.57 | 97.01 | 93.56 | 87.45 | 85.57 |
| **Image size 256x256** | | | | | | |
| | **Training without GC (ϒ=1)** | | **Training with GC (ϒ=1.5)** | | **Training with GC (ϒ=0.5)** | |
| Accuracy (%) | 95.02 | | 97.94 | | 89.14 | |
| Sensitivity (%) | 94.12 | 89.44 | 98.32 | 90.12 | 86.22 | 88.32 |
| F1-score (%) | 96.34 | 92.52 | 97.01 | 93.43 | 87.54 | 85.02 |

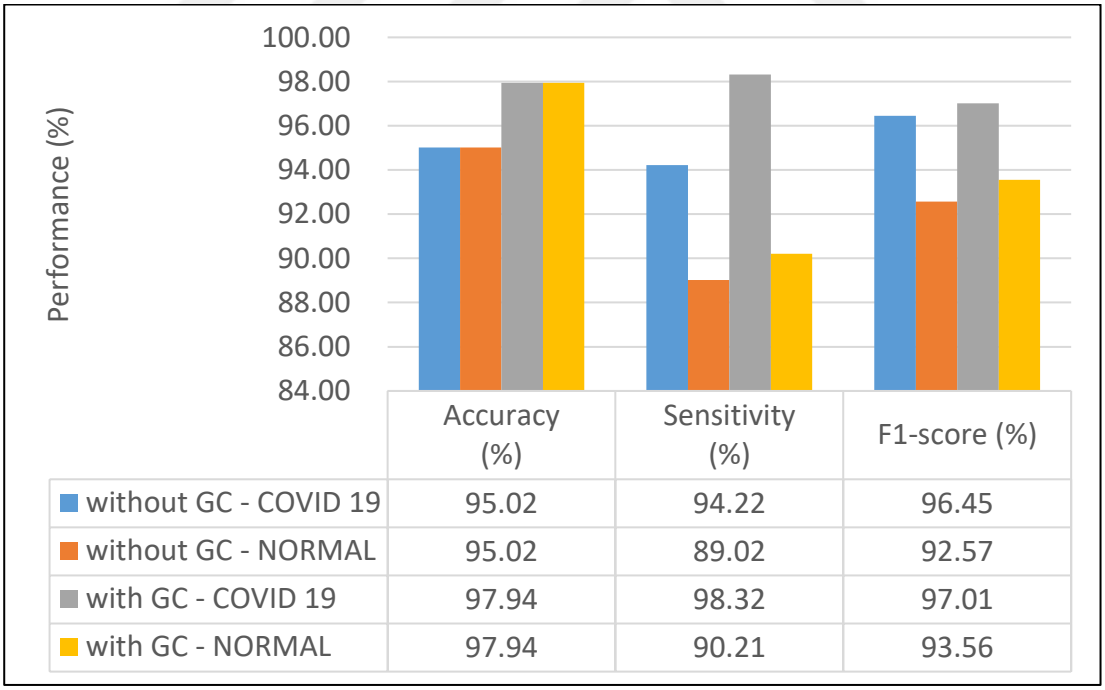


**Figure 4.2.** Covid-19 data-1 (80% training and 20% testing) the performance of training and testing XGBoost classifier.

In the absence of GC during training (Figure 4.2), the XGBoost classifier demonstrates exceptional accuracy, achieving a rate of 97.94%. Sensitivities for COVID-19 and normal cases are impressively high at 98.32% and 90.21%,

respectively. The F1-scores, reflecting a balance between precision and recall, are also noteworthy, standing at 97.01% for COVID-19 and 93.56% for normal cases.

However, when GC is introduced during training, a slight reduction in performance metrics is observed. The accuracy drops to 95.02%, and the sensitivities for COVID-19 and normal cases decrease to 94.22% and 89.02%, respectively. Similarly, F1-scores experience a modest decline, with values of 96.45% for COVID-19 and 92.57% for normal cases.

This nuanced performance difference between training with and without GC prompts a discussion on the impact of GC on the XGBoost classifier. While the absolute reduction in performance metrics is relatively small, it suggests that the inclusion of GC might introduce a subtle trade-off. The decrease in accuracy and sensitivities may indicate that the additional computational overhead introduced by GC during training could potentially affect the model's learning process. However, the high absolute values of all metrics, even with GC, reaffirm the robustness of the XGBoost classifier in effectively discriminating between COVID-19 and normal cases.

In practical terms, the choice of whether to include GC during training may depend on specific application requirements, computational resources, and the acceptable level of trade-off between model performance and training efficiency. Further investigation and experimentation could shed light on the optimal conditions for training the XGBoost classifier in a medical image classification scenario.

Where the main objective of the research is to investigate the power of deep learning and transfer learning in classifying medical images after implementing GC on CT images and deep features as well, we will compare the performance of CNN as a direct classifier and feature extraction step. As shown in Figure 4.3, CNN, after training its layers on the desired dataset, gives higher accuracy. On the other hand, the XGBoost classifier shows better sensitivity and F1-score, which reflects the lower number of false positive and negative outcomes of the XGBoost classifier. The presence of GC in preprocessing and as an enhancer for the newly extracted deep features shows a significant contribution to performance outcomes and COVID CT image detection.

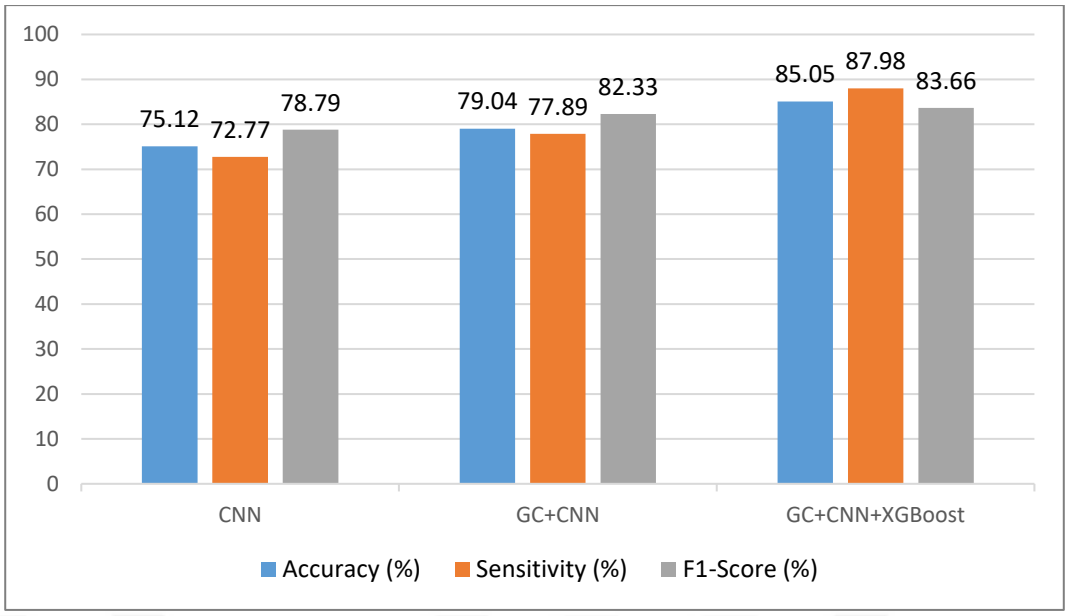


**Figure 4.3.** Classification performance of CNN and XGBoost classifier (features 128x128) (1.5 gamma).

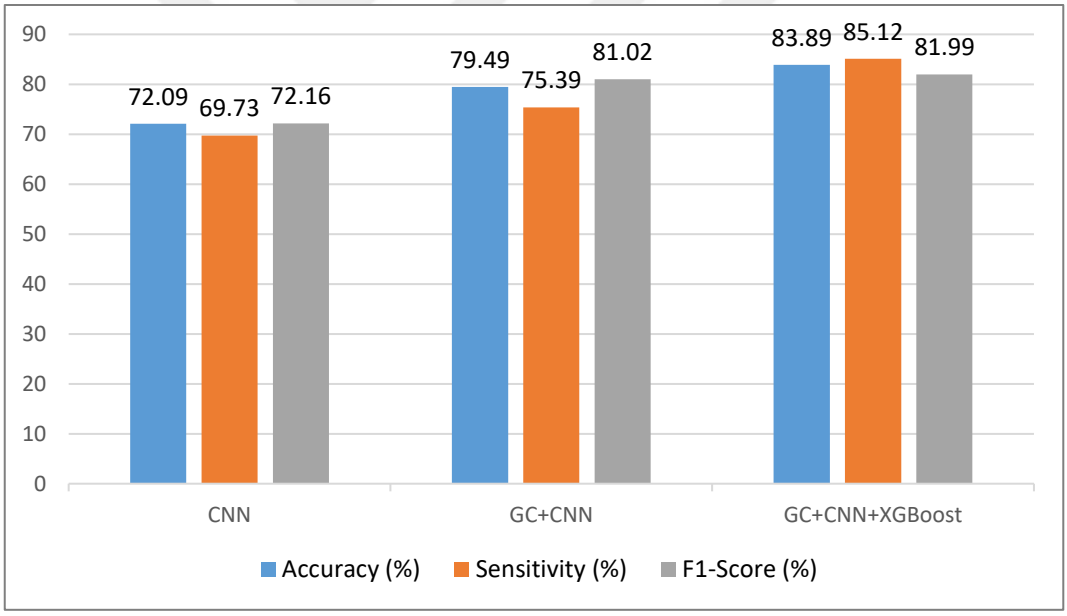


**Figure 4.4.** Classification performance of CNN and XGBoost classifier (features 128x128) (0.5 gamma).

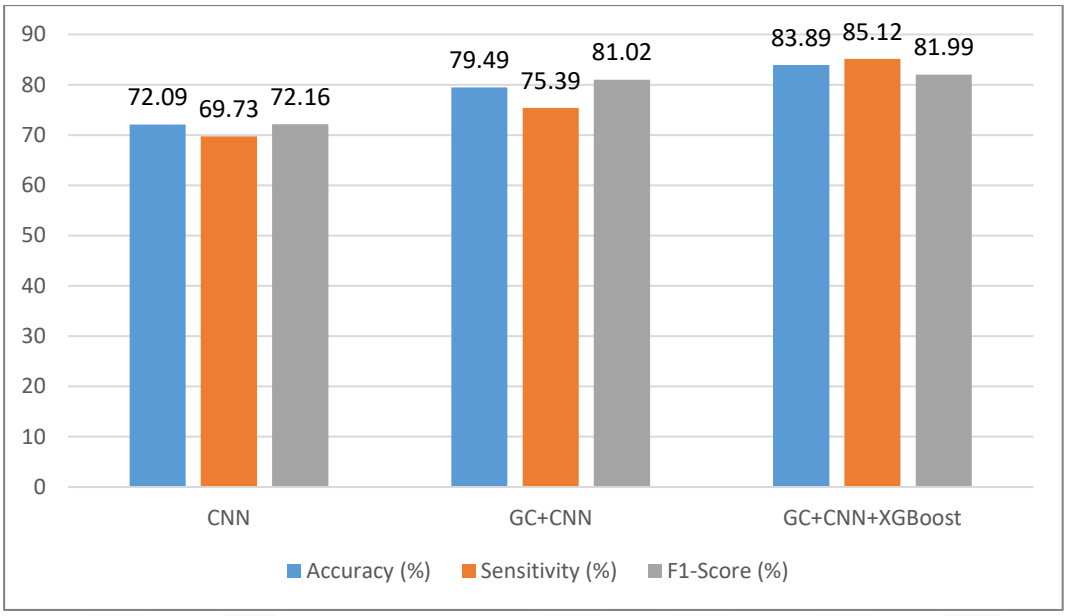


**Figure 4.5.** Classification performance of CNN and XGBoost classifier (features 128x128) (1 gamma).

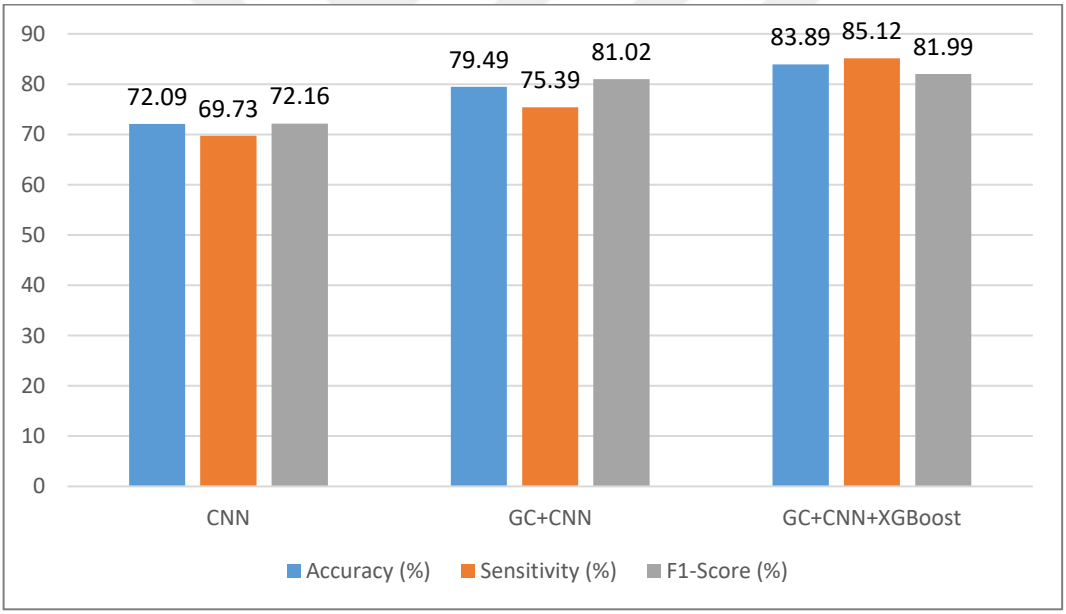


**Figure 4.6.** Classification performance of CNN and XGBoost classifier (features 256x256) (1.5 gamma).

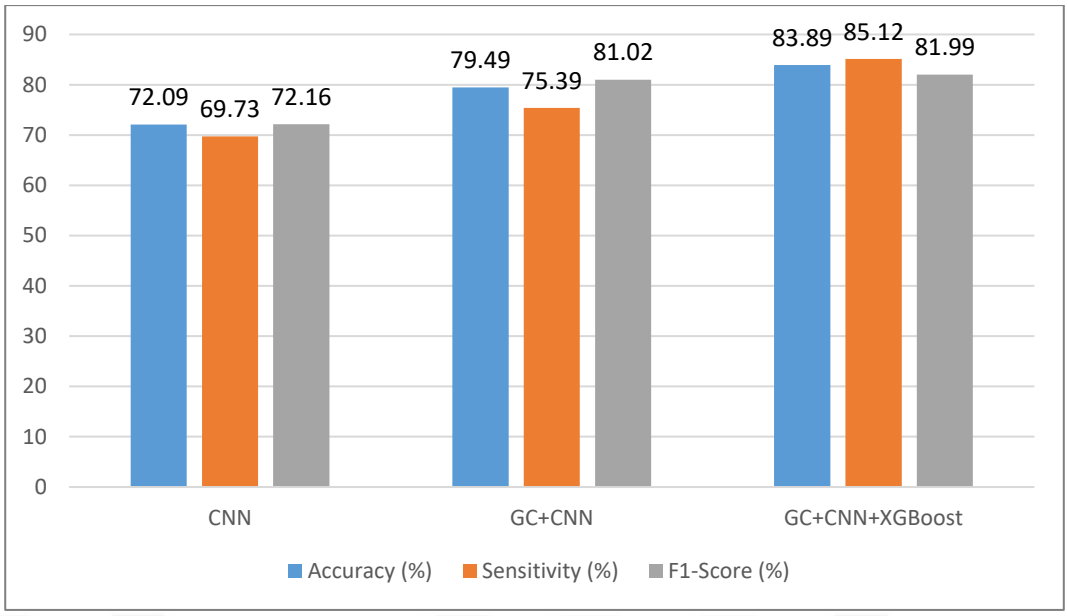


**Figure 4.7.** Classification performance of CNN and XGBoost classifier (features 256x256) (0.5 gamma).

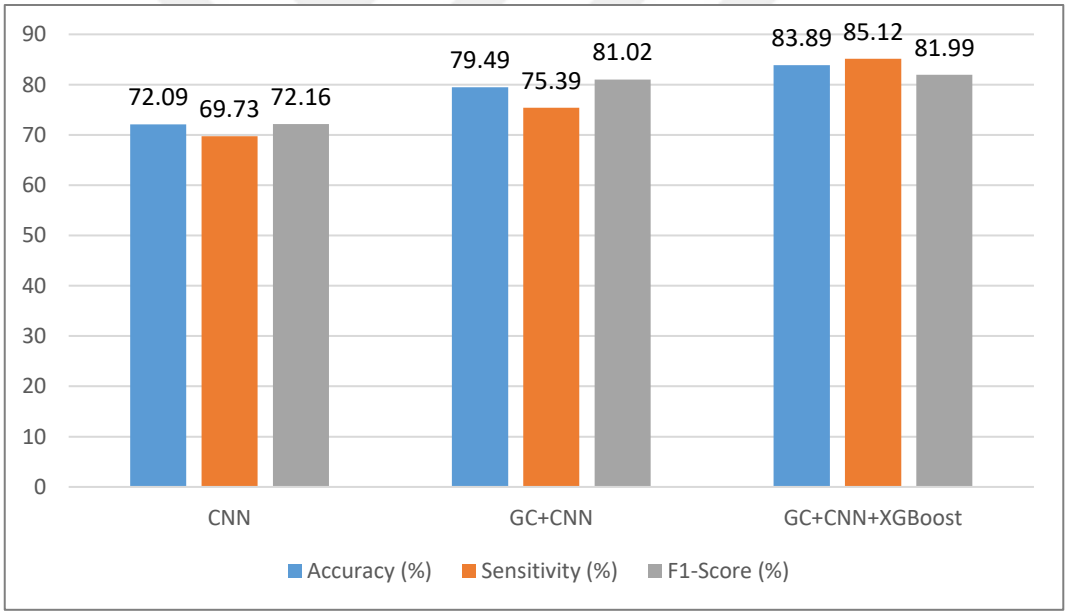


**Figure 4.8.** Classification performance of CNN and XGBoost classifier (features 256x256) (1 gamma).

### 4.1.2 Results of splitting Covid Data 1 into 70% training and 30% testing

Tables 4.3 and 4.4 present the performance metrics of training and testing two different classifiers, namely CNN and XGBoost, under two conditions: without GC and with GC. For the CNN classifier (Table 4.3), without GC, the accuracy is 78.54% for classifying COVID-19 cases and 91.34% for normal cases. Sensitivity, indicating the true positive rate, is 76.56% for COVID-19 and 75.23% for normal cases. The F1-score, a measure

of a model's accuracy, is 74.94% for COVID-19 and 72.9% for normal cases. With GC, the CNN classifier shows improved performance across all metrics, with accuracy increasing to 92.75% for COVID-19 and 91.85% for normal cases. Sensitivity also improves to 92.75% for COVID-19 and 91.85% for normal cases, while the F1-score rises to 91.55% for COVID-19 and 90.72% for normal cases. Similarly, for the XGBoost classifier (Table 4.4), without GC, the accuracy is 94.32% for COVID-19 and 97.32% for normal cases. Sensitivity is 92.67% for COVID-19 and 87.13% for normal cases, while the F1-score is 95.39% for COVID-19 and 92.45% for normal cases. With GC, the XGBoost classifier shows further improvement in accuracy, reaching 98.27% for COVID-19 and 89.41% for normal cases. Sensitivity also improves, with values of 98.27% for COVID-19 and 89.41% for normal cases. The F1-score increases to 96.56% for COVID-19 and 91.84% for normal cases.

**Table 4.3.** Covid-19 data-1 (70% training and 30% testing) the performance of training and testing the CNN net as a classifier.

| | **Training without GC (ϒ=1)** | | **Training with GC (ϒ=1.5)** | |
|---|---|---|---|---|
| | Covid-19 | Normal | Covid-19 | Normal |
| Accuracy (%) | 78.54 | | 91.34 | |
| Sensitivity (%) | 76.56 | 75.23 | 92.75 | 91.85 |
| F1-score (%) | 74.94 | 72.90 | 91.55 | 90.72 |

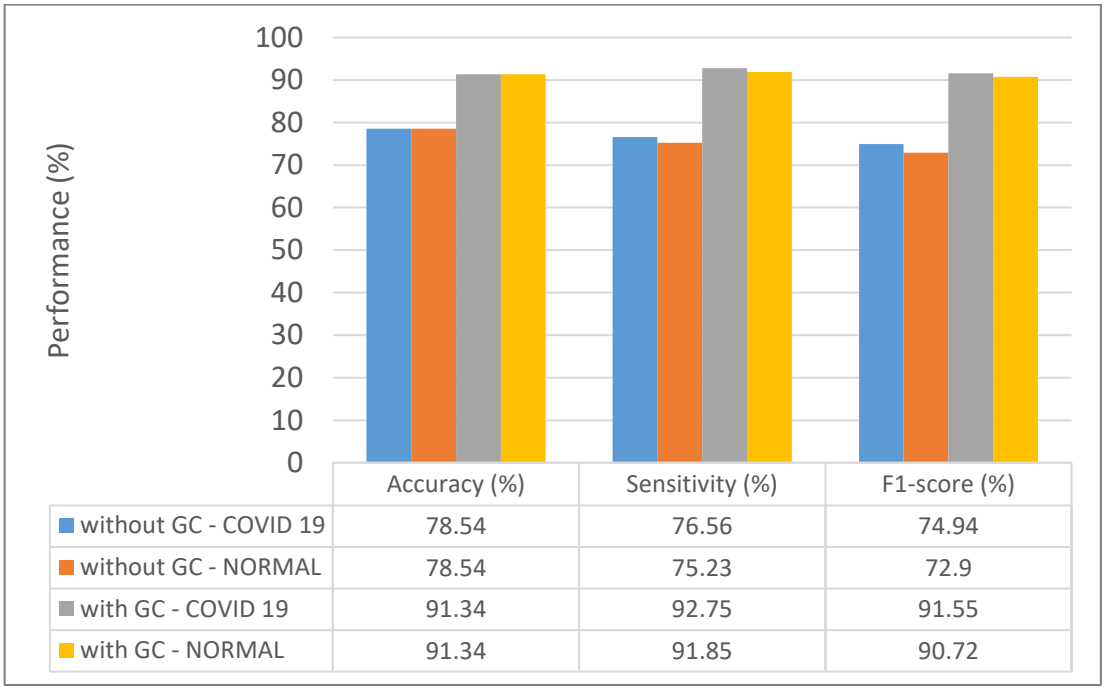


**Figure 4.9.** Covid-19 data-1 (70% training and 30% testing) the performance of training and testing the CNN net as a classifier.

**Table 4.4.** Covid-19 data-1 (70% training and 30% testing) the performance of training and testing XGBoost classifier.

| | **Training without GC (ϒ=1)** | | **Training with GC (ϒ=1.5)** | |
|---|---|---|---|---|
| | Covid-19 | Normal | Covid-19 | Normal |
| Accuracy (%) | 94.32 | | 97.32 | |
| Sensitivity (%) | 92.67 | 87.13 | 98.27 | 89.41 |
| F1-score (%) | 95.39 | 92.45 | 96.56 | 91.84 |

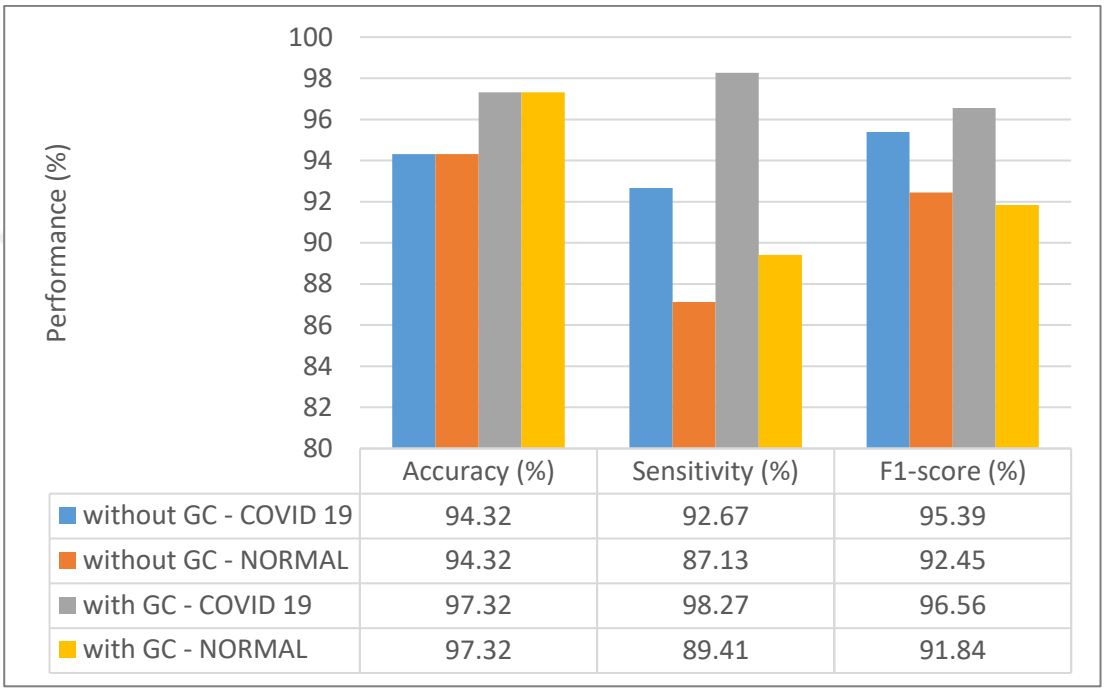


**Figure 4.10.** Covid-19 data-1 (70% training and 30% testing) the performance of training and testing XGBoost classifier.

Figure 4.11 presents the classification performance of four different configurations: CNN, CNN with GC, CNN with GC and XGBoost combined, and CNN with both GC and XGBoost combined. The accuracy, sensitivity, and F1-score metrics are provided for each configuration.

For the CNN classifier alone, the accuracy is 73.75%, the sensitivity is 71.98%, and the F1-score is 78.19%. When GC is applied to the CNN model, there is an improvement in performance across all metrics, with accuracy increasing to 78.69%, sensitivity to 77.12%, and F1-score to 80.56%.

Integrating XGBoost with GC-enhanced CNN further enhances the performance metrics. The configuration of GC-enhanced CNN combined with XGBoost shows an accuracy of 83.98%, sensitivity of 86.16%, and F1-score of 81.97%.

Finally, the configuration incorporating both GC and XGBoost demonstrates the highest performance across all metrics. The accuracy reaches 94.23%, the sensitivity is 96.36%, and the F1-score is 93.07%.

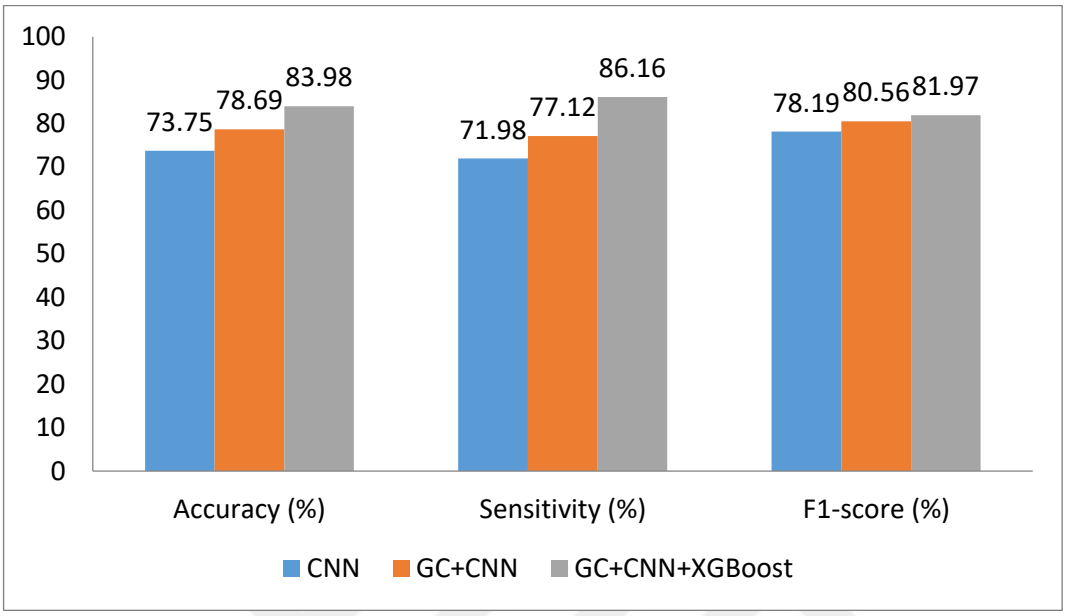


**Figure 4.11.** Covid-19 data-1 (70% training and 30% testing) classification performance of CNN and XGBoost classifier.

### 4.1.3. Results of splitting Covid Data 1 into 60% training and 40% testing

Tables 4.5 and 4.6 present the performance evaluation of training and testing two different classifiers, namely CNN and XGBoost, under two conditions: without GC and with GC.

For the CNN classifier (Table 4.5), without GC, the accuracy stands at 76.34% for classifying COVID-19 cases and 92.23% for normal cases. Sensitivity, indicating the true positive rate, is 76.64% for COVID-19 and 75.42% for normal cases. The F1-score, a measure of a model's accuracy, is 75.76% for COVID-19 and 73.29% for normal cases. With GC, the CNN classifier shows improvement across all metrics. Accuracy increases to 93.66% for COVID-19 and 90.45% for normal cases. Sensitivity also improves to 93.66% for COVID-19 and 90.45% for normal cases, while the F1-score rises to 91.9% for COVID-19 and 90.35% for normal cases.

Similarly, for the XGBoost classifier (Table 4.6), without GC, the accuracy is 95.34% for COVID-19 and 97.32% for normal cases. Sensitivity is 92.28% for COVID-19 and 87.91% for normal cases, while the F1-score is 95.05% for COVID-19 and 90.88% for normal cases. With GC, the XGBoost classifier shows further improvement in accuracy, reaching 97.43% for COVID-19 and 88.32% for normal cases. Sensitivity

also improves, with values of 97.43% for COVID-19 and 88.32% for normal cases. The F1-score increases to 96.75% for COVID-19 and 92.43% for normal cases.

**Table 4.5.** Covid-19 data-1 (60% training and 40% testing) the performance of training and testing the CNN net as a classifier.

| | **Training without GC (ϒ=1)** | | **Training with GC (ϒ=1.5)** | |
|---|---|---|---|---|
| | Covid-19 | Normal | Covid-19 | Normal |
| Accuracy (%) | 76.34 | | 92.23 | |
| Sensitivity (%) | 76.64 | 75.42 | 93.66 | 90.45 |
| F1-score (%) | 75.76 | 73.29 | 91.90 | 90.35 |

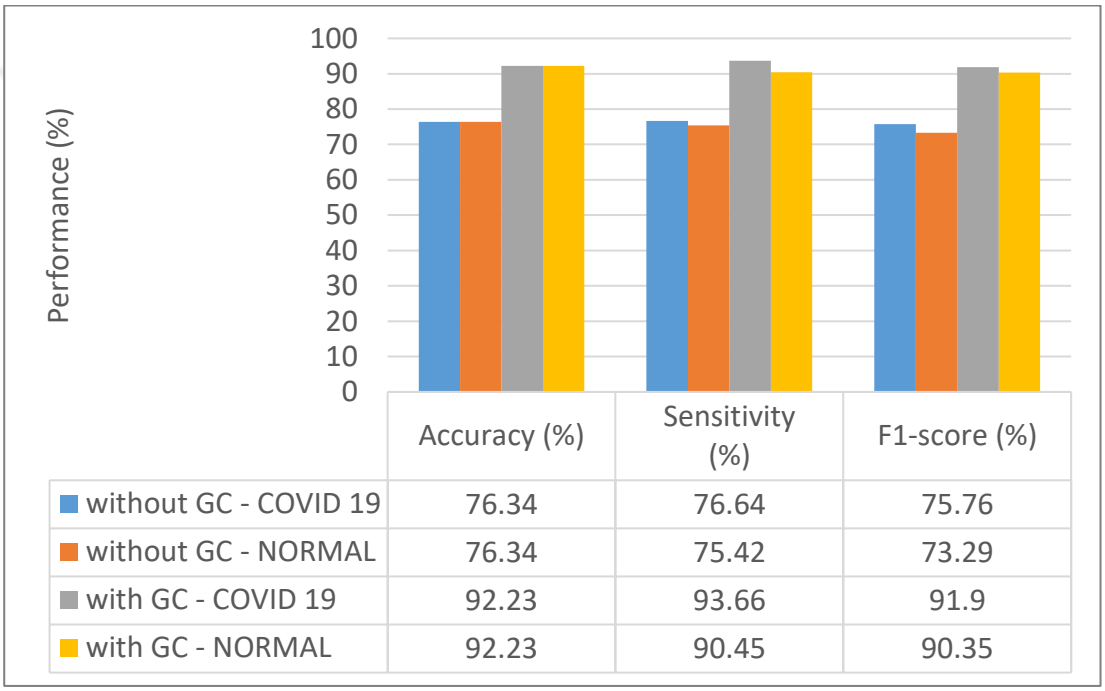


**Figure 4.12.** Covid-19 data-1 (60% training and 40% testing) the performance of training and testing the CNN net as a classifier.

**Table 4.6.** Covid-19 data-1 (60% training and 40% testing) the performance of training and testing XGBoost classifier.

| | **Training without GC (ϒ=1)** | | **Training with GC (ϒ=1.5)** | |
|---|---|---|---|---|
| | Covid-19 | Normal | Covid-19 | Normal |
| Accuracy (%) | 95.34 | | 97.32 | |
| Sensitivity (%) | 92.28 | 87.91 | 97.43 | 88.32 |
| F1-score (%) | 95.05 | 90.88 | 96.75 | 92.43 |

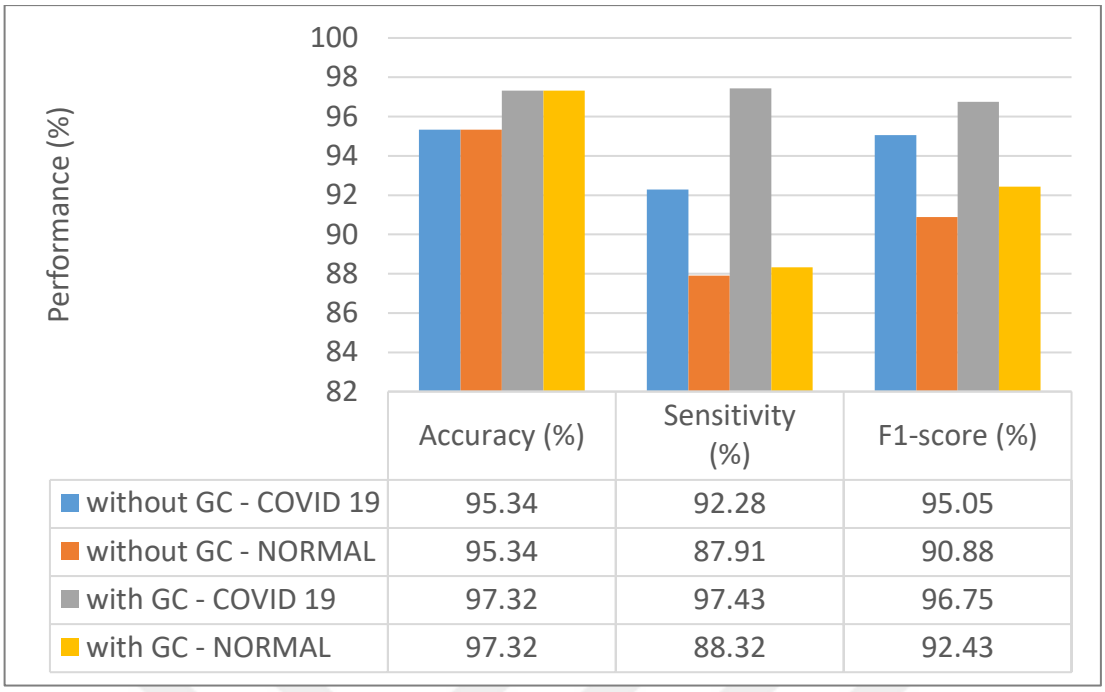


| | Accuracy (%) | Sensitivity (%) | F1-score (%) |
|---|---|---|---|
| without GC - COVID 19 | 95.34 | 92.28 | 95.05 |
| without GC - NORMAL | 95.34 | 87.91 | 90.88 |
| with GC - COVID 19 | 97.32 | 97.43 | 96.75 |
| with GC - NORMAL | 97.32 | 88.32 | 92.43 |

**Figure 4.13.** Covid-19 data-1 (60% training and 40% testing) the performance of training and testing XGBoost classifier.

Figure 4.14 illustrates the classification performance of four different configurations: CNN, CNN with GC, CNN with GC and XGBoost combined, and CNN with both GC and XGBoost combined. The table presents accuracy, sensitivity, and F1-score metrics for each configuration.

For the CNN classifier alone, the accuracy is 74.66%, the sensitivity is 71.93%, and the F1-score is 76.8%. Upon applying GC to the CNN model, there is a noticeable improvement in performance across all metrics. The accuracy increases to 77.77%, the sensitivity to 76.9%, and the F1-score to 80.73%.

Integrating XGBoost with GC-enhanced CNN further enhances the performance metrics. The configuration of GC-enhanced CNN combined with XGBoost demonstrates an accuracy of 84.42%, sensitivity of 87.43%, and F1-score of 83.02%.

Finally, the configuration incorporating both GC and XGBoost showcases the highest performance across all metrics. The accuracy reaches 94.18%, the sensitivity is 95.92%, and the F1-score is 93.22%.

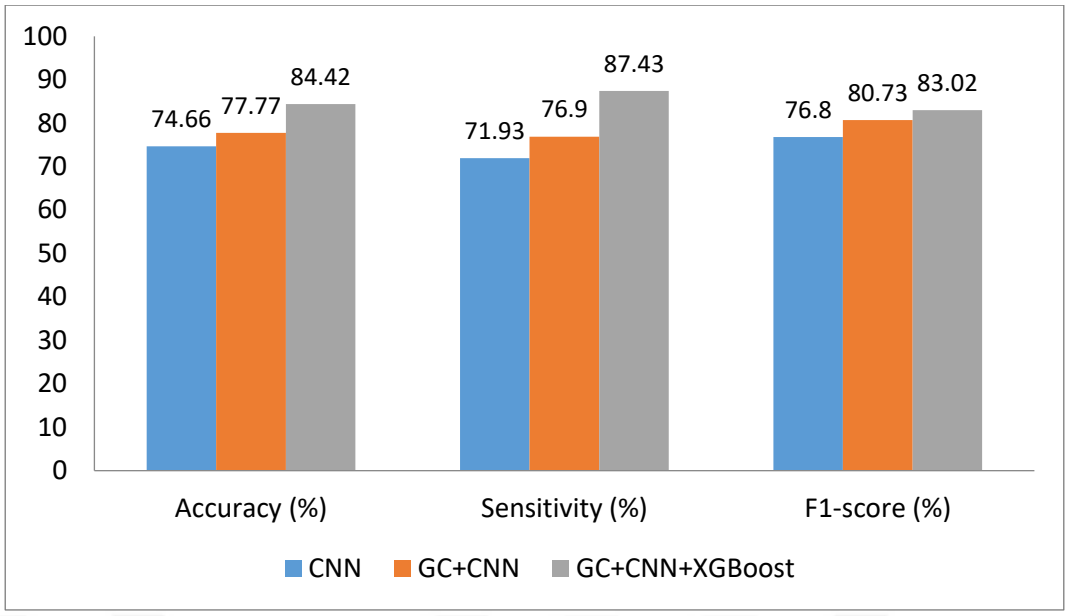


**Figure 4.14.** Covid-19 data-1 (60% training and 40% testing) classification performance of CNN and XGBoost classifier.

### 4.2. The results of the 2nd (Covid Data 2) Dataset

#### 4.2.1. Results of splitting Covid Data 2 into 80% training and 20% testing

For the CNN classifier (Table 4.7), without GC, the accuracy stands at 79.43% for identifying COVID-19 cases and 92.03% for normal cases. Sensitivity, representing the true positive rate, is 77.67% for COVID-19 and 75.96% for normal cases. The F1-score, a measure of a model's accuracy, is 76.3% for COVID-19 and 74.68% for normal cases. With GC, the CNN classifier exhibits improvement across all metrics. Accuracy increases to 93.23% for COVID-19 and 91.57% for normal cases. Sensitivity also improves to 93.23% for COVID-19 and 91.57% for normal cases, while the F1-score rises to 91.61% for COVID-19 and 90.96% for normal cases.

Similarly, for the XGBoost classifier (Table 4.8), without GC, the accuracy is 95.23% for COVID-19 and 97.12% for normal cases. Sensitivity is 94.08% for COVID-19 and 88.32% for normal cases, while the F1-score is 95.51% for COVID-19 and 92.13% for normal cases. With GC, the XGBoost classifier demonstrates further improvement in accuracy, reaching 97.45% for COVID-19 and 90.16% for normal cases. Sensitivity also improves, with values of 97.45% for COVID-19 and 90.16% for normal cases. The F1-score increases to 96.8% for COVID-19 and 93.01% for normal cases. These results underscore the effectiveness of employing GC in enhancing the performance of both CNN and XGBoost classifiers in accurately classifying COVID-19 cases and normal cases in medical imaging datasets.

**Table 4.7.** Covid-19 data-2 (80% training and 20% testing) the performance of training and testing the CNN net as a classifier.

| **Image size 128x128** | | | | | | |
|---|---|---|---|---|---|---|
| | **Training without GC (ϒ=1)** | | **Training with GC (ϒ=1.5)** | | **Training with GC (ϒ=0.5)** | |
| | Covid-19 | Normal | Covid-19 | Normal | Covid-19 | Normal |
| Accuracy (%) | 79.43 | | 92.03 | | 75.64 | |
| Sensitivity (%) | 77.67 | 75.96 | 93.23 | 91.57 | 74.67 | 73.54 |
| F1-score (%) | 76.30 | 74.68 | 91.61 | 90.96 | 73.63 | 73.68 |
| **Image size 256x256** | | | | | | |
| | **Training without GC (ϒ=1)** | | **Training with GC (ϒ=1.5)** | | **Training with GC (ϒ=0.5)** | |
| | Covid-19 | Normal | Covid-19 | Normal | Covid-19 | Normal |
| Accuracy (%) | 79.74 | | 92.43 | | 75.45 | |
| Sensitivity (%) | 77.97 | 75.96 | 93.54 | 91.57 | 74.14 | 73.53 |
| F1-score (%) | 76.86 | 74.68 | 91.43 | 90.96 | 73.63 | 73.68 |

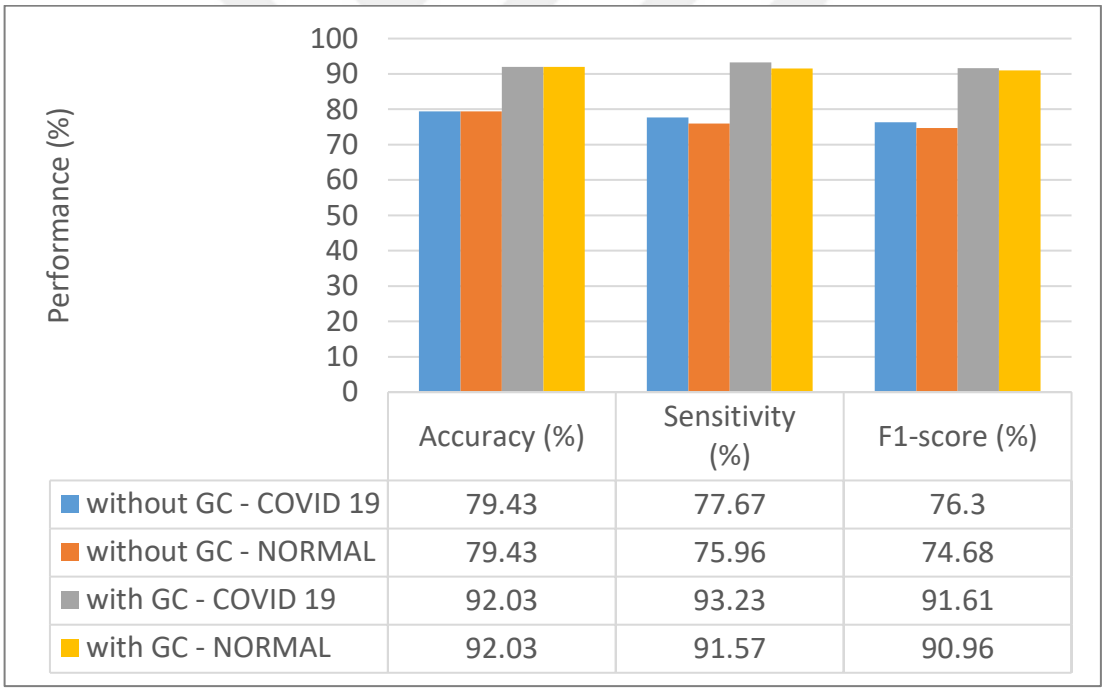


**Figure 4.15.** Covid-19 data-2 (80% training and 20% testing) the performance of training and testing the CNN net as a classifier.

**Table 4.8.** Covid-19 data-2 (80% training and 20% testing) the performance of training and testing XGBoost classifier.

| **Image size 128x128** | | | | | | |
|---|---|---|---|---|---|---|
| | **Training without GC (ϒ=1)** | | **Training with GC (ϒ=1.5)** | | **Training with GC (ϒ=0.5)** | |
| | Covid-19 | Normal | Covid-19 | Normal | Covid-19 | Normal |
| Accuracy (%) | 95.23 | | 97.12 | | 89.32 | |
| Sensitivity (%) | 94.08 | 88.32 | 97.45 | 90.16 | 92.21 | 84.43 |
| F1-score (%) | 95.51 | 92.13 | 96.80 | 93.01 | 94.32 | 89.32 |
| **Image size 256x256** | | | | | | |
| | **Training without GC (ϒ=1)** | | **Training with GC (ϒ=1.5)** | | **Training with GC (ϒ=0.5)** | |
| | Covid-19 | Normal | Covid-19 | Normal | Covid-19 | Normal |
| Accuracy (%) | 95.65 | | 97.76 | | 89.12 | |
| Sensitivity (%) | 94.22 | 88.32 | 97.32 | 90.16 | 92.11 | 84.32 |
| F1-score (%) | 95.23 | 92.43 | 96.23 | 93.44 | 94.32 | 89.29 |

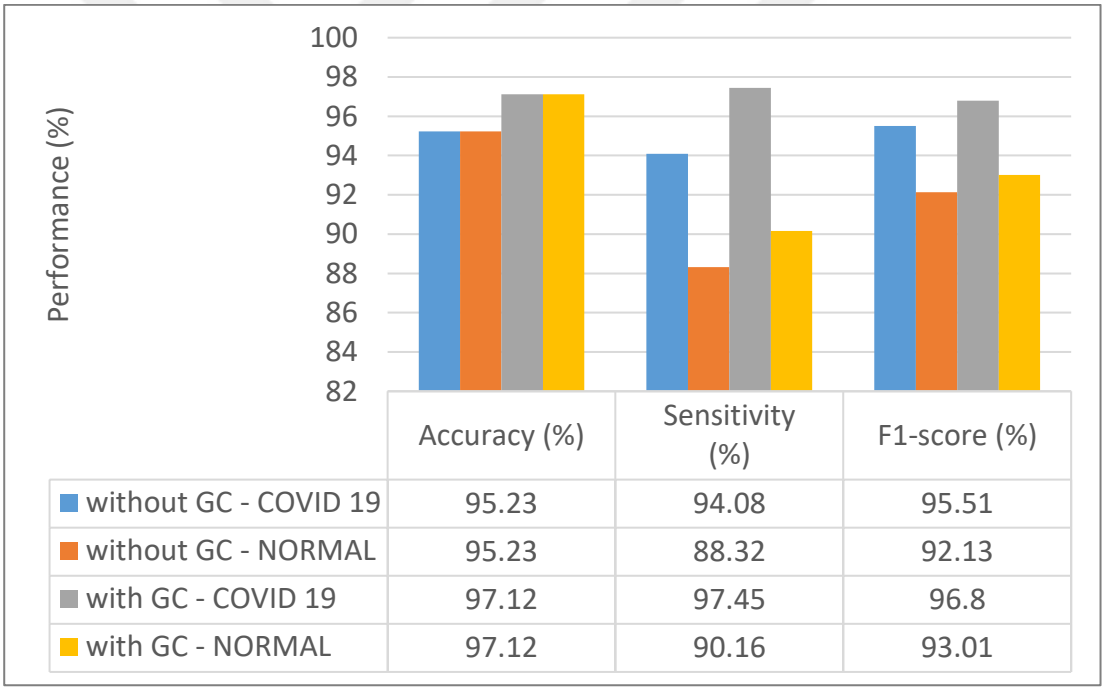


**Figure 4.16.** Covid-19 data-2 (80% training and 20% testing) the performance of training and testing XGBoost classifier.

Figure 4.17 presents the classification performance of four different configurations: CNN, CNN with GC, CNN with GC and XGBoost combined, and CNN with both GC and XGBoost combined. The table provides accuracy, sensitivity, and F1-score metrics for each configuration.

For the CNN classifier alone, the accuracy is 74.66%, the sensitivity is 71.83%, and the F1-score is 78.31%. Upon applying GC to the CNN model, there is an

improvement in performance across all metrics. The accuracy increases to 78.72%, the sensitivity to 77.33%, and the F1-score to 81.42%.

Integrating XGBoost with GC-enhanced CNN further enhances the performance metrics. The configuration of GC-enhanced CNN combined with XGBoost demonstrates an accuracy of 84.57%, sensitivity of 87.53%, and F1-score of 83.03%.

Finally, the configuration incorporating both GC and XGBoost showcases the highest performance across all metrics. The accuracy reaches 95.32%, the sensitivity is 97.01%, and the F1-score is 93.28%.

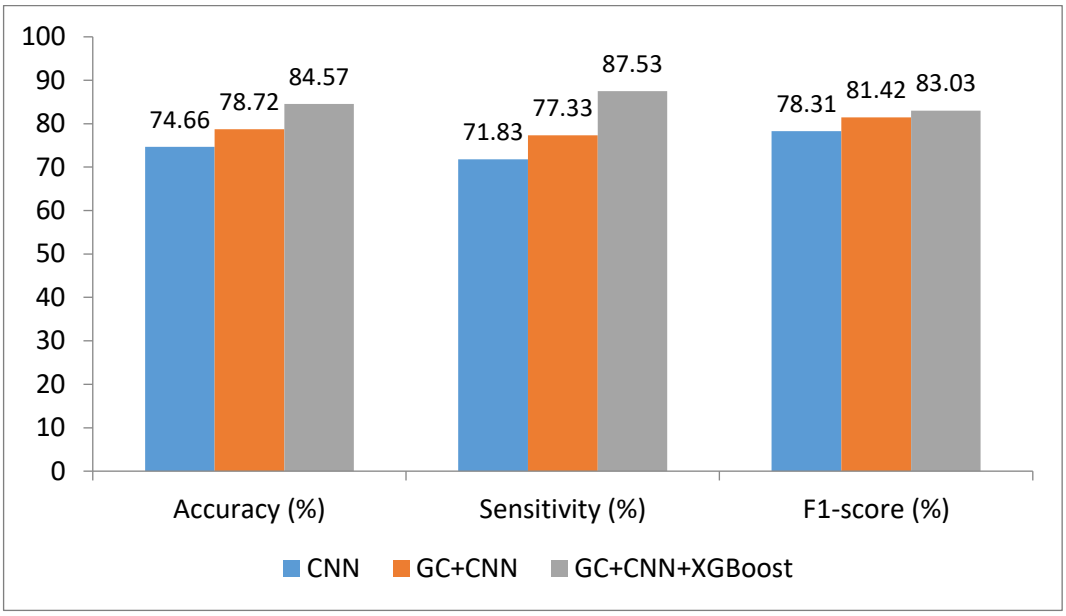


**Figure 4.17.** Covid-19 data-2 (80% training and 20% testing) classification performance of CNN and XGBoost classifier.

### 4.2.2. Results of splitting Covid Data 2 into 70% training and 30% testing

Tables 4.9 and 4.10 provide an overview of the performance evaluation of training and testing two different classifiers: CNN and XGBoost. This evaluation is conducted under two conditions: without GC and with GC.

For the CNN classifier (Table 4.9), without GC, the accuracy is 78.12% for identifying COVID-19 cases and 91.32% for normal cases. Sensitivity, indicating the true positive rate, is 74.8% for COVID-19 and 74.22% for normal cases. The F1-score, a measure of a model's accuracy, is 74.44% for COVID-19 and 72.23% for normal cases. With GC, the CNN classifier demonstrates improvement across all metrics. Accuracy increases to 92% for COVID-19 and 91.2% for normal cases. Sensitivity also improves to 92% for COVID-19 and 91.2% for normal cases, while the F1-score rises to 91.04% for COVID-19 and 89.28% for normal cases.

Similarly, for the XGBoost classifier (Table 4.10), without GC, the accuracy is 94.12% for COVID-19 and 97.52% for normal cases. Sensitivity is 92.12% for COVID-19 and 86.5% for normal cases, while the F1-score is 94.68% for COVID-19 and 91.51% for normal cases. With GC, the XGBoost classifier demonstrates further improvement in accuracy, reaching 97.74% for COVID-19 and 88.93% for normal cases. Sensitivity also improves, with values of 97.74% for COVID-19 and 88.93% for normal cases. The F1-score increases to 96.53% for COVID-19 and 91.13% for normal cases.

**Table 4.9.** Covid-19 data-2 (70% training and 30% testing) the performance of training and testing the CNN net as a classifier.

| | **Training without GC (ϒ=1)** | | **Training with GC (ϒ=1.5)** | |
|---|---|---|---|---|
| | Covid-19 | Normal | Covid-19 | Normal |
| Accuracy (%) | 78.12 | | 91.32 | |
| Sensitivity (%) | 74.80 | 74.22 | 92.00 | 91.20 |
| F1-score (%) | 74.44 | 72.23 | 91.04 | 89.28 |

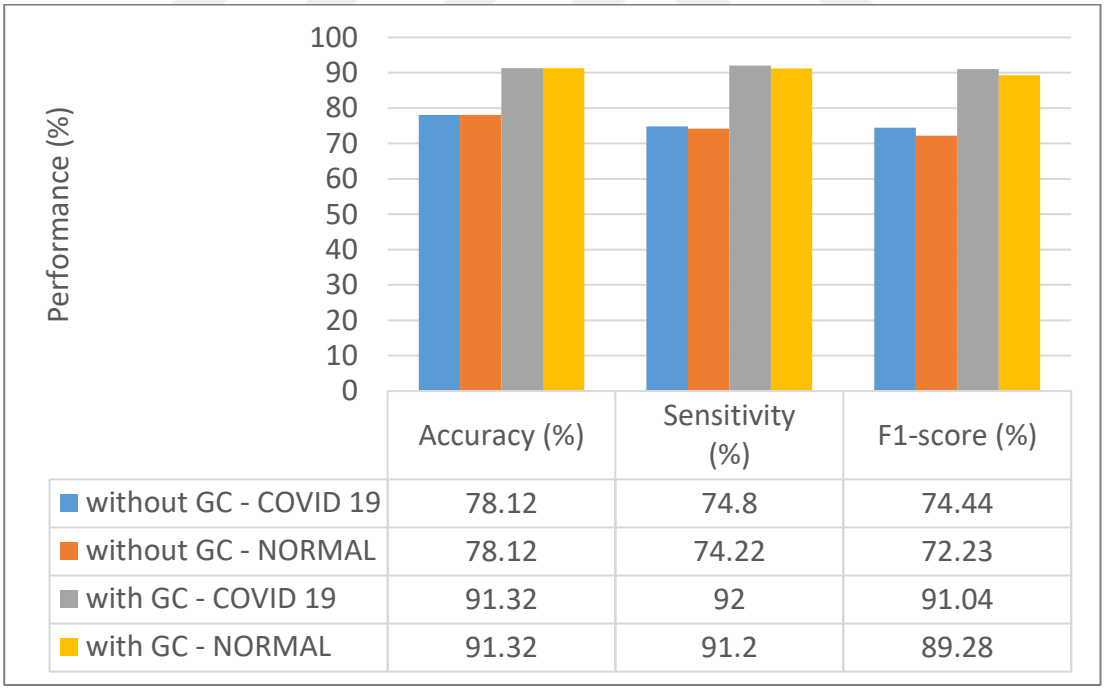


**Figure 4.18.** Covid-19 data-2 (70% training and 30% testing) the performance of training and testing the CNN net as a classifier.

**Table 4.10.** Covid-19 data-2 (70% training and 30% testing) the performance of training and testing XGBoost classifier.

| | **Training without GC (ϒ=1)** | | **Training with GC (ϒ=1.5)** | |
|---|---|---|---|---|
| | Covid-19 | Normal | Covid-19 | Normal |
| Accuracy (%) | 94.12 | | 97.52 | |
| Sensitivity (%) | 92.12 | 86.50 | 97.74 | 88.93 |
| F1-score (%) | 94.68 | 91.51 | 96.53 | 91.13 |

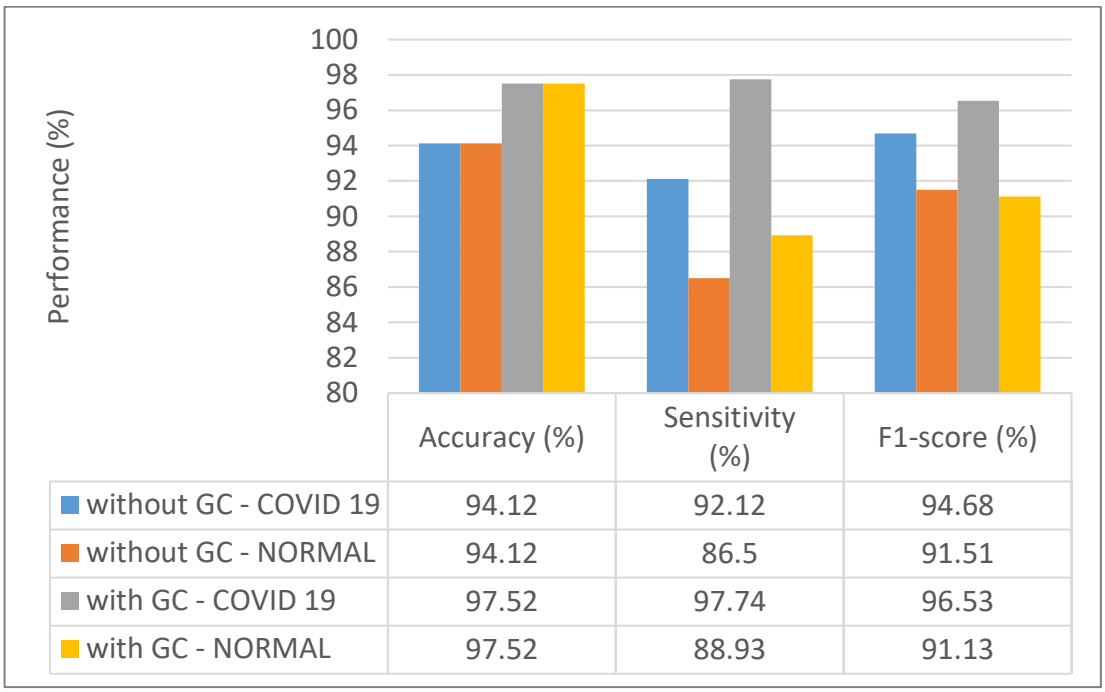


**Figure 4.19.** Covid-19 data-2 (70% training and 30% testing) the performance of training and testing XGBoost classifier.

Figure 4.20 depicts the classification performance of four different configurations: CNN, CNN with GC, CNN with GC and XGBoost combined, and CNN with both GC and XGBoost combined. The table provides accuracy, sensitivity, and F1-score metrics for each configuration.

For the CNN classifier alone, the accuracy is 73.66%, the sensitivity is 71.96%, and the F1-score is 77.89%. Upon applying GC to the CNN model, there is an improvement in performance across all metrics. The accuracy increases to 78.23%, the sensitivity to 77.02%, and the F1-score to 79.59%.

Integrating XGBoost with GC-enhanced CNN further enhances the performance metrics. The configuration of GC-enhanced CNN combined with XGBoost demonstrates an accuracy of 83.55%, sensitivity of 85.21%, and F1-score of 81.76%.

Finally, the configuration incorporating both GC and XGBoost showcases the highest performance across all metrics. The accuracy reaches 93.74%, the sensitivity is 96.32%, and the F1-score is 92.32%.

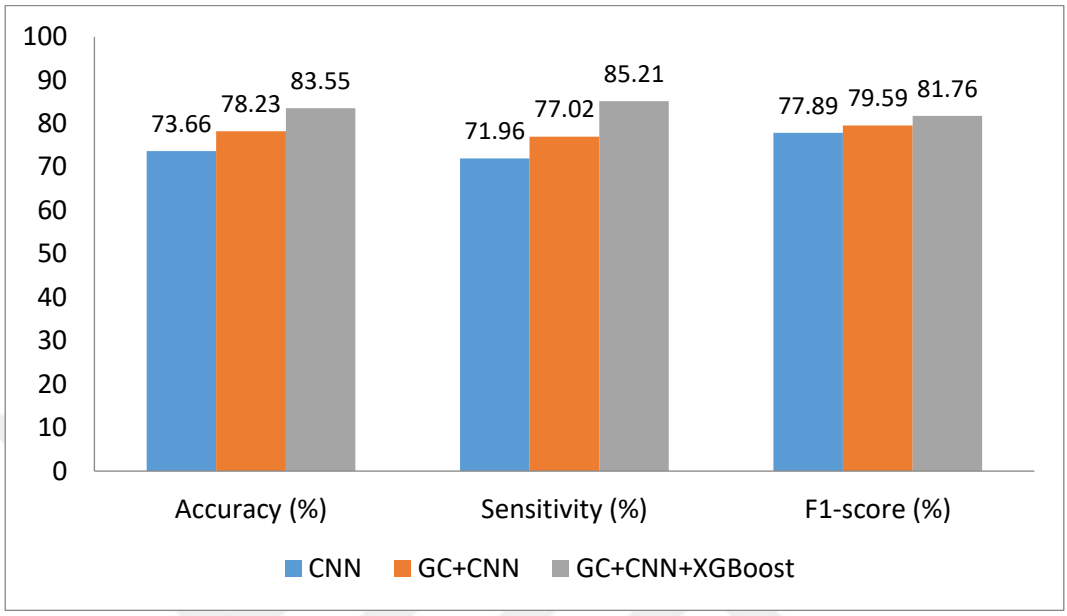


**Figure 4.20.** Covid-19 data-2 (70% training and 30% testing) classification performance of CNN and XGBoost classifier.

### 4.2.3. Results of splitting Covid Data 2 into 60% training and 40% testing

Table 4.21 and Table 4.12 present the performance evaluation of training and testing two different classifiers: CNN and XGBoost, under two conditions: without GC and with GC.

For the CNN classifier (Table 4.11), without GC, the accuracy stands at 76.64% for classifying COVID-19 cases and 92.87% for normal cases. Sensitivity, indicating the true positive rate, is 76.32% for COVID-19 and 75.17% for normal cases. The F1-score, a measure of a model's accuracy, is 75.42% for COVID-19 and 72.96% for normal cases. With GC, the CNN classifier shows improvement across all metrics. Accuracy increases to 93.63% for COVID-19 and 90.15% for normal cases. Sensitivity also improves to 93.63% for COVID-19 and 90.15% for normal cases, while the F1-score rises to 90.95% for COVID-19 and 90.11% for normal cases.

Similarly, for the XGBoost classifier (Table 4.12), without GC, the accuracy is 95.29% for COVID-19 and 97.83% for normal cases. Sensitivity is 91.31% for COVID-19 and 87.71% for normal cases, while the F1-score is 94.76% for COVID-19 and 90.12% for normal cases. With GC, the XGBoost classifier demonstrates further improvement in accuracy, reaching 97.06% for COVID-19 and 88.07% for normal

cases. Sensitivity also improves, with values of 97.06% for COVID-19 and 88.07% for normal cases. The F1-score increases to 95.95% for COVID-19 and 91.95% for normal cases.

**Table 4.11.** Covid-19 data-2 (60% training and 40% testing) the performance of training and testing the CNN net as a classifier.

| | **Training without GC (ϒ=1)** | | **Training with GC (ϒ=1.5)** | |
|---|---|---|---|---|
| | Covid-19 | Normal | Covid-19 | Normal |
| Accuracy (%) | 76.64 | | 92.87 | |
| Sensitivity (%) | 76.32 | 75.17 | 93.63 | 90.15 |
| F1-score (%) | 75.42 | 72.96 | 90.95 | 90.11 |

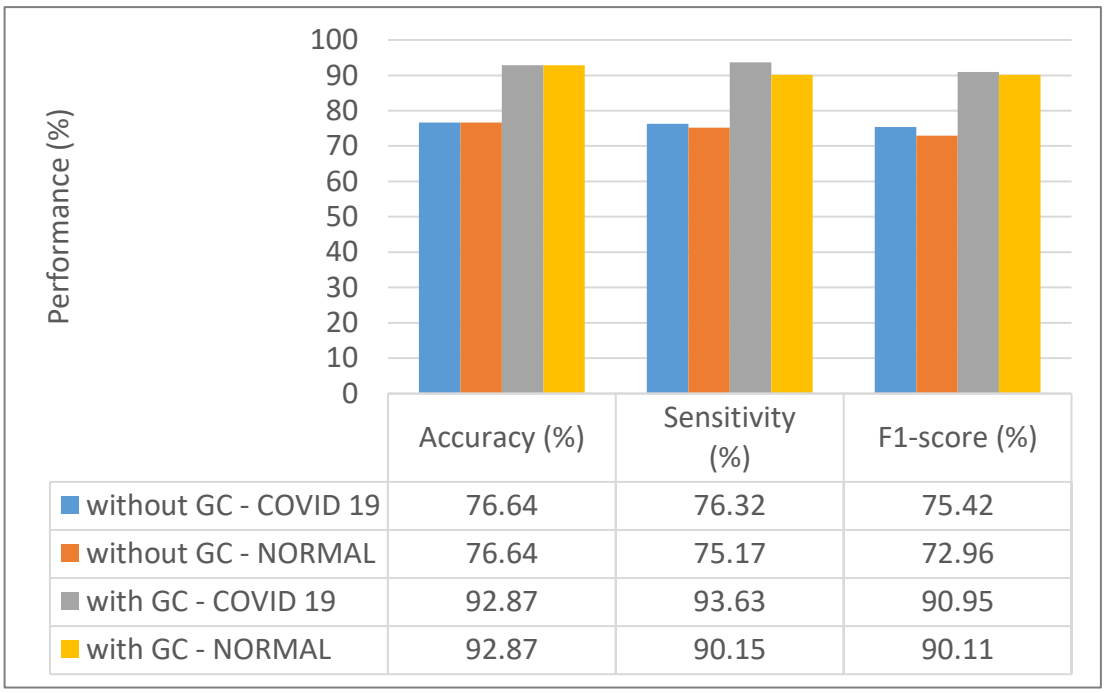


**Figure 4.21.** Covid-19 data-2 (60% training and 40% testing) the performance of training and testing the CNN net as a classifier.

**Table 4.12.** Covid-19 data-2 (60% training and 40% testing) the performance of training and testing XGBoost classifier.

| | **Training without GC (ϒ=1)** | | **Training with GC (ϒ=1.5)** | |
|---|---|---|---|---|
| | Covid-19 | Normal | Covid-19 | Normal |
| Accuracy (%) | 95.29 | | 97.83 | |
| Sensitivity (%) | 91.31 | 87.71 | 97.06 | 88.07 |
| F1-score (%) | 94.76 | 90.12 | 95.95 | 91.95 |

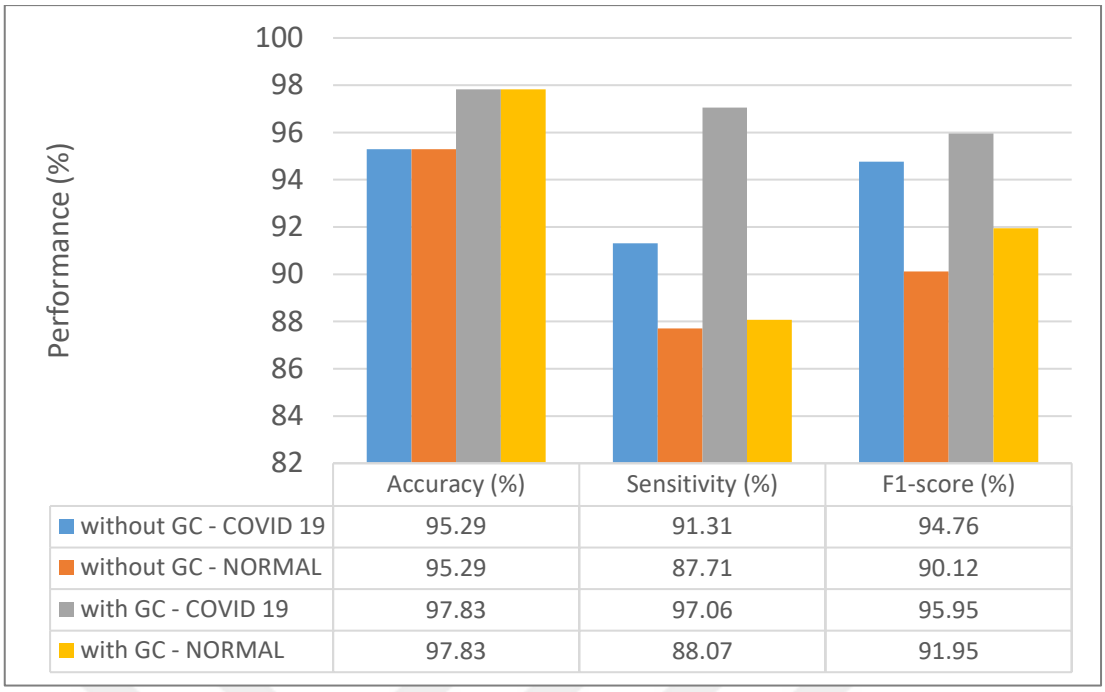


| | Accuracy (%) | Sensitivity (%) | F1-score (%) |
|---|---|---|---|
| without GC - COVID 19 | 95.29 | 91.31 | 94.76 |
| without GC - NORMAL | 95.29 | 87.71 | 90.12 |
| with GC - COVID 19 | 97.83 | 97.06 | 95.95 |
| with GC - NORMAL | 97.83 | 88.07 | 91.95 |

**Figure 4.22.** Covid-19 data-2 (60% training and 40% testing) the performance of training and testing XGBoost classifier.

Figure 4.23 illustrates the classification performance of four different configurations: CNN, CNN with GC, CNN with GC and XGBoost combined, and CNN with both GC and XGBoost combined. The table provides accuracy, sensitivity, and F1-score metrics for each configuration.

For the CNN classifier alone, the accuracy is 73.73%, the sensitivity is 71.72%, and the F1-score is 76.24%. Upon applying GC to the CNN model, there is an improvement in performance across all metrics. The accuracy increases to 76.87%, the sensitivity to 76.44%, and the F1-score to 80.29%.

Integrating XGBoost with GC-enhanced CNN further enhances the performance metrics. The configuration of GC-enhanced CNN combined with XGBoost demonstrates an accuracy of 83.5%, sensitivity of 87.12%, and F1-score of 82.98%.

Finally, the configuration incorporating both GC and XGBoost showcases the highest performance across all metrics. The accuracy reaches 93.55%, the sensitivity is 95.02%, and the F1-score is 92.7%.

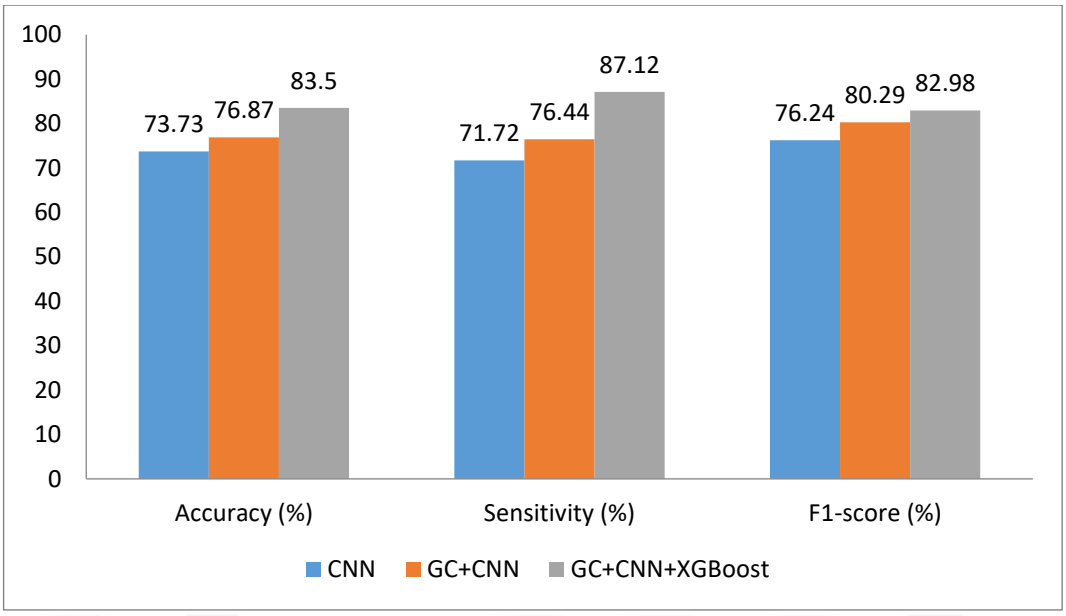


**Figure 4.23.** Covid-19 data-2 (60% training and 40% testing) classification performance of CNN and XGBoost classifier.

### 4.3. Comparison With Related Work

In comparing the performance of deep learning models across various studies, it becomes evident that each approach demonstrates impressive results in the classification of medical images related to COVID-19.

Amin et al. (2021) employed a deep learning model on a dataset comprising three classes—pneumonia, normal, and COVID-19—consisting of 194 images from the original pneumonia dataset and 163 images from the COVID-19 dataset. Their model achieved a remarkable 98% accuracy, with precision, recall, and F1 scores all equaling 0.97. Panwar et al. (2020) utilized the VGG model for feature extraction on a dataset of 142 COVID-19 images and 5863 Kaggle CXR healthy images, resulting in an accuracy of up to 99%. Demir et al. (2021) implemented a model with 20 convolutional layers on a dataset of 1061 CX images, achieving 100% accuracy in 80% of tests. Lastly, Sheykhivand et al. (2021) achieved a 92.43% accuracy on a diverse dataset containing healthy, COVID-19, bacterial, and viral images, demonstrating a high accuracy of 90% for all scenarios except one. These findings collectively underscore the effectiveness of deep learning models in the accurate classification of COVID-19 and related conditions, showcasing the potential for these models to contribute significantly to medical image analysis and diagnosis.

In this comparative analysis, the performance of the XGBoost model is evaluated against various deep learning models reported in different studies. For

instance, in comparison to Rajaraman et al.'s specialized CNN for CXR classification, the proposed XGBoost model achieves a testing accuracy of 95.55%, slightly below the 99.01% accuracy reported by Rajaraman et al. Hall et al.'s pre-trained ResNet50, which achieved an AUC of 95% and total accuracy of 89.2%, exhibits comparable accuracy levels to XGBoost. Similarly, Rahimzadeh et al.'s Xception and ResNet50V2 for multiclass CXR classification achieved 99.56% accuracy, slightly surpassing XGBoost. XGBoost competes well with models presented by Hemdan et al., where VGG19 and Dense Nets performed with F1 scores of 89% and 91%, respectively. In the context of chest CT images, XGBoost's performance aligns closely with Wang et al.'s three-stage DL technique, offering a potentially simpler alternative. Additionally, XGBoost outperforms Khalifa et al.'s testing accuracy of 87.1% using neutrosophic sets with deep transfer learning models. In comparison to Saad et al.'s deep feature concatenation (DFC) with CNNs, where XGBoost achieves a testing accuracy of 95.55%, the results are competitive, though slightly below Saad et al.'s reported accuracies for different methods.

**Table 4.13.** The performance of the proposed approach using different datasets.

| Ref. | DL Model | Dataset size | Ref. Results | Proposed method |
|---|---|---|---|---|
| (Amin et al., 2021) | Three different | - | (Amin et al., 2021) | Three different |
| (Panwar et al., 2020) | VGG as a model for feature extraction | 142 for COVID-19 images;5863 Kaggle CXR healthy images | accuracy up to 99% | 99.34% |
| (Demir et al., 2021) | 20 convolutional layers | 1061 CX images (361 COVID-19, 200 normal, and 500 pneumonia) | In 80% of tests, 100% performance was achieved for accuracy | 100% |
| (Sheykhivand et al., 2021 | - | Healthy: 2923 images; COVID-19:371; bacterial = 2778; viral = 2840 | 90% accuracy for all scenarios except one | 92.43% |

Serte et al.'s ResNet-50 for COVID-19 detection in CT scans, with an AUC of 96%, demonstrates comparable accuracy to XGBoost.

Moreover, while Singh et al.'s ensemble deep learning model outperformed existing models, XGBoost achieves high accuracy similar to Singh et al.'s ensemble approach. Kedia et al.'s CovNet-19 ensemble model, reporting an overall classification accuracy of 98.28%, slightly surpasses XGBoost's performance. Lastly, Ieracitano et al.'s CovNNet for COVID-19 pneumonia differentiation achieved an accuracy rate of over 80%, with XGBoost demonstrating a higher accuracy. In summary, the XGBoost model exhibits competitive performance, especially in terms of testing accuracy, across diverse applications. However, it's crucial to acknowledge that the choice of evaluation metrics and dataset characteristics may influence the comparative analysis, and each model's suitability depends on specific application requirements and dataset nuances.

# 5. CONCLUSION AND RECOMMENDATIONS

## 5.1. Conclusion

In recent years, the global landscape has witnessed a profound transformation attributable to the widespread impact of the COVID-19 pandemic. This transformative influence has spurred substantial progress in diagnostic technology, with a notable emphasis on the pivotal role of chest CT imaging. Beyond its primary utility in identifying COVID-19, this imaging modality has proven instrumental in detecting a spectrum of diverse ailments. The current research endeavors to contribute to this evolving landscape by investigating the efficacy of deep learning and transfer learning methodologies in the classification of medical images. A specific focus lies in the implementation of GC on CT images and the utilization of deep features.

In this study, the comparison between training the XGBoost classifier without and with GC yields insightful findings regarding its classification performance for distinguishing COVID-19 cases from normal ones. Across various image sizes and training scenarios, it's evident that incorporating GC enhances the classifier's performance metrics, including accuracy, sensitivity, and F1-score. Notably, when GC is applied (with $\gamma$ values of both 1.5 and 0.5), there's a noticeable improvement in the classifier's ability to accurately classify COVID-19 cases, especially in terms of sensitivity and F1-score. This suggests that GC effectively enhances the discriminative power of the XGBoost model by correcting for gradient discrepancies, thereby improving its capability to distinguish between different classes within medical imaging datasets.

In summary, the analysis of classifiers' performance, particularly CNN and XGBoost, on two distinct datasets (Covid Data 1 and Covid Data 2), underscores the impact of various training scenarios and image sizes, along with the significance of GC integration. For Covid Data 1, employing GC during training consistently enhances performance metrics across both classifiers. Notably, with an 80% training and 20% testing split, the XGBoost classifier achieves accuracy scores ranging from 89.32% to 97.76% for different image sizes and GC parameters ($\Upsilon$=1, $\Upsilon$=1.5, and $\Upsilon$=0.5). Similarly, sensitivity and F1-score metrics also exhibit notable improvements with GC utilization. Conversely, for Covid Data 2, akin to Covid Data 1, analogous trends in performance enhancement are discernible across diverse training splits and image sizes. Noteworthy accuracies ranging from 89.12% to 97.83% are attained by the XGBoost

classifier under different configurations, showcasing the efficacy of GC incorporation with varying gamma values. This highlights the robustness of preprocessing techniques and underscores the importance of tailored model training strategies for optimal performance in medical image classification tasks, accounting for dataset-specific nuances and variations.

The primary research objective involves a comprehensive examination of the capabilities of deep learning and transfer learning in the proposed medical image classification framework. A distinctive feature of this investigation is the incorporation of gamma correction as a preprocessing step and an enhancer for newly extracted deep features. A comparative analysis is conducted, scrutinizing the performance of the CNN both as a direct classifier and in its capacity as a feature extraction step. In contrast, the XGBoost classifier exhibits heightened sensitivity and F1-score, indicative of its proficiency in minimizing false positive and negative outcomes. The strategic inclusion of gamma correction in the preprocessing stage, coupled with its role as an enhancer for the newly extracted deep features, emerges as a pivotal factor contributing significantly to the performance outcomes, especially in the detection of COVID-19 in CT images.

In adopting a scientific approach, this study contributes to the growing body of knowledge surrounding medical image classification, offering insights into the nuanced interplay between advanced artificial intelligence systems, preprocessing techniques, and feature extraction methods. The findings pave the way for further refinement of diagnostic tools and underscore the potential for continued advancements in therapeutic diagnostics through the integration of sophisticated computational approaches.

### 5.2. Recommendations

The potential for growth in this field is vast. As an initial extension, further exploration of designs incorporating gamma correction and pre-processing tools is warranted. Enhancing the complexity of the models calls for investigating training options that accommodate larger GPU memory limits. This opens the door to utilizing inception modules and incorporating numerous dense layers, potentially unlocking more intricate patterns and correlations within the data. This avenue promises not only improved diagnostic capabilities but also a deeper understanding of the nuances of medical imaging.

Beyond the technical enhancements, the next frontier of research lies in expanding the classification scope to cover diverse ailments. Investigating how

architectural variations impact the diagnosis of specific conditions could be a pivotal step. If certain architectural styles prove more effective for particular illnesses, it could lead to targeted model development for specialized diagnostics. Additionally, delving into the reasons behind performance variations induced by different diseases holds the potential to uncover valuable insights into the intricacies of medical image analysis.

Exploring alternative data splitting methods, such as k-fold data splitting, stands as another avenue for future investigation. This could provide a more robust validation framework, ensuring the model's generalizability across diverse datasets. Moreover, such approaches could shed light on the robustness of the proposed model in handling variations and ensure its reliability in real-world scenarios. Continual refinement of these methodologies is crucial to bolstering the credibility and applicability of the developed model in clinical settings.

## 6. REFERENCES


Abebe, E. C., Dejenie, T. A., Shiferaw, M. Y., & Malik, T. (2020). The newly emerged COVID-19 disease: a systemic review. Virology journal, 17(1), 1-8.

Ahuja, A. S. (2019). The impact of artificial intelligence in medicine on the future role of the physician. PeerJ, 7, e7702.

Alshayeji, M. H., ChandraBhasi Sindhu, S., & Abed, S. E. (2022). CAD systems for COVID-19 diagnosis and disease stage classification by segmentation of infected regions from CT images. BMC bioinformatics, 23(1), 1-28.

Amin, H., Darwish, A., & Hassanien, A. E. (2021). Classification of COVID19 X-ray images based on transfer learning InceptionV3 deep learning model. In Digital Transformation and Emerging Technologies for Fighting COVID-19 Pandemic: Innovative Approaches (pp. 111-119). Cham: Springer International Publishing.

Ardakani, A. A., Kanafi, A. R., Acharya, U. R., Khadem, N., & Mohammadi, A. (2020). Application of deep learning technique to manage COVID-19 in routine clinical practice using CT images: Results of 10 convolutional neural networks. Computers in biology and medicine, 121, 103795.

Baek, I., & Kim, S. B. (2022). 3-Dimensional convolutional neural networks for predicting StarCraft II results and extracting key game situations. Plos one, 17(3), e0264550.

Basu, S., Mitra, S., & Saha, N. (2020). Deep learning for screening COVID-19 using chest x-ray images. In 2020 IEEE Symposium Series on Computational Intelligence (SSCI) (pp. 2521-2527). IEEE.

Berger, K., & Kaner, R. J. (2023). Diagnosis and Pharmacologic Management of Fibrotic Interstitial Lung Disease. Life, 13(3), 599.

Bharati, S., Podder, P., Mondal, M., & Prasath, V. B. (2021). Medical imaging with deep learning for COVID-19 diagnosis: a comprehensive review. arXiv preprint arXiv:2107.09602.

Brittain, E. L., & Hemnes, A. R. (2022). Introduction to Review Series on Pulmonary Vascular Disease and Right Ventricular Heart Failure. Circulation Research, 130(9), 1362-1364.

Camacho-Gonzalez, A., Spearman, P. W., & Stoll, B. J. (2013). Neonatal infectious diseases: evaluation of neonatal sepsis. Pediatric Clinics, 60(2), 367-389.

Canayaz, M. (2021). MH-COVIDNet: Diagnosis of COVID-19 using deep neural networks and meta-heuristic-based feature selection on X-ray images. Biomedical Signal Processing and Control, 64, 102257.

Canayaz, M., Şehribanoğlu, S., Özdağ, R., & Demir, M. (2022). COVID-19 diagnosis on CT images with Bayes optimization-based deep neural networks and machine learning algorithms. Neural Computing and Applications, 34(7), 5349-5365.

Chan, H. P., Hadjiiski, L. M., & Samala, R. K. (2020). Computer-aided diagnosis in the era of deep learning. Medical physics, 47(5), e218-e227.

Chua, F., Desai, S. R., Nicholson, A. G., Devaraj, A., Renzoni, E., Rice, A., & Wells, A. U. (2019). Pleuroparenchymal fibroelastosis. A review of clinical, radiological, and pathological characteristics. Annals of the American Thoracic Society, 16(11), 1351-1359.

Constantino, K., Gottlieb, M., & Long, B. (2023). Interstitial Lung Disease: A Focused Review for the Emergency Clinician. The Journal of Emergency Medicine.

Cottin, V., Hirani, N. A., Hotchkin, D. L., Nambiar, A. M., Ogura, T., Otaola, M., ... & Wells, A. U. (2018). Presentation, diagnosis and clinical course of the spectrum of progressive-fibrosing interstitial lung diseases. European Respiratory Review, 27(150).

Cui, H., Xie, N., Banerjee, S., Ge, J., Jiang, D., Dey, T., ... & Liu, G. (2021). Lung myofibroblasts promote macrophage profibrotic activity through lactate-induced histone lactylation. American journal of respiratory cell and molecular biology, 64(1), 115-125.

Cypel, M., & Keshavjee, S. (2020). When to consider lung transplantation for COVID-19. The Lancet Respiratory Medicine, 8(10), 944-946.

Damseh, N., Quercia, N., Rumman, N., Dell, S. D., & Kim, R. H. (2017). Primary ciliary dyskinesia: mechanisms and management. The application of clinical genetics, 67-74.

Demir, F. (2021). DeepCoroNet: A deep LSTM approach for automated detection of COVID-19 cases from chest X-ray images. Applied soft computing, 103, 107160.

Dorr, F., Chaves, H., Serra, M. M., Ramirez, A., Costa, M. E., Seia, J., ... & Barmaimon, G. (2020). COVID-19 pneumonia accurately detected on chest radiographs with artificial intelligence. Intelligence-based Medicine, 3, 100014.

Ezzat, D., Hassanien, A. E., & Ella, H. A. (2021). An optimized deep learning architecture for the diagnosis of COVID-19 disease based on gravitational search optimization. Applied Soft Computing, 98, 106742.

Farhan, A. M. Q., & Yang, S. (2023). Automatic lung disease classification from the chest X-ray images using hybrid deep learning algorithm. Multimedia Tools and Applications, 1-27.

File, T. M. (2000, September). The epidemiology of respiratory tract infections. In Seminars in respiratory infections (Vol. 15, No. 3, pp. 184-194).

Fu, M., Yi, S. L., Zeng, Y., Ye, F., Li, Y., Dong, X., ... & Zhang, Q. (2020). Deep learning-based recognizing COVID-19 and other common infectious diseases of the lung by chest ct scan images. MedRxiv, 2020-03.

Galani, I. E., Rovina, N., Lampropoulou, V., Triantafyllia, V., Manioudaki, M., Pavlos, E., ... & Andreakos, E. (2021). Untuned antiviral immunity in COVID-19 revealed by temporal type I/III interferon patterns and flu comparison. Nature immunology, 22(1), 32-40.

Gallacher, D. J., Hart, K., & Kotecha, S. (2016). Common respiratory conditions of the newborn. Breathe, 12(1), 30-42.

Guarnera, A., Santini, E., & Podda, P. (2022). COVID-19 Pneumonia and Lung Cancer: A Challenge for the Radiologist Review of the Main Radiological Features, Differential Diagnosis and Overlapping Pathologies. Tomography, 8(1), 513-528.

Gunraj, H., Wang, L., & Wong, A. (2020). COVIDnet-ct: A tailored deep convolutional neural network design for detection of COVID-19 cases from chest ct images. Frontiers in medicine, 7, 608525.

Halalli, B., & Makandar, A. (2018). Computer aided diagnosis-medical image analysis techniques. Breast imaging, 85, 85-109.

Hall, L. O., Paul, R., Goldgof, D. B., & Goldgof, G. M. (2020). Finding COVID-19 from chest x-rays using deep learning on a small dataset. arXiv preprint arXiv:2004.02060.

Hammoudi, K., Benhabiles, H., Melkemi, M., Dornaika, F., Arganda-Carreras, I., Collard, D., & Scherpereel, A. (2021). Deep learning on chest X-ray images to detect and evaluate pneumonia cases at the era of COVID-19. Journal of medical systems, 45(7), 75.

Han, Z., Wei, B.,... & Zhang, W. (2020). Accurate screening of COVID-19 using attention-based deep 3D multiple instance learning. IEEE transactions on medical imaging, 39(8), 2584-2594.

Hemdan, E. E. D., Shouman, M. A., & Karar, M. E. (2020). COVIDx-net: A framework of deep learning classifiers to diagnose COVID-19 in x-ray images. arXiv preprint arXiv:2003.11055.

Ieracitano, C., Mammone, N., Versaci, M., Varone, G., Ali, A. R., Armentano, A., ... & Morabito, F. C. (2022). A fuzzy-enhanced deep learning approach for early detection of COVID-19 pneumonia from portable chest X-ray images. Neurocomputing, 481, 202-215.

Kedia, P., & Katarya, R. (2021). CoVNet-19: A Deep Learning model for the detection and analysis of COVID-19 patients. Applied Soft Computing, 104, 107184.

Khalifa, N. E. M., Smarandache, F., Manogaran, G., & Loey, M. (2021). A study of the neutrosophic set significance on deep transfer learning models: An experimental case on a limited COVID-19 chest x-ray dataset. Cognitive Computation, 1-10.

Khalifa, N. E. M., Taha, M. H. N., Hassanien, A. E., & Elghamrawy, S. (2022, November). Detection of coronavirus (COVID-19) associated pneumonia based on generative adversarial networks and a fine-tuned deep transfer learning model using chest X-ray dataset. In Proceedings of the 8th International Conference on Advanced Intelligent Systems and Informatics 2022 (pp. 234-247). Cham: Springer International Publishing.

Khan, A. I., Shah, J. L., & Bhat, M. M. (2020). CoroNet: A deep neural network for detection and diagnosis of COVID-19 from chest x-ray images. Computer methods and programs in biomedicine, 196, 105581.

Kim, S. J., Azour, L., & Moore, W. H. (2020). Pleural disease: A review for the general radiologist. Applied Radiology, 49(6), 17-22.

Ko, H., Chung, H., Kang, W. S., Kim, K. W., Shin, Y., Kang, S. J., ... & Lee, J. (2020). COVID-19 pneumonia diagnosis using a simple 2D deep learning framework with a single chest CT image: model development and validation. Journal of medical Internet research, 22(6), e19569.

Leung, J. M., Yang, C. X., Tam, A., Shaipanich, T., Hackett, T. L., Singhera, G. K., ... & Sin, D. D. (2020). ACE-2 expression in the small airway epithelia of smokers and COPD patients: implications for COVID-19. European Respiratory Journal, 55(5).

Li, L., Qin, L.,... & Xia, J. (2020). Using artificial intelligence to detect COVID-19 and community-acquired pneumonia based on pulmonary CT: evaluation of the diagnostic accuracy. Radiology, 296(2), E65-E71.

Li, Q., Guan, X.,... & Feng, Z. (2020). Early transmission dynamics in Wuhan, China, of novel coronavirus–infected pneumonia. New England journal of medicine.

Loey, M., Smarandache, F., & M. Khalifa, N. E. (2020). Within the lack of chest COVID-19 X-ray dataset: a novel detection model based on GAN and deep transfer learning. Symmetry, 12(4), 651.

Martinez-Pitre, P. J., Sabbula, B. R., & Cascella, M. (2020). Restrictive lung disease.

Minaee, S., Kafieh, R., Sonka, M., Yazdani, S., & Soufi, G. J. (2020). Deep-COVID: Predicting COVID-19 from chest X-ray images using deep transfer learning. Medical image analysis, 65, 101794.

Mohammad, R., & Abolfazl, A. (2020). A new modified deep convolutional neural network for detecting COVID-19 from x-ray images. arXiv preprint arXiv:2004.08052.

Nayak, S. R., Nayak, D. R., Sinha, U., Arora, V., & Pachori, R. B. (2021). Application of deep learning techniques for detection of COVID-19 cases using chest X-ray

images: A comprehensive study. Biomedical Signal Processing and Control, 64, 102365.

Newell Jr, J. D., Sieren, J., & Hoffman, E. A. (2013). Development of quantitative CT lung protocols. Journal of thoracic imaging, 28(5).

Oh, Y., Park, S., & Ye, J. C. (2020). Deep learning COVID-19 features on CXR using limited training data sets. IEEE transactions on medical imaging, 39(8), 2688-2700. 23.

Oluwasanmi, A., Aftab, M. U., Qin, Z., Ngo, S. T., Doan, T. V., Nguyen, S. B., & Nguyen, S. H. (2021). Transfer learning and semisupervised adversarial detection and classification of COVID-19 in CT images. Complexity, 2021, 1-11.

Panahi, L., Amiri, M., & Pouy, S. (2020). Risks of novel coronavirus disease (COVID-19) in pregnancy; a narrative review. Archives of academic emergency medicine, 8(1).

Panwar, H., Gupta, P. K., Siddiqui, M. K., Morales-Menendez, R., Bhardwaj, P., & Singh, V. (2020). A deep learning and grad-CAM based color visualization approach for fast detection of COVID-19 cases using chest X-ray and CT-Scan images. Chaos, Solitons & Fractals, 140, 110190.

Panwar, H., Gupta, P. K., Siddiqui, M. K., Morales-Menendez, R., & Singh, V. (2020). Application of deep learning for fast detection of COVID-19 in X-Rays using nCOVnet. Chaos, Solitons & Fractals, 138, 109944.

Patel, Z., Franz, C. K., Bharat, A., Walter, J. M., Wolfe, L. F., Koralnik, I. J., & Deshmukh, S. (2022). Diaphragm and phrenic nerve ultrasound in COVID-19 patients and beyond: imaging technique, findings, and clinical applications. Journal of Ultrasound in Medicine, 41(2), 285-299.

Rajaraman, S., Siegelman, J., Alderson, P. O., Folio, L. S., Folio, L. R., & Antani, S. K. (2020). Iteratively pruned deep learning ensembles for COVID-19 detection in chest X-rays. Ieee Access, 8, 115041-115050.

Rehman, A., Naz, S., Khan, A., Zaib, A., & Razzak, I. (2022, April). Improving coronavirus (COVID-19) diagnosis using deep transfer learning. In Proceedings

of International Conference on Information Technology and Applications: ICITA 2021 (pp. 23-37). Singapore: Springer Nature Singapore.

Rguibi, Z., Hajami, A., Zitouni, D., Elqaraoui, A., & Bedraoui, A. (2022). Cxai: Explaining convolutional neural networks for medical imaging diagnostic. Electronics, 11(11), 1775.

Saad, W., Shalaby, W. A., Shokair, M., El-Samie, F. A., Dessouky, M., & Abdellatef, E. (2022). COVID-19 classification using deep feature concatenation technique. Journal of Ambient Intelligence and Humanized Computing, 1-19.

Serte, S., & Demirel, H. (2021). Deep learning for diagnosis of COVID-19 using 3D CT scans. Computers in biology and medicine, 132, 104306.

Shan, F., Gao, Y., Wang, J., Shi, W., Shi, N., Han, M., ... & Shi, Y. (2020). Lung infection quantification of COVID-19 in CT images with deep learning. arXiv preprint arXiv:2003.04655.

Shazia, A., Xuan, T. Z., Chuah, J. H., Usman, J., Qian, P., & Lai, K. W. (2021). A comparative study of multiple neural network for detection of COVID-19 on chest X-ray. EURASIP journal on advances in signal processing, 2021(1), 1-16.

Sheykhivand, S., Mousavi, Z., Mojtahedi, S., Rezaii, T. Y., Farzamnia, A., Meshgini, S., & Saad, I. (2021). Developing an efficient deep neural network for automatic detection of COVID-19 using chest X-ray images. Alexandria Engineering Journal, 60(3), 2885-2903.

Shukla, S. D., Vanka, K. S., Chavelier, A., Shastri, M. D., Tambuwala, M. M., Bakshi, H. A., ... & O'toole, R. F. (2020). Chronic respiratory diseases: An introduction and need for novel drug delivery approaches. In Targeting chronic inflammatory lung diseases using advanced drug delivery systems (pp. 1-31). Academic Press.

Singh, D., Kumar, V., & Kaur, M. (2021). Densely connected convolutional networks-based COVID-19 screening model. Applied Intelligence, 51, 3044-3051.

Singhal, T. (2020). A review of coronavirus disease-2019 (COVID-19). The indian journal of pediatrics, 87(4), 281-286.

Smith, D. J., & Jenkins, R. G. (2023). Contemporary Concise Review 2022: Interstitial lung disease. Respirology (Carlton, Vic.).

Subramanian, N., Elharrouss, O., Al-Maadeed, S., & Chowdhury, M. (2022). A review of deep learning-based detection methods for COVID-19. Computers in Biology and Medicine, 105233.

Sunarti, S., Rahman, F. F., Naufal, M., Risky, M., Febriyanto, K., & Masnina, R. (2021). Artificial intelligence in healthcare: opportunities and risk for future. Gaceta Sanitaria, 35, S67-S70.

Ucar, F., & Korkmaz, D. (2020). COVIDiagnosis-Net: Deep Bayes-SqueezeNet based diagnosis of the coronavirus disease 2019 (COVID-19) from X-ray images. Medical hypotheses, 140, 109761.

Verleden, G. M., Raghu, G., Meyer, K. C., Glanville, A. R., & Corris, P. (2014). A new classification system for chronic lung allograft dysfunction. The Journal of Heart and Lung Transplantation, 33(2), 127-133.

Wang, L., Lin, Z. Q., & Wong, A. (2020). COVID-net: A tailored deep convolutional neural network design for detection of COVID-19 cases from chest x-ray images. Scientific reports, 10(1), 1-12.

Wang, S., Zha, Y., Li, W., Wu, Q., Li, X., Niu, M., ... & Tian, J. (2020). A fully automatic deep learning system for COVID-19 diagnostic and prognostic analysis. European Respiratory Journal, 56(2).

Wiersinga, W. J., Rhodes, A., Cheng, A. C., Peacock, S. J., & Prescott, H. C. (2020). Pathophysiology, transmission, diagnosis, and treatment of coronavirus disease 2019 (COVID-19): a review. Jama, 324(8), 782-793.

Yang, X., He, X., Zhao, J., Zhang, Y., Zhang, S., & Xie, P. (2020). COVID-CT-dataset: a CT scan dataset about COVID-19. arXiv preprint arXiv:2003.13865.

Yeasmin, S. (2019). Benefits of artificial intelligence in medicine. In 2019 2nd International Conference on Computer Applications & Information Security (ICCAIS) (pp. 1-6). IEEE.

Zheng, C., Deng, X., Fu, Q., Zhou, Q., Feng, J., Ma, H., ... & Wang, X. (2020). Deep learning-based detection for COVID-19 from chest CT using weak label. MedRxiv, 2020-03.

Zoorob, R., Sidani, M. A., Fremont, R. D., & Kihlberg, C. (2012). Antibiotic use in acute upper respiratory tract infections. American family physician, 86(9), 817.

**CURRICULUM VITAE**

| Student Information | |
|---|---|
| **Name/Surname:** | RANA SABRY ABBAS AL-BAYATI |
| **Nationality:** | IRAQ |
| **Orcid No:** | 0000-0002-9099-3346 |

| School Information | |
|---|---|
| **Undergraduate Study** | |
| **University** | MUSTANSIRIYAH UNIVERSITY |
| **Faculty** | COLLEGE OF COMPUTER SCIENCE AND MATHEMATICS |
| **Department** | COMPUTER |
| **Graduation Year** | 2011/2012 |
| **Graduate Study** | |
| **University** | KIRŞEHİR AHİ EVRAN UNIVERSİTY |
| **Institute** | INSTITUTE OF NATURAL AND APPLIED SCIENCES |
| **Department** | DEPARTMENT OF ADVANCED TECHNOLOGIES |
| **Graduation Year** | 2024 |

| Articles and Papers Produced from the Thesis |
|---|
| Abbas, R.S. (2024) Detection of COVID-19 infection using CT scan images and deep learning model. Journal of Utilitas Mathematica. |